MODULATION OF CELL ADHESION STRENGTHENING BY NANOSCALE GEOMETRIES AT THE ADHESIVE INTERFACE

A Dissertation
Presented to
The Academic Faculty

by

Sean R. Coyer

In Partial Fulfillment
of the Requirements for the Degree
Doctor of Philosophy in
Bioengineering

Georgia Institute of Technology
August 2010

MODULATION OF CELL ADHESION STRENGTHENING BY NANOSCALE GEOMETRIES AT THE ADHESIVE INTERFACE

Approved by:

Dr. Andrés García, Advisor
School of Mechanical Engineering
Georgia Institute of Technology

Dr. Larry McIntire
Department of Biomedical Engineering
Georgia Institute of Technology

Dr. Emmanuel Delamarche
IBM Zurich Research Laboratory

Dr. Cheng Zhu
Department of Biomedical Engineering
Georgia Institute of Technology

Dr. Andrew Kowalczyk
Department of Cell Biology
Emory University

Date Approved: May 1, 2010

To my Mother and Father, for their guidance and encouragement

ACKNOWLEDGEMENTS

There are many people who have made this project possible and to them I owe my sincerest gratitude. First and foremost, I thank my advisor, Andrés García. Out of the multitude of lessons I have learned from Andrés, there are a few that resonate the loudest. He showed me that there's a time to think about things and there's a time to do things. He reminded me to enjoy the process and crack a joke as often as possible. He reassured me that hard work and persistence, no matter how daunting the task, pays off in the end. And that's why he's the PI! Thank you, Andrés, for your support and friendship.

I thank Emmanuel Delamarche for his support during my stay at IBM Zurich Research Labs. His fascination with science is infectious and his drive to help young scientist succeed is inspiring. Emmanuel taught me to be efficient with my time, to collaborate with others so that everyone benefits, and to enjoy a break from science on occasion to tell stories about snowboarding adventures and the unique ways that kids combine gum and pebbles with leather seats and electronics.

Thank you to the members of my committee for their participation and valuable input. Dr. Cheng Zhu provided critical input on this project and challenged me to find balance between engineering and biology. Dr. Andrew Kowalczyk clarified the important questions in biology and was a tremendous proponent throughout the project. Dr. Larry McIntire has strongly supported the project and has helped me to explore the implications of this work beyond the lab.

The path to a Ph.D. started well before I arrived at Georgia Tech, and through it all my family has given me their support. Thank you to my Mom and Dad for always letting me explore and supporting my independence, for teaching me a strong work ethic and letting me be

stubborn, and for passing on their appreciation for the pursuit of knowledge. I owe special thanks to my grandparents for showing me through example what it means to be dedicated to your family and your career. I thank my Grandpa Coyer, whose insatiable desire to learn and high spirits made a strong impression on a young boy who grew up to be an engineer like his Grandpa. To my Grandpa Dolan I owe my gratitude for showing me how to make your own path no matter how difficult and always maintain poise. Thank you, Grandma Coyer, for always cheering me on and teaching me to make the best of whatever comes my way. Thank you, Grandma Dolan, for being an example of how selflessness and fierce determination can make a difference for humanity. To my brother Jim I give my thanks for being the guy I wanted to grow up to be just like with a passion for figuring out how things work and having the coolest toys. Thanks to my sister Kelly for always keeping track of me and laughing at my Coyer sense of humor. I thank my sister Kathy for reminding me through example to enjoy the little things and for letting me get the kids worked up right before bed. Thanks to all of my family for their unwavering support even when they were not quite sure exactly what I was doing.

Thank you to my girlfriend and best friend, Shetal, who was there every day to do more for me than words can express. She has given me her full support and made gracious sacrifices so that I could reach my goals. Thank you, Shetal, for helping me when times were tough, sharing my excitement when it all worked out, and for laughing with me at jokes that only we get.

The members of the García Lab, past and present, made the lab more than an environment that produces excellent research. They made it motivating, hilarious, chaotic, challenging, inquisitive, and much more. First, my thanks to the original members for creating a lab environment that continues to benefit every student that joins the group. I owe many thanks

to Kristin Michael for showing me the ropes and cheering me on as I learned the art of the cell adhesion project. Her balance of patience, skill, and kindness makes her an excellent mentor. Nate Gallant was responsible for developing many of the techniques and know-how that made my project possible. Thanks, Nate, for leading the way and always being willing to help the next in line. Thank you to Jenn Phillips, one of my original first row cohorts, for being a great example of hard work paying off and for pushing in your chair … sometimes. Thanks to all the lab members who each taught me valuable lessons: Huengsoo Shin, Catherine Reyes, Charles Gersbach, Ben Keselowsky and Jeff Capadona.

I give my sincerest thanks to the lab members who helped complete this project and continue to inspire me to do my best. Thanks to Dave Dumbauld for being my fierce proponent, conscientious critic, and avid pep-talker. He shared the wild ride including forgotten homework assignments, tests that caused people to pass out, and desks and benches where the dividing line blurred in a shared effort to overcome the obstacles. Thanks DD! Kellie Templeman has been the best lab mom a graduate student could ask for. She has an amazing talent for balancing all of the demanding needs of the lab while sharing a contagious sense of humor and sincere desire to help others succeed. Thanks K-Dog, for always having my back, and for an endless stream of jokes, stories, and side-hurting laughs (Old Greg, mmm, creamy beige). My thanks to Tim Petrie come in two parts. First, Tim showed me what dedication to the pursuit of knowledge is truly about. Tim goes above and beyond that of a mere mortal to achieve success for himself and everyone around him. Second, Tim has given me a lifetime of fantastic stories that would be hard to believe if I didn't see it myself. Thanks Big T! Thanks to Abbey Wojtowicz for being the nicest person I've ever met. She wore a never-ending smile that was a gentle reminder to look on the brighter side of things. She showed me that it really was possible to graduate, and even though

the end would be rough, it was possible to do it with grace. Abbey, I won't forget that it's central not southern Illinois. Thanks to Amanda Bridges for being a rock, seemingly unfazed by the stress of the lab, and always ready to let it roll off and move on. Thanks, Amanda, for keeping it real and trading stories with the guys. I thank Joe Charest who is one of the best engineers I know. Thanks Joe, especially for the pig roasts! Thank you, Ed Phelps, for always being willing to help, for taking on the monumental challenge of keeping the lab computers alive, and for a fantastic City Chase. Ted Lee has recently joined the lab but quickly became an intricate part with a big personality and a great sense of humor that will lead him to great places. Thanks for keeping it OG, T. Lee. I thank Asha Shekaran for her razor sharp intellect and wit. It takes a strong person to join the ranks of the first row, and Asha did it, finding a way to give it as much … or maybe more than she gets. Nduka Enemchukwu, thank you for our tissue-culture discussions that often started with science and ended with something completely different. Watch out for the bike-stealing gangs of Ninjas. Many thanks to Rachel Whitmire for taking on the thankless job of leading the charge against lab chaos and for delicious baked goods. Ram Selvam, thank you for battling it out against the confocal with me and introducing me to Indian cuisine for a bachelor. Thank you to Stacie Gutowski for all the sugar-rush goodies, especially those oreo cookie treats that are ridiculous good. Sincere thanks to Iming, Patricia, Imen, and Ankur for their considerable contributions to making the lab more than just a lab.

The 2D crew is determined to work hard and play harder. Thank you to Angela Lin for surviving with me on Mondays by reliving stories from Saturday. I thank Mela Johnson for dishing it until I gave up even if you were always in my way in the lab. Thanks to Yash Kolambkar for demonstrating how to overcome any challenge while staying super cool. Thanks

to Julia “Razor” Henkels, Brent (aka Teen Wolf), Jessica, Ashley, Hazel, Joel, Tamim, Dosier, and the rest of the 2D family for being part of and continuing the Lair of Inefficiency.

During my year at IBM Zurich Research labs, I worked with a talented group of researchers who taught me a new way to approach science. Tobias Kraus is the kind of person that you hope you have the opportunity to work with again because he brings such strong dedication and determination but does it effortlessly and always with a hearty laugh. He is equally fearless on the rock wall as at the lab bench and I owe him many thanks for being a great friend. Thank you to Ute Drechsler, Heiko Wolf, Heike Riel, Emanuel Lörtscher, Martin Zimmermann, Jörg Ziegler, Dan Solis, Walter Riess, Paul Seidler, the entire NSSD group, and IBM staff.

I owe thanks to many people at Georgia Tech who contributed to the success of this project. Thank you to all my colleagues in IBB and Whitaker for their support including Meg McDevitt, Chris Ruffin, Sally Gerrish, James Godard, Alyceson Andrews, Floyd Wood, Katharine Montgomery, Vivian Johnson, Steve Woodard, and Allen Echols. Thank you to the MiRC Cleanroom for their assistance including Devin Brown, Gary Spinner, and the cleanroom staff.

TABLE OF CONTENTS

LIST OF TABLES

LIST OF FIGURES

LIST OF SYMBOLS AND ABBREVIATIONS

AFM	Atomic Force Microscope
BSA	Bovine Serum Albumin
DTSSP	3,3 dithiobis(sulfosuccinimidylpropionate)
ECM	Extracellular Matrix
EDC	1-Ethyl-3-(3-dimethylaminopropyl)carbodiimide Hydrochloride
EG_3	Tri(ethylene glycol)-terminated Alkanethiol
EG_6-COOH	Carboxylic Acid-terminated Alkanethiol
f	Fraction of Adherent Cells
FAK	Focal Adhesion Kinase
FN	Fibronectin
ISP	Ink-Subtract-Print
MEF	Mouse Embryonic Fibroblast
MHA	Mercaptohexadecanoic Acid
μ	Fluid Viscosity
μCP	Microcontact Printing
NCS	Newborn Calf Serum
NgCAM	Neuron-glia Cell Adhesion Molecule
NHS	N-hydroxysulfosuccinimide
NMP	N-methyl Pyrrolidinone
OEG	Oligo(Ethylene-Glycol)
PBS	Phosphate Buffered Saline
PDMS	Polydimethylsiloxane
PEG	Poly(Ethylene-Glycol)

PEI	Poly(ethylene imine)
PLL-g-PEG	Poly(L-Lysine)-g-Poly(Ethylene-Glycol)
PMMA	Poly(methyl methacrylate)
r	Radial Distance
ρ	Fluid Density
ROCK	Rho Kinase
σ, SCD	Surface Charge Density
SAM	Self-Assembled Monolayer
τ	Wall Shear Stress
τ_{50}	Wall Shear Stress at 50% Adherent Fraction
TRITC	Tetramethyl Rhodamine Iso-Thiocyanate
ω	Rotational Speed

SUMMARY

Cell adhesion to extracellular matrices (ECM) is critical to differentiation, proliferation, migration, and apoptosis. Alterations in adhesive mechanisms are central to the behavior of cells in pathological conditions and aging, including cancer, atherosclerosis, and defects in wound healing. Cell adhesion is a significant consideration in biomedical and biotechnology applications including biomaterials, tissue engineering, and cell culture supports.

This research project focused on quantitatively analyzing the adhesive responses while systematically modulating the adhesive interface. The *objective* of this project was to analyze the role of nanoscale geometry of the adhesive interface in regulating integrin recruitment to adhesive contacts and modulating cell adhesion strengthening to ECM. Our central *hypothesis* was that the size and location of clusters of recruited integrin modulates cell adhesion strengthening in response to nanoscale organization of the adhesive interface.

Technical limitations have made it challenging to analyze the role of nanoscale spatial geometry in biological functionality. To overcome this limitation, we developed an experimental platform that provides control over the nanoscale geometry of the adhesive interface on samples that match the needs of cell biology studies. We first focused on developing a technique for producing high resolution patterns of proteins in biologically relevant geometries. To this end, the subtractive patterning technique was used to produce a pattern of proteins on a flat elastomer using a silicon nanotemplate which was then transferred to a final substrate by contact and release. Atomic force microscopy and fluorescence microscopy analysis demonstrated that this technique can produce patterns of antibodies with sizes as small as 90 nm with high contrast and high reproducibility. A wide range of pattern geometries were demonstrated by printing lines, linelets, and squares with spacing between features ranging from hundreds of nanometers to 64 μm. Patterns comprising two types of antibodies with intrinsic self-alignment were produced by the successive inking, subtraction, and printing of antibodies. Our results introduce a facile, high-

throughput technique for patterning proteins on surfaces that enables the production of arrays of multiple types of proteins with high resolution, high contrast, and self-alignment in geometries that are relevant to cell adhesion studies.

In order to use the subtractive patterning technique for cell adhesion experiments, a robust immobilization strategy was required that maintained the original geometry of the protein patterns under extended cell culture conditions. The objective of our next study was to develop a method for producing cell adhesion arrays that constrain adhesion to nanoscale patterns of protein that are surrounded by a non-fouling background. To this end, we combined the subtractive patterning technique with mixed self-assembled monolayers. A mixed self-assembled monolayer was produced by assembling mixed carboxylic acid- and tri(ethylene glycol)-terminated alkanethiols into self-assembled monolayers on gold-coated substrates. The carboxylic acid-terminated alkanethiol component provided an anchoring point for immobilization of proteins into patterns. The tri(ethylene glycol)-terminated alkanethiol component provided a protein-resistant background when setup into a self-assembled monolayer. The subtractive patterning technique was used to produce complex patterns with multi-length scale dimensions. Following activation of COOH-end groups of the self-assembled monolayer, proteins transferred from the elastomer to the substrate during printing and tethered by coupling of protein primary amines to surface groups presenting NHS-esters.

Patterns of the cell adhesion protein fibronectin were produced to demonstrate the ability of the technique to immobilize proteins in controlled geometries while maintaining protein activity. Activity of the tethered FN was verified by binding of the FN-specific HFN7.1 monoclonal antibody which is receptor-mimetic. The background regions between FN-tethered regions remained devoid of antibody indicating that the non-fouling background effectively resists protein adsorption. Taken together, these results verify that protein activity is maintained during patterning and immobilization and that the non-patterned areas are resistant to protein adsorption.

Complex patterns of proteins with spacing and sizes varying across multiple length scales are desirable for studies of biological processes whose functionality requires coordination across the same scales. Previous experimental techniques typically achieve either micro- or nano-meter features but not both or are not able to maintain high-throughput or large sample areas that are needed for many biology experiments. In order to demonstrate the ability of our strategy to overcome these limitations, arrays of patterns of proteins were produced over large areas (~500 mm^2) in geometries that include feature dimensions at both micro- and nanometer length scales. Features measuring as small as several hundred nanometers were simultaneously patterned and printed with micron feature sizes of 2×2 μm^2. These results demonstrate the ability of this technique to overcome previous technical limitations by producing patterns with dimensions across multiple length scales.

Covalent immobilization of proteins and a protein-resistant background of alkanethiols were used to ensure robust arrays of protein that could maintain a controlled adhesive interface during extended periods of cell culture. We verified that proteins were tethered to the carboxylic acid-terminated alkanethiol and that the mixed-SAM background would resist cell adhesion by plating cells on substrates with various alkanethiol treatments. These results confirm that protein tethering occurs through carboxylic acid-terminated alkanethiols that have been activated by NHS/EDC chemistry. Further, the non-adhesive character of mixed SAMs including >95% tri(ethylene glycol)-terminated alkanethiols was maintained during printing and was able to resist deposition of protein from solution and/or cells. Taken together, these results demonstrate that printing to mixed-SAMs is applicable to cell studies that require the ability to control the location of cell adhesion.

Our patterning technique was shown to be a useful approach to controlling cellular processes by using FN patterns to direct the formation of focal adhesions in adherent cells. Staining of the focal adhesion component vinculin in cells spread on non-patterned FN showed areas of high intensity at sites of vinculin localization, indicating the formation of elongated focal adhesions that are typical of spread cells. Vinculin staining of cells adhered to patterns

consisting of eight squares with dimensions of 1 × 1 μm^2 showed constrained localization of focal adhesions to the patterned region. These results demonstrate that focal adhesion formation can be directed with high precision by modulating the geometry of the adhesive region. Combined, these results demonstrate that the combination of the subtractive patterning technique with mixed self-assembled monolayers produces robust cell adhesion arrays in which the geometry of the adhesion region can be used to direct cellular processes.

The objective of our next study was to analyze the recruitment of integrins into adhesive clusters in response to nanoscale geometry of the adhesive interface (adhesion area, spacing, and clustering) and determine the functional implications of integrin recruitment by quantifying variations in adhesion strength. Patterns of FN consisting of features with a range of nanoscale geometries (adhesion islands with dimensions of 1000, 500, 333, and 250 nm in clusters of 1, 2, 4, or 9) were produced using the subtractive patterning technique to directly immobilize proteins by covalent tethering onto surfaces presenting mixed self-assembled monolayers of alkanethiols. Cells seeded on the arrays were limited to one cell per pattern and adhesion was constrained to the adhesion region presented by the protein pattern. Spreading in between the patterns is prevented by the non-fouling background. Patterned substrates were shown to maintain the original pattern dimensions and resist FN deposition from cells using immunostaining with FN antibodies. These results demonstrate that the patterned arrays constrain cell adhesion to defined regions and that the adhesion patterns maintain their original design throughout the experiment.

Integrin recruitment was assessed using two metrics: 1) pad occupancy, which is defined as the number of adhesion pad locations that have integrin recruitment, and 2) integrin clustering characteristics, which includes the quantity of integrins that are recruited to a cluster, the localization of integrins within a cluster, and the area of the cluster. Three patterns were used with the same total area (12 μm^2) but in different area splitting configurations of 1000 nm × 1, 500 nm × 4, and 333 nm × 9 (square island edge dimension in nm × number of islands in cluster). A smaller total area (6 μm^2) was achieved with the pattern configuration of 250 nm × 4. Integrin clustering characteristics were analyzed by creating heat map images of α5 integrin

recruitment by averaging individual images of integrin staining in cells on patterns. Results show that as the size of adhesion islands decreases, integrin recruitment is reduced until reaching a pattern size that is too small to support integrin clustering. These results establish a threshold size between 333 nm and 250 nm at which an adhesion area-dependent transition that occurs from adhesion areas that support formation of clusters with high levels of integrin binding to adhesion areas that result in low level integrin binding at low frequency. These results demonstrate that the recruitment of bound integrins into clusters is directed by the nanoscale geometry of the adhesive interface.

The second metric of integrin recruitment that we analyzed was pad occupancy which describes the extent of cell adhesion that is supported on different pattern geometries. Cells on 1000 nm × 1 patterns predominantly occupied three or more pads (out of eight total pads) with over half of the locations showing pad occupancy on all adhesive pads. In contrast, cells on 250 nm × 9 patterns showed low pad occupancy with over 90% of locations having two or less pads occupied. Patterns 500 nm × 4 and 333 nm × 9 generated pad occupancies that were equally distributed from partial to full occupancy. These results indicate a range of adhesion that occurs on patterns with nanoscale geometries. Larger adhesion patterns provide the highest level of pad occupancy and therefore a greater extent of adhesion. Decreased adhesion occurs with decreased pattern size until limited cell adhesion occurs at pattern sizes below the threshold for recruitment of integrin clusters. Interestingly, no difference in pad occupancy occurs between the 500 nm and 333 nm pattern. These results establish a relationship between geometry of available adhesion areas and the ability of cells to generate integrin clusters that are required for adhesion and spreading.

Contractile forces in adherent cells are known to be important in the formation and maintenance of adhesive structures. In order to determine the effect of contractile forces on adhesion to nanopatterns, integrin recruitment was analyzed in cells on 500 nm × 4 patterns after treatment with an inhibitor of Rho-kinase. The inhibitor Y-27632 has been shown to reduce contractility and focal adhesion assembly. Cells treated with inhibitor showed no difference in

pad occupancy compared to control cells. However, cells treated with inhibitor exhibited a decrease in the level of integrin recruitment. These results indicate that cells with inhibited contractile forces are still able to recruit integrins to nanoscale adhesive contacts in a similar response as control cells. However, a decrease in the level of integrin recruitment occurs due to an inhibition of contractile forces.

Adhesion strength on nanoscale patterns was quantified in order to assess the functional dependence of cell adhesion on nanoscale geometry of the adhesion interface.
Adhesion strength was analyzed as a function of total adhesion area, spacing between adhesion points, and size of individual adhesion points at nanoscale dimensions in order to uncover their roles in generation of adhesive force. Analysis of adhesion strength on various patterns uncovered several unexpected roles for nanoscale geometry in modulation of adhesion strength. The importance of nanoscale area was determined by results showing that adhesion strength decreased with a decrease in total pad area. Adhesion strength was also shown to depend on area splitting. When total pad area was kept constant but adhesive pads were broken down into multiple islands of smaller dimensions, adhesion strength decreased. This area splitting effect occurred at pattern dimensions of both 1000 nm and 500 nm indicating a range of sizes over which this effect can occur. In another set of experiments, no differences in adhesion strength occurred with changes to the space between adhesion islands. Further analysis determined a relationship between adhesion strength and the size of individual adhesion islands independent of the number of islands per pad. No difference in adhesion strength occurred on patterns of 500 nm × 4 and 500 nm × 1. Combined with results from integrin recruitment analysis, these results suggest that pad occupancy plays a dominant role in generation of adhesion strength and that a integrin clusters with sizes ranging between 0.25 μm^2 to1 μm^2 can produce similar adhesion forces.

This thesis project has developed a unique experimental approach to analyze recruitment of bound integrins into clusters and quantify modulation of adhesion strength in response to systematic variation of the area, spacing, and clustering of adhesion areas. We determined that

integrin recruitment is directed by changes in the size, clustering, and orientation of adhesion regions. We established a threshold pattern area between 333 × 333 nm^2 (0.11 μm^2) and 250 × 250 nm^2 (0.06 μm^2) below which integrin recruitment switches from robust integrin clusters to low frequency punctate formations. The role of area splitting in adhesion strengthening was established where adhesion strength changes despite no change to the total available adhesion area. A relationship was established between adhesion strength and area of individual adhesion islands. Patterns with adhesion areas below the threshold were unable to generate adhesion strength. Adhesion strength is seen to vary with integrin pad occupancy and not with the level of integrin clustering at adhesion regions. Furthermore, our results suggest that integrin clusters with areas between 0.25 μm^2 and 1 μm^2 generate equal adhesion strengths. As a whole, this project provides new insights on the role of size and location of clusters of recruited integrin in the modulation of adhesion strength in response to nanoscale geometry of the adhesive interface.

CHAPTER 1

SPECIFIC AIMS

Cell adhesion to extracellular matrices (ECM) is critical to differentiation, proliferation, migration, and apoptosis. Alterations in adhesive mechanisms are central to the behavior of cells in pathological conditions and aging, including cancer, atherosclerosis, and defects in wound healing. Cell adhesion is a significant consideration in biomedical and biotechnology applications including biomaterials, tissue engineering, and cell culture supports. The adhesion process begins with integrins on the cell surface binding to adhesion ligands present in the ECM such as fibronectin (FN). Integrin binding is followed by clustering of integrins and formation of focal adhesion complexes that consist of structural and signaling molecules. Although significant progress has been made in identifying molecules involved in adhesion, the mechanisms that dictate the generation of strong adhesive forces remain poorly understood. Specifically, the role of nanoscale geometry of the adhesive interface, integrin clusters, and focal adhesions in adhesion forces remains elusive.

The *objective* of this project is to analyze the role of nanoscale geometry of the adhesive interface in regulating integrin recruitment to adhesive contacts and modulating cell adhesion strengthening to ECM. Our central *hypothesis* is that the size and location of clusters of recruited integrin modulates cell adhesion strengthening in response to nanoscale organization of the adhesive interface. The *rationale* of this project is that new insights into the regulation of adhesive interactions can be elucidated through a rigorous analysis of adhesion strengthening using an integrated set of unique techniques that allow systematic variation of the nanoscale geometry of the adhesive interface and quantitative analysis of adhesion strength. The objective of this project will be addressed in the following specific aims:

I: Develop an experimental technique capable of producing nanoscale patterns of proteins on surfaces for cell adhesion arrays.

The *working hypothesis* is that arrays of cells adherent to nanoscale patterns of active proteins will be achieved by using a modified microcontact printing technique to tether patterns of proteins onto surfaces coated with mixed self-assembled monolayers. A new soft-lithography technique will be developed in order to overcome previous technical limitations that prevented high-resolution patterning for cell adhesion studies. The patterning technique will achieve the following requirements: patterns will be produced with high resolution and high contrast, protein activity will be maintained throughout the procedure, the technique will be high-throughput, and final substrates will consist of tethered protein in patterns surrounded by a non-adhesive background that maintains high fidelity under extended cell culture conditions.

II: Analyze the recruitment of integrins into adhesive clusters in response to nanoscale geometry of the adhesive interface (adhesion area, spacing, and clustering)

The *working hypothesis* is that a nanoscale threshold exists at which integrin clusters transition from punctate entities to robust bonds to the surface in which the size and quantity of recruited integrins is directed by the adhesive interface geometry. We will determine the characteristics of various categories of integrin clusters ranging from small punctate formations to robust integrin clusters. A threshold area will be elucidated under which integrin clusters do not form on nanoscale patterns. Nanoscale patterns consisting of a range of adhesion areas, spacing, and clustering will be used to direct integrin recruitment.

III: Analyze the effect of adhesive interface organization on adhesion strengthening using controlled geometries of nanoscale patterns of proteins.

The *working hypothesis* is that variations in the nanoscale organization of the adhesive interface significantly modulate cell adhesion strength. Adhesion strength will be analyzed as a function of total adhesion area, spacing between adhesion points, and size of individual adhesion islands at nanoscale dimensions in order to uncover the role of geometry in generation of adhesive force. A threshold area will be elucidated under which nanoscale patterns are unable to

participate in generation of adhesion strength. A relationship between adhesion strength and integrin recruitment will be established.

Project Significance

Cell adhesion to the extracellular matrix provides spatial and chemical cues that determine cell functionality and fate. Integrin-mediated cell-ECM adhesion is central to cell survival, migration, differentiation, and proliferation [De Arcangelis and Georges-Labouesse Trends in Genetics 2000, Danen Sonnenberg J Pathology 2003]. Adhesions between cells and the extracellular matrix ligands are responsible for providing mechanical and biochemical signals that drive cell function. While significant contributions have been made identifying key adhesion components involved and the role they play in cell adhesion, migration, and signaling, the adhesive characteristics that drive the generation of strong adhesive forces remain poorly understood. **This research project is *significant* because it provides systematic analysis of the various categories of integrin clusters that occur in adhesive cells and the effect of nanoscale geometry on cell functionality as measured through adhesion strength. These analyses will provide a mechanistic link between structural elements at the adhesive complex and the adhesive function of adhesion strength.** This project will provide new insights into the modulation of adhesive interactions by the adhesive interface as well as the role of integrin recruitment in cell adhesion. A new understanding of integrin recruitment and clustering will be achieved by identifying categories based on size, spacing, and orientation. As well, we will elucidate the roles of adhesive interface and adhesive contact geometry at nanoscale dimensions in modulation of adhesion strength. In order to achieve this analysis, this project aims to develop a novel patterning technique that provides precise control over the adhesive interface and combine it with a well-established adhesion analysis system. This platform provides a novel method for systematic variation of characteristics of the adhesive interface and quantitative analyses of the effect on cell functionality. The facile and flexible

nature of this experimental platform makes it highly applicable to a wide variety of biological studies.

CHAPTER 2

LITERATURE REVIEW

Adhesion Strengthening

Cell adhesion to ECM proteins, such as fibronectin (FN), is primarily mediated by integrin receptors on the cell surface (Hynes, 2002). Integrins are a family of heterodimeric (αβ) receptors that consist of an intracellular and extracellular component. The integrin receptor consists of a large extracellular domain formed by both α and β subunit, a single transmembrane pass, and two short cytoplasmic tails. Integrin-mediated adhesion requires activation of integrins and mechanical coupling to extracellular ligands (Choquet et al., 1997; Faull et al., 1993; Garcia et al., 1998; Ginsberg et al., 2005). Bound integrins rapidly associate with cytoskeleton components before clustering together to form focal adhesions (Fig 2.1). Focal adhesions are supramolecular complexes comprised of structural (vinculin, talin, α-actinin) and signaling (FAK, Src, paxillin) molecules. Focal adhesions act as mechanochemical linkages between the cell cytoskeleton and the extracellular matrix (ECM) to generate adhesive force and transduce molecular signals (Chen et al., 2004).

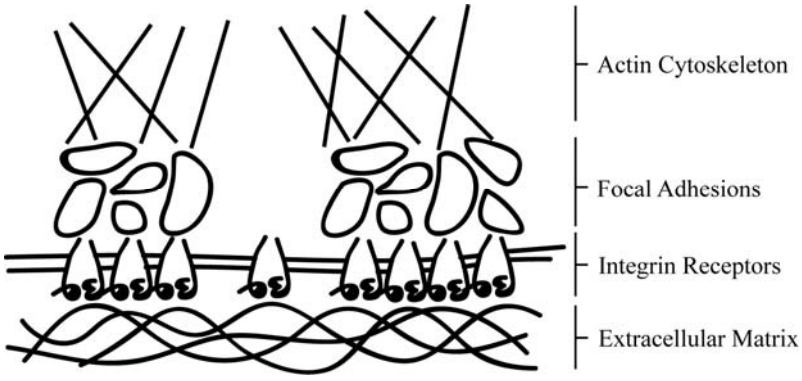

Figure 2.1: Cell adhesion begins with binding of integrins to extracellular matrices. After integrins associate with the cytoskeleton, clustering of integrins occurs, followed by formation of focal adhesions. Clustering of integrins and focal adhesion formation is critical to generation of force by the cell.

The cytoskeleton is an important component for generating adhesive force. The cytoskeleton includes three types of filaments – actin filaments, intermediate filaments, and microtubules. The cytoskeleton is a critical component in generating mechanical tension within the cell that regulates cell shape and behavior (Chicurel et al., 1998). Coordination of cytoskeleton components (actin, myosin II) and the initiation of adhesion sites are required for control of lamellipodium protrusion that occurs during cell motility (Giannone et al., 2007). Actomyosin contractility is required by cells to modulate the size and orientation of focal adhesions through mechanical forces (Balaban et al., 2001).

McClay and Erickson proposed the widely accepted model for adhesion strength in which a two-step process occurs consisting of initial integrin-ligand binding followed by rapid strengthening (Lotz et al., 1989). Adhesion strengthening comes from (i) increases in the cell-substrate contact area (spreading), (ii) recruitment of receptors to anchoring sites (integrin clustering), and (iii) interactions with cytoskeletal elements that combine to make adhesive structures that enhance force distribution by stiffening of the local membrane (focal adhesion assembly). These mechanisms have been verified experimentally using a variety of approaches (Balaban et al., 2001; Choquet et al., 1997; Hato et al., 1998; Maheshwari et al., 2000; Stupack et al., 1999). Strengthening of cytoskeleton linkages occurs in response to a force applied using fibronectin-coated beads and an optical trap (Choquet et al., 1997). Atomic force microscopy measurements demonstrated that integrin-ligand bond lifetimes are prolonged by application of force in a behavior called catch bonds (Kong et al., 2009). Analyses with elastic substrates demonstrated that focal adhesions act as strong anchorage points to the ECM and are involved in generation of forces in migrating cells (Balaban et al., 2001; Beningo et al., 2001; Tan et al., 2003). Clustering of integrins is required for cell motility using surfaces presenting clusters of adhesive ligands (Maheshwari et al., 2000). Garcia and coworkers have used a unique experimental system that combines an adhesion assay with micropatterning and biochemical assays to produce a quantitative assessment of the

contributions of adhesive area, bound integrins, and focal adhesion assembly to adhesion strengthening (Gallant et al., 2002; Gallant et al., 2005; Michael et al., 2009).

Integrin Clustering and Adhesive Responses

One of the most intensively studied areas in cell adhesion has been the role of integrins in the adhesion process. Integrin activity, distribution, clustering, and interactions with adhesion ligands have been extensively investigated. Yamada and colleagues showed that ligand binding targets integrin receptors to integrin-FN adhesion sites (Laflamme et al., 1992). The ability of integrins to mediate a complex variety of functions was connected to the receptor aggregation and occupancy by showing that each separate receptor activity or the combined activities produced different responses. Integrin occupancy by monovalent ligand resulted in redistribution of the receptor, but minimal protein signaling or recruitment of the cytoskeleton. Aggregation of integrins induced accumulation of FAK and tensin, but not other focal adhesion proteins such as talin. Combining occupancy and aggregation induced accumulation of various cytoskeletal proteins, including alpha-actinin, talin, and F-actin. This is a similar result to the activity of multivalent interactions with fibronectin (Miyamoto et al., 1995a; Miyamoto et al., 1995b). These results establish the importance of integrin activity in adhesive responses.

One area of focus has been studying the effects of integrin clustering on cell adhesion and spreading. Erickson and colleagues used microbeads coated with oligomeric constructs presenting multiple copies of the cell adhesive domain of FN to examine adhesion events (Coussen et al., 2002). They showed that trimers and pentamers, but not monomers or dimers, supported binding to actin followed by rearward translocation. Additionally, trimer- but not monomer-coated beads were associated with a talin-dependent slip bond (Jiang et al., 2003). These results suggest that clustering of integrins is required to enable binding to the cytoskeleton which leads to mature

adhesion. Furthermore, results demonstrating a required space between ligands of the adhesive domain RGD of 440 nm for cell spreading and 140 nm for focal adhesion assembly suggest that the organization of the integrins within the cluster is also important (Massia and Hubbell, 1991). These conclusions were verified by Spatz and coworkers who used block co-polymer micelle lithography to show that integrin spacing below 73 nm is required for focal adhesion assembly and adhesion (Arnold et al., 2004). Recently, clustering of α5β1-fibronectin bonds were determined to play a role unique from other integrins in maintaining structural adhesive bonds (Roca-Cusachs et al., 2009). Koo et al demonstrated that reinforcement of cell adhesion strength is dependent on the level of clustering of ligands on surfaces where clusters of 3 or more ligands can produce an increase in the force required to detach cells (Koo et al., 2002). Recently, AFM force measurements determined that a spacing between ligands of ≥ 90 nm was shown to inhibit focal adhesion formation and lead to significantly decreased adhesion strength compared to spacings of ≤50 nm (Selhuber-Unkel et al., 2010).

Focal Adhesion Size and Adhesive Responses

The size and distribution of focal adhesion in adherent cells has been observed and correlated with cell function. Focal adhesions have been observed to range in size from 0.25 to 10 μm^2 (Dugina et al., 2001; Geiger et al., 2001; Riveline et al., 2001; Zimerman et al., 2004). The range of sizes have been correlated to different categories of focal adhesions that include small, initial focal complexes (Nobes and Hall, 1995) and larger, mature focal contacts (Balaban et al., 2001; Ballestrem et al., 2001; Gumbiner, 1996).

In migrating cells, focal adhesion size has been shown to vary with location and function. Small nascent focal adhesions at the leading edge produce strong propulsive traction forces while larger mature focal adhesions exert weaker forces, suggesting a transition for focal adhesions from generators of strong propulsive forces to passive

anchorage devices based on size (Beningo et al., 2001). Focal adhesions at the leading edge of migrating cells go through a transition from early stage complexes into mature focal adhesions during which the composition of the focal adhesions changes (Zaidel-Bar et al., 2003). The range in function of focal adhesions that comes with variation in spatial distribution, size, and composition provides balance between adhesion and contraction in migrating cells (Gupton and Waterman-Storer, 2006).

Focal adhesion size and distribution have been correlated to the ability of cells to adhere and spread using a variety of techniques to produce surfaces with controlled patterns of adhesive protein. Lehnert and coworkers determined that cells are able to adhere to and spread on adhesion regions of 0.25 μm^2 and larger, but that adhesion with no spreading occurred on 0.1 μm^2 (Lehnert et al., 2004). Formation of focal adhesions on the smallest pattern size was verified by localization of vinculin and paxillin. Researchers used live-imaging to determine that 0.1 μm^2 dots were often removed from the substrate and internalized by cells. This suggests that focal adhesion formation occurred on these patterns and was robust enough to apply a force to overcome hydrophobic forces binding the FN dot to the substrate. Cell spreading was shown to directly correlate to the amount of adhesion area available, but irrespective of the geometrical pattern (Lehnert et al., 2004). Malstrom et al combined polystyrene particles, lift-off techniques, and PLL-g-PEG to produce circular patterns of FN with diameter 200, 500, or 1000 nm (0.03 to 0.8 μm^2). Results showed that cell adhesion, spreading, and focal adhesion formation vary with adhesion area. Vinculin staining of focal adhesions showed that focal adhesions increase in size with increased adhesion area. Cell spreading and focal adhesion formation was impaired on patterns with adhesion areas of 0.03 μm^2 and spacing of 300 nm. Bridging of focal adhesions between adhesion areas occurred on 1000 nm diameter patterns and rarely on 500 nm diameter patterns (Malmstrom et al., 2010). Frey and coworkers produced pattern sizes of 90 to 100 nm using metal evaporation onto surfaces coated with spheres followed by thiol- and poly(ethylene glycol)-functionalization of the

surface and fibronectin adsorption. These patterns were used to assess the effect of fibronectin pattern area on cell behavior. Researcher found that a minimum area of 0.05-0.1 μm^2 is needed to support cell spreading and proliferation (Slater and Frey, 2008). The ability of focal adhesions to apply force to surfaces of PDMS posts was linked to the size of the focal adhesion for areas larger than 1 μm^2, but no correlation existed between force and focal adhesion size for areas smaller than 1 μm^2 (Tan et al., 2003).

Cell Adhesion Strengthening

García and coworkers have made significant progress in analyzing the process of adhesion strengthening (Dumbauld et al., 2010a; Dumbauld et al., 2010b; Gallant et al., 2002; Gallant et al., 2005; Michael et al., 2009). These results have come from a unique experimental system that combines micropatterning with a spinning disk adhesion assay. Micropatterned surfaces consisting of arrays of proteins with diameters down to 2 μm were used to culture fibroblasts (NIH3T3 and mouse embryonic fibroblasts (MEFs)) onto a surface where the adhesion interface is controlled. The spinning disk assay uses fluid flowing over the cell array to detach the cells from the surface. The spinning speed of the disk determines the applied fluid shear stress and thereby the force that is required to detach the cell, i.e. the adhesion strength. The protein arrays used to culture cells consist of the adhesion protein fibronectin (FN). Blocking antibodies against human FN or integrin α5β1 completely eliminated adhesive force, demonstrating that adhesion is mediated solely by α5β1 binding to FN.

Adhesion analysis experiments using this system have provided unique information concerning the role of time, adhesion area, and focal adhesion composition in adhesion strengthening. The organization of integrins plays a critical role in regulating adhesion strength. Visualization of integrins showed that integrin organization on large features was punctuated and discrete while on small features the integrin coverage was uniform. These results combined with biochemical quantification of the number of bound

integrins indicated that on large adhesion areas the number of integrins is not limited which results in formation of many separate clusters of integrins. On small adhesion areas, when the number of bound integrins is limited, integrins are distributed evenly across the adhesion area (Gallant et al., 2005). These results suggest that integrin clustering and focal adhesion geometry are responsible for modulation of adhesion strength.

The role of focal adhesion kinase (FAK) and actin-myosin contractility in adhesion strengthening was also investigated. A novel role for FAK in integrin activation during early stages of adhesion was demonstrated. FAK expression in FAK-null cells was shown to enhance integrin activation and regulate time-dependent generation of adhesive forces (Michael et al., 2009). The role of contractility was investigated by either blocking phosphorylation of myosin light chain (inhibition of myosin light chain kinase or Rho-kinase) or inhibiting myosin II (blebbistatin) which resulted in reductions in adhesion strength to similar levels. This loss in adhesion strength correlated with a loss of vinculin and talin but not bound integrin from focal adhesions. Using vinculin-null cells and FAK expressing cells, contractility modulation of adhesion strengthening was shown to require FAK-and vinculin-containing focal adhesions (Dumbauld et al., 2010a; Dumbauld et al., 2010b).

Cell Adhesion Strengthening Model

Several theoretical models have been developed for receptor-mediated cell adhesion (Dembo et al., 1988; Evans, 1985; Hammer and Lauffenburger, 1987; Kloboucek et al., 1999; Olivier and Truskey, 1993; Ward and Hammer, 1993), but are limited either by not modeling long term adhesion or by the parameters being used not being easily controlled experimentally. A simple model overcoming these limitations was developed by Gallant et al (Gallant and Garcia, 2007) to correlate adhesion strengthening to the density and distribution of integrin-ligand bonds (both coupled and uncoupled to

the cytoskeleton) within the adhesion area. This microscopic model examines the adhesion force exerted by the cell through an adhesive area that is divided into segments (Fig 2.2). Within each segment are bonds that connect the cell to the substrate. Three conditions are considered: (i) bonds that are distributed uniformly across the adhesive area, (ii) clustered bonds (the outermost segment is filled first with clustered bonds until a saturation value is reached, then the next segment is filled), (iii) focal adhesion-associated bonds (bonds were distributed as in the clustering condition, but a fraction of the bonds were associated with the cytoskeleton). Detachment of the cell is assumed to occur by membrane peeling. For the uniformly distributed and clustered scenarios, bond loading was specified to decay exponentially from the periphery towards the center of the cell, while focal adhesion associated bonds are considered rigid, i.e. all bonds must break simultaneously. The resultant force and moment produced by each segment (Fi) is given by

$$F_i = f \cdot B_i \left[\chi + (1 - \chi) e^{1-i} \right]$$

where f is the individual bond strength, Bi is the number of bonds in segment i, and χ is the fraction of bonds associated with focal adhesions. Summing the forces and moments for all segments gives the total adhesion force. Several adhesion situations were examined using this model and correlated to experimental results. Under the condition of uniformly distributed bonds, the total adhesion force increased linearly with number of bonds. When integrin clustering occurred, the adhesion strength increased exponentially with bond number. This was due to localization of the bonds to the periphery where a higher moment arm allowed higher adhesion forces to be supported. Integrin clustering with focal adhesion formation also provided exponential increases in adhesion strength with bond number, and further enhanced the total adhesion force over integrin clustering alone. These results agree with experimental obtained adhesion values for long term adhesion and linear increases in adhesion strength at short adhesion times (Gallant et al., 2005; Garcia et al., 1998). Interestingly, the modeling results predict that an adhesion

area as small as 200 nm can produce the same mechanical behavior observed for focal adhesions of conventional sizes. These results are based on the assumption that detachment occurs by peeling in which most of the force resisting detachment occurs on bonds farthest from the center of adhesion area, and when these bonds break, the cell detaches. This model explains the importance of integrin clustering and focal adhesion formation in enhancement of adhesion strength over values obtained by bond number alone. Further experimentation combined with this model is needed to gather critical information concerning the precise focal adhesion spatial distribution and number of integrin clusters that allow advancement to mature adhesion.

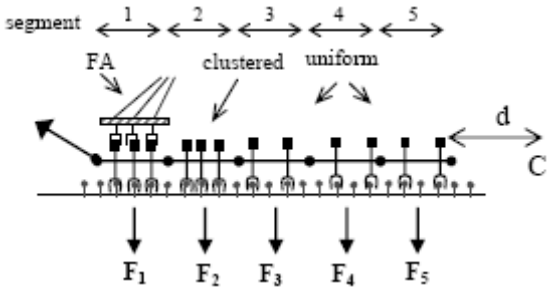

Figure 2.2: Mechanical model of adhesion strength. Adhesive segments contain bonds to the surface that are either uniformly distributed, clustered, or clustered with FA formation. Detachment forces for individual segments generated during membrane peeling are summed to give total adhesion force of the cell. (Gallant *et al., J. Biomech.* 2007)

Adhesion Quantification by Spinning Disk Assay

The García group has extensive experience using the spinning disk adhesion assay for studies of adhesion strength (Gallant et al., 2005; Garcia et al., 1997; Garcia et al., 1998). This experimental method uses a hydrodynamic flow to produce a shear stress that detaches cells from the surface. The detachment force imparted on the cell adhesion surface is proportional to the hydrodynamic wall shear stress, τ. The equation for the wall shear stress is

$$\tau = 0.8r\sqrt{\rho\mu\omega^3}$$

where r is the radial distance from the center of spinning, ρ is the fluid density, μ is the fluid viscosity, and ω is the rotational speed. The wall shear stress and therefore the detachment force increases with radial distance from the center. This characteristic of the system produces one substrate over which a range of detachment forces are applied to a large population of cells (~6000 cells/substrate). At the center of the disk where detachment forces are negligible, fully adherent cell populations remain after spinning. As the radius increases, the number of cells being detached from the surface increases. After spinning, the remaining cells are fixed, stained, and counted. The resulting detachment profile compares the fraction of adherent cells, f, to the wall shear stress. The fraction of adherent cells is calculated by dividing the number of cells in a counting field by the number of cells in the center counting field where detachment forces are negligible. The value for mean adhesion strength is defined to be the wall shear stress at which 50% of the cells are detached, (Fig 2.3). This value is obtained by fitting the experimental data to the sigmoid, $f = \frac{1}{1+e^{b(\tau-\tau_{50})}}$. The mean adhesion strength is the value used to quantify adhesion strength in various testing conditions including changes to adhesion time and the geometry of the adhesion area.

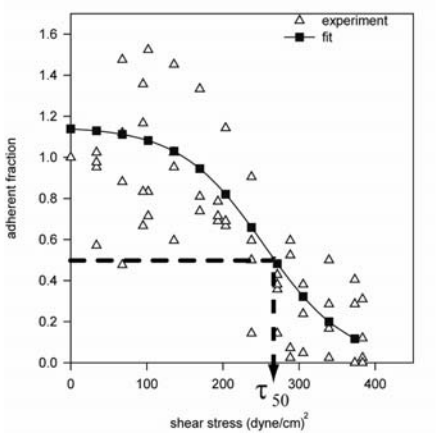

Figure 2.3: In the adhesion profile, the fraction of adherent cells is plotted as a function of the applied shear stress. The mean adhesion strength, τ_{50}, is defined as the shear stress value at which 50% of the cell population detaches. (Gallant *et al., J. Biomech.* 2007)

Protein Patterning

The ability to control the patterning of proteins is not only important for gaining insights into biological phenomena (Sniadecki et al., 2006) but is also a prerequisite for high-performance biosensors (Blank et al., 2003; Cornell et al., 1997) and novel fabrication paradigms (Lutolf and Hubbell, 2005). Many approaches have been pursued for patterning proteins on surfaces with high resolution, including dip-pen lithography, (Lee et al., 2002) microcontact printing,(Bernard et al., 1998; Lopez et al., 1993; Mayer et al., 2004; Renault et al., 2003; Von Philipsborn et al., 2006) self-assembly,(Yan et al., 2003) ablation of patterns into monolayers of proteins/organic molecules using various techniques,(Rundqvist et al., 2007) and nanografting based on scanning probe methods (Liu and Amro, 2002).

Microcontact Printing

Microcontact printing (μCP) has emerged as a highly effective patterning technique for biological applications due to its parallel patterning capabilities, low cost, and ease of use. Microcontact printing was originally developed by Whitesides and coworkers to pattern self-assembled monolayers (SAMs) of alkanethiols onto gold (Kumar and Whitesides, 1993). In μCP, a stamp is produced by replica molding of a template, often made in silicon using photolithography. Pattern transfer occurs from the inked stamp to the final substrate at regions of contact between the stamp and the surface.

The stability of the stamp material dictates the pattern resolution that can be achieved. Collapse of the stamp by buckling of the stamp features or sagging between features can occur (James et al., 1998). Most variations of microcontact printing, which conventionally use polydimethylsiloxane (PDMS) as the stamp material, are limited to feature sizes larger than 1 μm (Whitesides et al., 2001). As well, the spacing between features must be minimized to maintain stamp stability.

The applicability of μCP was greatly expanded when it was extended to patterns of biological materials. Proteins were patterned onto surfaces using adsorption to microcontact printed SAMs (Lopez et al., 1993). Bernard et al demonstrated direct transfer of patterns of proteins to a surface without the preliminary step of patterning SAMs by printing fluorescently tagged IgG (Bernard et al., 1998). James et al used microcontact printing to produce patterns of polylysine on glass coverslips (James et al., 1998). Application of microcontact printing stamps to biologically relevant systems was shown by affinity-contact printing where selective immobilization of antigens from solution to capture IgGs on the surface of a PDMS stamp was completed. Neuronal cells were seeded on patterns of neuron-glia cell adhesion molecules (NgCAM) printed by affinity-contact printing (Bernard et al., 2001). The role of wettability in protein transfer was determined by Chen and coworkers using printed patterns of SAMs on surfaces (Tan et al., 2002). These results show that transfer of proteins outside of solution occurs from a hydrophobic to hydrophilic surface. This approach was used to produce micrometer patterns of proteins by using a silicon template to selectively remove protein from a PDMS stamp (Renault et al., 2002).

As the size requirements for patterning have surpassed the micron regime, modifications to traditional microcontact printing have helped advance the field. Schmid et al developed variations of PDMS that are capable of producing feature sizes as small as 80 nm (Schmid and Michel, 2000). Renault et al used these advanced stamp materials to directly pattern one or several protein molecules by inking a stamp comprised of 100-nm posts with low concentration protein solution (5 μg/ml) (Renault et al., 2003).

Microcontact printing has developed into a valuable tool for patterning biological materials. Several issues remain to be resolved including the ability to obtain high-resolution patterns of proteins while maintaining the systems ease of use and high-throughput capabilities. Advancements in these areas will be critical to its applicability to exploring complex biological phenomena.

Patterning Proteins with Self-Assembled Monolayers

Self-assembled monolayers (SAMs) are assemblies of organic molecules that absorb onto surfaces in highly ordered arrays (Love et al., 2005). The molecular components of the SAM consist of a carbon backbone, a head group that provides chemical functionality, and an end group, that provides affinity for binding of the molecule to a surface. The most often used SAM molecules are alkanethiols that have a thiol end group which binds gold. Various head groups are used to control the chemical nature of a surface (wettability, friction, adhesion) (Keselowsky and Collard, 2004; Tan et al., 2002) or provide specific affinity to other molecules through activation. Mixed-SAMs are monolayers comprised of a mixture of unique SAM-components.

Self-assembled monolayers have been widely applied to biological studies. Multiple surface functionalities can be achieved based on head group selection. These include surfaces that 1) resist passive adsorption of biomolecules, 2) promote adsorption of biomolecules based on surface chemistry, or 3) covalently immobilize proteins or ligands. Protein-resistant surfaces are achieved using SAMs composed of oligo- or poly(ethylene glycol) (OEG or PEG). Tri-(ethylene glycol) alkanethiols have been used extensively to produce surfaces that resist protein deposition from solution or cells in culture over extended periods of time (Dumbauld et al., 2010b; Gallant et al., 2005).

SAMs have found extensive application to biological systems as a method for patterning biomolecules either by adsorption from solution or patterning by microcontact printing. Lahiri et al introduced a method for immobilizing proteins to mixed-SAMs from solution. Activation of carboxylic acid-terminated alkanethiols to reactive N-hydroxysuccinimidyl esters allowed coupling of these groups to amines on proteins or ligands from solution (Lahiri et al., 1999a). In reactive microcontact printing, a microcontact printing stamp is used to bring in contact and react a molecule presenting an amine group with an active ester-terminated SAM on the surface thereby transferring and immobilizing the molecule. Combinations of various species, activation schemes, and

reactive groups have been used. Whitesides and coworkers printed *n*-hexadecylamine onto activated carboxylic acid SAM as well as poly(ethylene imine) (PEI) onto a reactive SAM by binding primary and secondary amines in the PEI polymer to anhydride groups on the SAM end groups (Yan et al., 1999; Yan et al., 1998). As well, they immobilized various ligands including biotin and benzenesulfonamide using activation of carboxylic acid-terminated SAMs to pehntafluorpenyl esters (Lahiri et al., 1999b).

Dip-pen Nanolithography

Dip-pen nanolithography is an additive printing technique where molecules are deposited from an atomic force microscope (AFM) tip onto surfaces with nanoscale resolution. Dip-pen was first used to pattern alkanethiols with line width resolution of 30-nanometers (Piner et al., 1999). Patterning of structures consisting of multiple molecular components aligned at high resolution was demonstrated with patterns of 16-mercaptohexadecanoic acid (MHA) and 1-octadecanethiol (ODT). Patterns of MHA were used to immobilize proteins onto features with sizes ranging from 100 to 350 nm which were used for binding antigens from solution as well as seeding cells (Lee et al., 2002). Dip-pen nanolithography has also been used to covalently immobilize DNA with hexanethiol groups (Demers et al., 2002) and antibodies for detection of HIV-1 antigens (Lee et al., 2004). More recently, arrays of tips (up to 55,000) have been used to increase throughput for patterning proteins with feature resolution as small as 150 nm (Lee et al., 2006; Salaita et al., 2006).

Colloidal Lithography using Diblock Copolymers

Diblock copolymer micelles loaded with gold nanoparticles are coated onto surface by dip coating followed by chemical treatment to dissolve the copolymer leaving behind an array of gold nanoparticles whose spacing can be controlled by varying the molecular weight of the diblock copolymers (Spatz et al., 1999). Application to

biological systems was shown by immobilizing peptides to gold nanoparticles to produce arrays of adhesive ligand with controlled spacings of 28, 58, 73, and 85 nm (Arnold et al., 2004). Combining block copolymer micellar monolayers with electron-beam lithography was used to produce nanoscale patterns consisting of clusters of gold nanoparticles, thereby overcoming a limitation of pure self-assembly of non-periodic feature dimensions (Glass et al., 2003). Surfaces with uniform patterns of ligands with controlled spacing have been used to determine a minimum spacing required for integrin clustering (Arnold et al., 2004), to study FA dynamics (Cavalcanti-adam et al., 2007), and cell polarization and migration (Arnold et al., 2008). Most recently, arrays of ligand with controlled spacing were combined with AFM force measurements to show that ligand spacings ≥ 90 nm inhibited focal adhesion formation and detachment forces were decreased significantly compared to spacings of ≤ 50 nm (Selhuber-Unkel et al., 2010).

Additional Techniques for Nanopatterning Proteins

A wide variety of other techniques have been used to produce patterns of proteins on surfaces (Christman et al., 2006). DNA self-assembly has been used to produce a DNA lattice with biotin incorporated at lattice points which is then used to immobilize streptavidin into protein arrays (Yan et al., 2003). Ablation of proteins on surfaces uses electron beam pulses to remove protein from a coated surface thereby producing patterns of fibronectin at length scales as small as tens of nanometers although proteins may be rendered inactive during the process (Rundqvist et al., 2007). Nanografting uses a scanning probe to uncover gold on the surface which binds thiol molecules from the AFP tip. This technique was used to pattern alkanethiols on surfaces and immobilize BSA protein on 200 × 250 nm^2 features and IgG molecules on 40 × 40 nm^2 features (Liu and Amro, 2002). Nanoimprint lithography presses a silicon template, usually fabricated with high resolution features by ebeam lithography, into a polymer-coated surface heated to above the glass transition temperature. After cooling, the template is removed, and the

patterned polymer surface can be chemically modified to immobilize active proteins, such as streptavidin, in lines smaller than 100 nm (Hoff, 2004).

CHAPTER 3

FACILE PREPARATION OF COMPLEX PROTEIN ARCHITECTURES ON SURFACES WITH SUB-100 NM RESOLUTION

Summary

Proteins on surfaces are important in responses to implanted biomedical devices, diagnostic assays, pathological states, and cell adhesion. The nanoscale spatial organization of proteins plays a critical role in the activity of these systems. To determine the role of proximity in the functionality of protein complexes requires an experimental system that can systematically vary the protein environment. We report here a powerful yet simple technique in which multiple proteins can be patterned simultaneously into complex architectures with high resolution. The subtractive patterning technique achieves pattern sizes as small as 90nm with high contrast and high reproducibility. The contact printing characteristics of the technique make it high-throughput and able to be used outside of a cleanroom environment. Pattern geometries with a wide range of sizes, shapes, and spacing are demonstrated. These capabilities make the subtractive patterning technique well-suited for a variety of applications including studies of biological systems.

Introduction

Proteins on surfaces play an ubiquitous and central role in host responses to implanted biomedical devices and biotechnological applications (Anderson et al., 1990), including in vitro surface-based diagnostic assays (Koch, 2004) and cell culture supports (Capadona et al., 2005). In many cases, complex biological functionality results from the

* Modified from Coyer, S.R., Garcia, A.J., Delamarche, E. Facile preparation of complex protein architectures with sub-100-nm resolution on surfaces. *Angewandte Chemie-International Edition* **46**, 6837-6840.

interplay of multiple types of proteins, such as in immune responses involving antigen-presenting cells (Mossman et al., 2005), bone regeneration (Lutolf and Hubbell, 2005), and cell adhesion (Gallant et al., 2002). The activity of these systems is particularly dependent on a spatial organization that occurs primarily on the nanoscale, which has spurred the development of novel bioinspired materials and nanofabrication routes (Anderson et al., 2004; Gates et al., 2005; Stevens and George, 2005). The ability to control the patterning of proteins is therefore not only important for gaining insights into biological phenomena (Sniadecki et al., 2006) but is also a prerequisite for high-performance biosensors (Blank et al., 2003; Cornell et al., 1997) and novel fabrication paradigms (Lutolf and Hubbell, 2005).

Many approaches have been pursued for patterning proteins on surfaces with high resolution, including dip-pen lithography (Lee et al., 2002), microcontact printing (Bernard et al., 1998; Lopez et al., 1993; Mayer et al., 2004; Renault et al., 2003; Von Philipsborn et al., 2006), self-assembly (Yan et al., 2003), ablation of patterns into monolayers of proteins/organic molecules using various techniques (Rundqvist et al., 2007), and nanografting based on scanning probe methods (Liu and Amro, 2002). Despite these efforts, no single technique has been widely applied to investigate the role of proteins on surfaces in biological phenomena because of practical limitations. These limitations include the time required for high-throughput production of samples with nanoscale features over large areas, the need for specific surface chemistry to adsorb proteins from solution in selected areas of a surface, and the challenge of molding high-resolution features in elastomers that are mechanically stable.

Here, we present a method that combines the advantages of virtually any high-resolution lithographic method and microcontact printing by transferring a pattern of proteins from a nanotemplate to a substrate using a planar elastomer as the transfer vehicle. This method can be used to generate patterns with one or multiple types of

proteins with sub-100 nm resolution and having arbitrary geometries. Moreover, co-aligning proteins into complementary patterns is simply accomplished with this method. The intrinsic design of this method allows the production of a wide variety of complex protein architectures using easily accessible techniques and equipment.

Materials and Methods

Preparation of Nanotemplates

High-resolution nanotemplates were produced using electron-beam lithography. Silicon wafers (4") were spin-coated with poly(methyl methacrylate) (PMMA):anisole at a ratio of 2:1 for 40 s at 3000 RPM followed by a postbaking step at 180 °C for 90 s. The resulting thickness of the PMMA layer was ~100 nm. The PMMA resist was exposed in an e-LiNE electron-beam lithography system (voltage: 20 kV, aperture: 10 μm, beam current: 29 pA) (Raith GmbH, Dortmund, Germany), developed in a solution of MIBK:isopropanol at a 1:3 ratio for 30 s, immersed in isopropanol for 1 min, and blown dry under a stream of N2. The PMMA pattern was transferred into the silicon substrate using a low-etch-rate reactive ion etcher in a balanced process that used SF6 as a precursor for the etching and C4F8 for passivation of the sidewalls (Alcatel Vacuum Technology France, Annecy, France) that lasted for 25 s. The resulting Si structures were ~60 nm deep. The PMMA resist was removed by immersion in acetone for ~1 min. Generally, dicing was not completed prior to or after patterning to prevent particle contamination of the wafer. If dicing had to be completed prior to or after patterning, a sacrificial layer of PMMA was spin-coated on the wafer, dicing was completed, and then the PMMA was removed.

Nanotemplate design

Several types of geometries were used during these experiments. Patterns of lines, meshes of lines overlapping to form right angles, linelets, and squares gave results with

different resolution limits and ease of use. Patterns with large spaces between features (squares, linelets) were difficult to locate using atomic force microscopy (AFM). The highest-resolution features were obtained with patterns of meshes. High resolution patterns of squares were difficult to create.

Preparation of planar elastomers

PDMS planar elastomers were polymerized using Sylgard 184 prepolymers (Dow Corning, Midland, MI) at a ratio of 10:1 (base polymer:curing agent). An automatic mixer/dispenser (DOPAG Micro-Mix E, Cham, Switzerland) was used to uniformly mix the prepolymers before dispensing them into planar Petri dishes (Falcon 1001 and 1013, Becton Dickinson, NJ). PDMS was then cured at 60 ºC for at least 24 h. The planar elastomers had a final thickness of ~2 mm. Complete mixing of the PDMS is crucial to ensure homogeneous curing of the elastomer. If incomplete curing occurs locally, this may result in PDMS residues left on the nanotemplate, which might be difficult to remove.

Protein inking of planar elastomers

The polymerized PDMS was cut while still in contact with the Petri dish into ~5 × 5 mm2 pieces of elastomer. The side of the elastomer that was not in contact with the Petri dish was marked by making a shallow cut with a scalpel. The elastomers were cleaned by sonication in a 1:3 solution of isopropanol:deionized water for 5–10 min, rinsed using deionized water produced using a Millipore Simplicity System (Millipore Corporation, Billerica, MA), rinsed using ethanol, and blown dry under a stream of N2. The side of the elastomer that was in contact with the Petri dish was inked with ~100 μL of antibody solution for 30 min at room temperature. Using the pipette tip, the antibody solution was spread over the entire elastomer surface without contacting the surface. TRITC-labeled goat anti-rabbit IgG (T6778, Sigma, St. Louis, MO) was used at a

concentration of 0.5 mg mL–1 in phosphate buffered saline (PBS) (A7906, Sigma). AlexaFluor 647-labeled goat anti-rabbit IgG (A21244, Invitrogen, Carlsbad, CA) was used at a concentration of 0.1 mg mL–1 in PBS. Elastomers inked with antibodies were rinsed using PBS and deionized water, and blown dry under a stream of N2 for approximately 30 s.

Subtraction and Printing of proteins

Microscope glass slides (Menzel GmbH, Braunschweig, Germany) and silicon wafer pieces (Siltronic AG, Munich, Germany) were used as substrates for printing. Prior to printing, substrates were cleaned by sonication in a 1:3 solution of isopropanol:deionized water for 5-10 min, rinsed in deionized water, rinsed in ethanol, and blown dry under a stream of Ni. Silicon substrates and nanotemplates were treated in an oxygen plasma at 200 W for 60 s (Technics Plasma 100-E, Florence, KY). Proteins on homogenously inked elastomers were removed in selected areas by bringing the elastomers into contact with the nanotemplate for 15 s. The elastomers were brought into contact and released from the nanotemplate by hand without bending the elastomers to prevent the introduction of distortions in the resulting protein patterns. The protein patterns were transferred from the elastomers to the final substrates using a 30-s-long printing step. Intimate contact between the elastomer and the nanotemplate/substrate occurred after placing the elastomer on the nanotemplate/substrate by hand and applying a slight pressure with tweezers. The displacement of air by a propagating contact line between the elastomer and the contacted surface was easily seen by eye and confirmed uniform contact between the surfaces. Nanotemplates were cleaned of organic material by repeating the treatment with oxygen plasma before reusing. When completing patterns involving multiple subtraction or printing steps, a mark on the back of the elastomer created by making a shallow cut with a scalpel was used as an alignment marker to assure that successive steps were being completed in the same area.

Visualization

Fluorescence micrographs were acquired using a Nikon Eclipse 90i (Nikon Corporation, Tokyo, Japan) fitted with a Nikon Digital Sight DS-1QM/H-cooled CCD camera (Nikon Corporation). Black and white images captured from individual channels were color-coded and combined into one image for analysis using NIS-Elements 2.30 (Nikon Corporation). Scanning electron microscopy images were obtained using a LEO 1550 (LEO Electron Microscopy, Inc., Throrwood, NY) to verify the quality and dimensions of the nanotemplate. AFM images were obtained using a Nanoscope Dimension 3000 (Digital Instruments, Santa Barbara, CA) operated in tapping mode using standard silicon cantilevers (174–191 kHz, Nanosensors, Neuchâtel, Switzerland). AFM images were planarized, displayed, and analyzed using WSxM (Nanotec Electronica, Madrid, Spain).

The size of the total area containing patterns on the nanotemplate was important for (i) locating the pattern of proteins on the final substrate using immunofluorescence microscopy or AFM, (ii) locating the patterns on the nanotemplate using scanning electron microscopy, and (iii) ensuring correct location of the elastomer on the nanotemplate and substrate during contact steps. A pattern size of 1000 μm × 1000 μm was found to be optimal. Rectangular features with dimensions of 80 μm × 30 μm were placed at the corners of the area containing patterns on the nanotemplate to help locate the pattern.

Results

Figure 3.1 illustrates this method in which the main steps are to ink (I) a planar, hydrophobic elastomer using the spontaneous adsorption of proteins from solution onto hydrophobic surfaces, to subtract (S) proteins from the elastomer using a nanotemplate during a brief contact step, and to print (P) the remaining protein pattern from the elastomer onto a final substrate. These three steps are combined to form the “ISP”

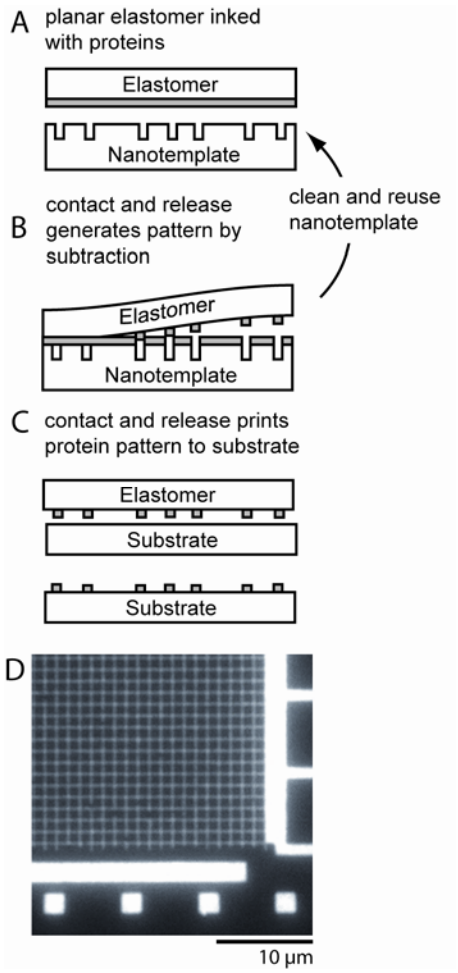

Figure 3.1. Experimental design to transfer patterns of proteins from a nanotemplate to substrates using a planar elastomer. (A) A planar elastomer is homogeneously inked with a monolayer of protein. (B) Contacting the inked elastomer with a nanotemplate results in the selective subtraction of proteins from the elastomer. (C) Proteins remaining on the elastomer subsequently transfer onto a target substrate during a printing step. (D) Fluorescence micrograph showing TRITC-labeled antibodies patterned on glass including micrometer (squares) and sub-micrometer (mesh) features using the ink-subtract-print (ISP) strategy.

strategy. The robustness of the ISP strategy is demonstrated by patterns of proteins with micrometer and sub-micrometer sizes (Fig. 3.1D). The only requirement for this method is to use a nanotemplate and final substrate having a higher work of adhesion for water than the elastomer (Tan et al., 2002), thereby yielding complete protein transfer. This requirement was easily accomplished in the following experiments using silicon nanotemplates and silicon or glass substrates by treating these surfaces with oxygen plasma to clean them and increase their surface hydrophilicity. Many other surfaces that are less hydrophobic than the elastomer can be used for this purpose (Bernard et al., 1998; Tan et al., 2002). Poly(dimethylsiloxane) (PDMS) was used as the elastomer material because of its higher hydrophobicity over glass and silicon and its conformability to surface topographies (Kumar et al., 1994).

We assessed the resolution and contrast of the ISP method using atomic force microscopy (AFM) to analyze patterns of isolated micrometer squares and nanoscale lines (Fig. 3.2). Arrays of high-contrast patterns of proteins were obtained (Fig. 3.2A) in which efficient printing from elastomer to substrate resulted in patterns of homogeneous layers of proteins. The profile of the pattern (Fig. 3.2B) shows small variation from a height consistent with that of a monolayer of protein (Liu and Amro, 2002). Patterns of right-angle meshes (Fig. 3.2C) exhibit no visible distortion along the lines or in the corners of the pattern, suggesting that once inked on the elastomer, proteins retain their positions during subtraction and printing without diffusing laterally (Geissler et al., 2000). High-resolution patterns (width < 100 nm) (Fig. 3.2D) were achieved with only a few optimization cycles of the nanotemplate preparation. These patterns are representative of those obtained over large areas (0.25 mm2). The mechanical stability of the nanotemplate suggests that uniform patterning of proteins might be completed over much larger areas. Such patterns can be used to array large numbers of individual biological elements on a surface with the advantage of enabling the simultaneous study of individual elements and the collection of data on statistically meaningful populations

(Stamou et al., 2003). The controlled adhesion of single cells onto surfaces patterned with user-defined protein architectures provides a unique experimental system for cell biology studies (Arnold et al., 2004; Chen et al., 1997; Gallant and Michael, 2005; Koo et al., 2002). We therefore generated patterns of proteins having a range of sizes and spacings (Fig. 3.3). Arrays were obtained of ~260-nm-wide linelets (Fig. 3.3C), with the spacing between geometries ranging from 1 to 64 μm (Fig. 3.3A). Patterns of proteins with nanoscale features separated by many micrometers would be very difficult to produce using microcontact printing stamps made from commercially available materials or even advanced polymer compositions due to collapse between or buckling of the features on the stamp (Bietsch and Michel, 2000). Square patterns with a minimum size of ~280 nm (Fig. 3.3F) were printed in clusters of 1, 2, or 4 (Fig. 3.3D). These arbitrary patterns were simultaneously completed in less than one hour, a time which included inking of the elastomer (30 min), subtraction with the nanotemplate (1 min), and patterning to the final substrate (1 min).

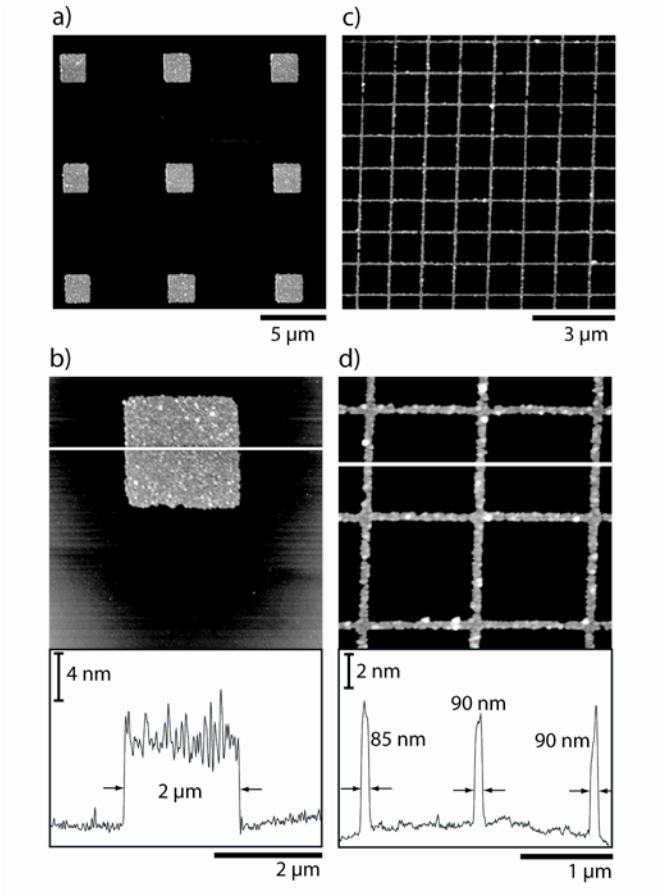

Figure 3.2. Noncontact mode AFM analysis of high-resolution patterns of antibodies obtained using a nanotemplate produced by electron-beam lithography. Complete protein transfer from the elastomer to the nanotemplate results in high-contrast patterns having (A) and (B) micrometer and (C) and (D) sub-100 nm sizes. A planar PDMS (Sylgard 184™) elastomer and a silicon substrate were used for these experiments.

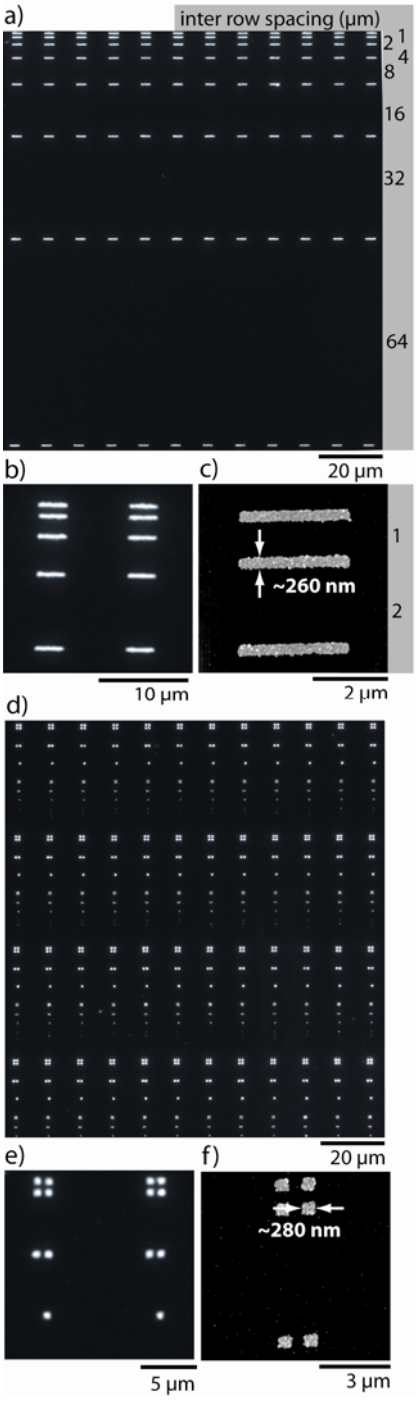

Figure 3.3. Fluorescence and AFM images revealing high-resolution patterns of TRITC-labeled antibodies on glass and silicon, respectively. The low fill factor of the patterns in (A)-(C) and the geometric variability in (D)-(F) did not pose particular problems to the patterning method used here. In (C) and (F), AFM was used to assess the dimensions of the patterns.

Combining the I, S, and P steps provides a variety of avenues for creating complex architectures of multiple proteins (Fig. 3.4). In one strategy, two different types of proteins are separately patterned by subtraction on separate elastomers prior to being printed onto one substrate (2×ISP) (Fig. 3.4A). By varying the in-plane orientation of the elastomers during printing to the final substrate, patterns of proteins were produced having regions of overlapping antibodies (Fig. 3.4B). Nonoverlapping patterns of proteins can also be produced with various spatial organizations (Fig. 3.4C). This robust method might be used to produce patterns of two proteins whose functionality results from their interaction to investigate the role of spatial orientation and density on the activity of the two proteins.

In a second strategy, one elastomer is inked with the first antibody, subtracted using a nanotemplate, inked with a second antibody, subtracted again, and then contacted with the final substrate to print the proteins (ISISP) (Fig. 3.4D). Individual channels for the antibodies present in the final pattern show the complementary nature of patterns that are intrinsically aligned because of the simultaneous patterning by subtraction from one nanotemplate during the second subtraction step (Fig. 3.4E). As proteins from solution will not adsorb to previously patterned proteins, boundaries between neighboring features consist of two adjacent patterns of proteins. The flexibility of this technique enables a multitude of variations in the size, spacing, and orientation of the patterns of proteins by simple changes in the procedure. By rotating the second nanotemplate with respect to the pattern obtained by the first subtraction step, the spacing of the two proteins is proportionally varied between a minimum and maximum spacing that is defined by the layout of the nanotemplates (Fig. 3.4F).

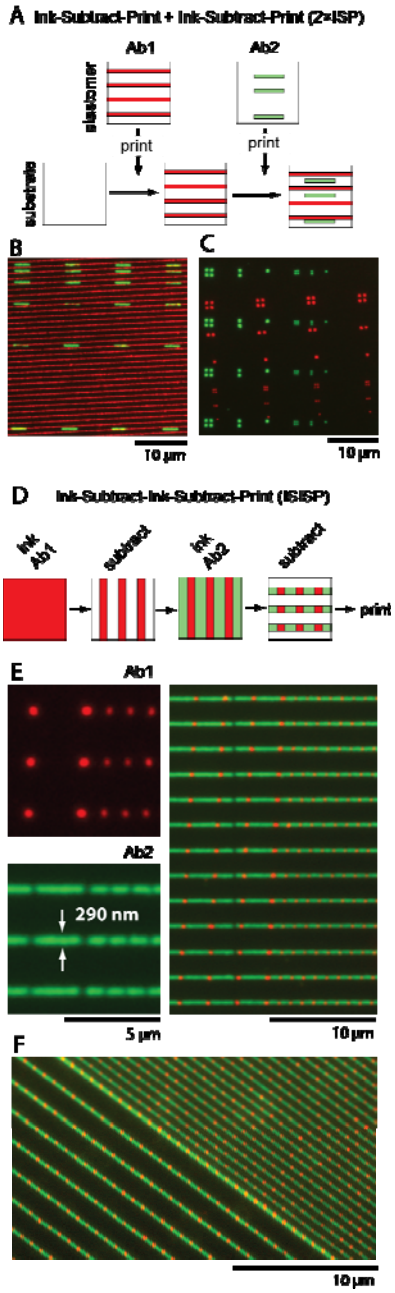

Figure 3.4. Complex protein architectures produced using combinatorial printing methods and visualized by fluorescence microscopy. (A) The successive inking, subtraction, and printing of antibodies on a glass substrate results in patterns comprising two types of antibodies. Depending on the geometry of the patterns, the different types of proteins might overlay on the surface (B) or be adjacent (C). (D) The repeated inking and subtraction of multiple types of proteins followed by one printing step produces complementary patterns of proteins as shown in the combined fluorescence image in (E). Intrinsically aligned patterns of proteins are produced using this method irrespectively of lateral shifts and angle variations between the two subtractive steps (F). The positions of each type of antibody were recorded separately and digitally recombined using, as encoding colors, red and green for TRITC-labelled IgG (Ab1) and Alexa Fluor® 647-labelled IgG (Ab2), respectively.

Discussion

The method shown here for patterning proteins on surfaces enables the production of arrays of multiple types of proteins with high resolution, high contrast, and self-alignment. In contrast to many techniques used for patterning surfaces at high resolution, a nanotemplate is the only key component needed to implement this method. The template does not necessarily have to be fabricated by means of electron-beam lithography but can also be prepared at various scales and from many materials using in-house or commercially available sources. The template can be reused or made disposable by structuring polymers with molding, hot embossing, or nano-imprint techniques. We believe that the method presented here enables a broad range of researchers to easily pattern proteins on surfaces at very high resolution while spending only a minimum effort on generating a patterned template. As most proteins adsorb from solution onto hydrophobic surfaces and transfer by printing from a less wettable to a more wettable substrate, this method should be widely applicable to the patterning of a variety of proteins and substrates. The contiguous placement of multiple types of proteins on the nanometer scale creates complex architectures at which advanced functionalities can be expected. These are, for example, the selective anchoring of protein complex, vesicles, or even cells with high specificity and control over the orientation.

Conclusion

Our results introduce a novel method for producing patterns of proteins on surfaces. The flexibility of this strategy allows production of a wide variety of patterns with high resolution and contrast. Single and multiple proteins can be printed in self-aligned patterns with precise control over feature geometry, size, and spacing. The flexibility of this technique makes it applicable to a wide variety of applications including

analysis of biological systems in which functionality occurs at nanometer length scales or through the combination of multiple proteins into complex architectures.

CHAPTER 4

TETHERING OF PROTEINS INTO MICRO- AND NANOSCALE PATTERNS BY PRINTING ONTO SELF-ASSEMBLED MONOLAYERS

Summary

Surfaces engineered with controlled spatial arrangement of biomolecules have supported design of advanced biosensor and biomaterials and opened opportunities in fundamental studies of protein-protein interactions and cell biology. This work presents a strategy for printing high-resolution patterns of proteins on surfaces using direct covalent immobilization. A mixed self-assembled monolayer was produced by assembling mixed carboxylic acid- and tri(ethylene glycol)-terminated alkanethiols into self-assembled monolayers on gold-coated substrates. Complex patterns with multi-length scale dimensions are produced by subtracting protein from a flat elastomer stamp. Following activation of COOH-end groups of the self-assembled monolayer, proteins transferred from the elastomer to the substrate during printing and tethered by coupling of protein primary amines to surface groups presenting NHS-esters. We demonstrate broad applicability to biological studies by controlling the spatial arrangement of cell adhesive proteins to control assembly of adhesive structures in adherent cells. Substrate areas that were not printed with proteins remained resistant to non-specific protein adsorption and cell adhesion. This method is useful because it provides direct covalent immobilization of proteins, control over micron and nanoscale pattern geometries, and a robust protein-resistant background.

Introduction

Engineering surfaces of functionalized bioactive components is of great importance in medical applications including protein biochips and biosensors (Jonkheijm et al., 2008) as well as fundamental life sciences studies (Sniadecki et al., 2006). Patterning of biomolecules onto surfaces has been extensively investigated as a way to achieve control over the spatial arrangement of chemical signals (Christman et al., 2006; Schmidt and Healy, 2009). Specifically, spatial control at length scales of both cellular focal contacts (micrometer scale) and individual proteins (nanometer scale) has been highly sought after as a way to produce surfaces with specific biological responses. A major challenge has been combining features with micron and nanometer dimensions onto one sample while maintaining a protein-resistant background that is stable for extended periods under experimental conditions. Sample production must also be high-throughput and low cost in order to be useful for examining biological questions.

Patterning of proteins onto surfaces in biologically-relevant spatial arrangements is an active area of investigation (Mossman et al., 2005). Traditional microcontact printing has been successful in producing micro-scale patterns for biological studies quickly and inexpensively (Chen et al., 1997), but faces limitations when approaching submicron resolution of patterns due to the diffraction limit of light and the instability of elastomer stamp materials. Scanning probe based techniques have made feature sizes of tens of nanometers accessible through a variety of methods for controlling protein placement, such as depositing or scraping off molecules using a cantilever (ie, dip-pen lithography) (Lim et al., 2003). While patterns approaching single proteins produced with this technique are desirable for a variety of applications, standard equipment is only capable of writing areas of 100 × 100 μm2 which impedes its use in biology studies where high-throughput is required to produce large numbers of samples. Colloidal lithography is useful for producing patterns of biologically relevant molecules with nanometer spacing over large areas. While diblock copolymers have provided control

over the nanoscale spacing between ligands for studies of cell adhesion (biophysical journal 07) and apopotosis (Ranzinger et al., 2009), the pattern geometries are limited to predetermined spacings by micelle chemistry. As well, achieving micrometer patterns with nanometer features requires lithographic processing one sample at a time which is time intensive.

In this work, we introduce a technique that produces multi-length scale patterns of proteins that are tethered to an activated surface and surrounded by a protein-resistant background. The subtractive patterning technique uses a reusable template and a flat elastomer to pattern and print proteins with resolution as high as several hundred nanometers. During printing, patterns of protein covalently tethered to surfaces consisting of mixed SAMs presenting COOH-functional groups within a protein adsorption-resistant background. The versatility of this technique is demonstrated by producing patterns of proteins with both micron and nanometer dimensions in various spatial arrangements. Patterns of the adhesive protein fibronectin are printed on a non-adhesive background to produce arrays of single cells where adhesion is constrained to the region of tethered protein. The applicability of the technique to biological studies is demonstrated by producing arrays of adherent cells on which focal adhesion size and spatial arrangement is modulated according to the geometry of the adhesive region.

Materials and Methods

Cells and Reagents

NIH3T3 fibroblasts (American Type Culture Collection, Manassas, VA) were cultured in DMEM (Invitrogen, Carlsbad, CA) supplemented with 10% newborn calf serum (NCS) (HyClone, Logan, UT) and 1% penicillin-streptomycin (Invitrogen, Carlsbad, CA). Cell culture reagents, including human plasma FN and Dulbecco's phosphate-buffered saline (DPBS), were purchased from Invitrogen (Carlsbad, CA).

Albumin from bovine serum (BSA) was purchased from Sigma-Aldrich (St. Louis, MO). Antibodies against vinculin (clone VIN-11-5, Sigma Aldrich), and human FN (anti-hFN polyclonal antibody, Sigma Aldrich) were used for immunostaining. Blocking antibody against human FN (HFN7.1) was acquired from the Developmental Studies Hybridoma Bank (University of Iowa, Iowa City, IA). AlexaFluor 488- and 555-conjugated secondary antibodies and Alexa Fluor 555 succinimidyl ester were purchased from Invitrogen (Carlsbad, CA). Cross-linker 3,3 dithiobis(sulfosuccinimidylpropionate) (DTSSP) was purchased from Pierce Chemical (Rockford, IL). Poly(dimethylsiloxane) (PDMS) elastomer and curing agent (Sylgard 184) were produced by Dow Corning (Midland, MI). ZEP520A was purchased from Zeon Chemicals (Tokyo, Japan). Amyl acetate was produced by Mallinckrodt Baker (Phillipsburg, NJ), and n-methyl pyrrolidinone (NMP, 1165 Remover) was obtained from MicroChem (Newton, MA). Tri(ethylene glycol)-terminated alkanethiol (HS-$(CH_2)_{11}$–$(OCH_2CH_2)_3$–OH; EG_3) and carboxylic acid-terminated alkanethiol (HS-$(CH_2)_{11}$–$(OCH_2CH_2)_6$–OCH_2–COOH; EG_6-COOH) were purchased from ProChimia Surfaces (Sopot, Poland). Peptide tethering reagents, N-hydroxysuccinimide (NHS) and N-(3-dimethylaminopropyl)-N'-ethylcarbodiimide hydrochloride (EDC) were obtained from Sigma-Aldrich (St. Louis, MO). 2-(N-morpho)-ethanesulfonic acid was purchased from Sigma-Aldrich (St. Louis, MO).

Monolayer Surface Preparation

Self-assembled monolayers (SAMs) of alkanethiols on gold were used to present anchoring groups for covalent immobilization of FN within a non-fouling background. Surfaces of mixed SAMs were prepared using tri(ethylene glycol)-terminated alkanethiol (HS-$(CH_2)_{11}$–$(OCH_2CH_2)_3$–OH; EG_3) and carboxylic acid-terminated alkanethiol (HS-$(CH_2)_{11}$–$(OCH_2CH_2)_6$–OCH_2–COOH; EG_6-COOH). Gold-coated substrates were prepared by sequential deposition of titanium (100 Å) and gold (200 Å) films via an

electron beam evaporator (Thermionics Laboratories, Hayward, CA, 2×10-6 Torr, 1 Å /s) onto clean 25 mm-diameter glass coverslips (Bellco Glass, Vineland, NJ). Mixed SAM surfaces were prepared on substrates by immersing in a mixed solution of EG_3 + EG_6-COOH thiols (100 parts EG_3 to one part EG_6-COOH, 1.0 mM final concentration in 200 proof ethanol) overnight in untreated polystyrene dishes with a nitrogen cap and sealed with parafilm. Several ratios of EG_3 to EG_6-COOH were tested to determine an optimal balance between providing enough sites for tethering protein during printing while maintaining a protein-resistant background. Following washing in ethanol for 15 min, twice in deionized water, and MES buffer (0.1M 2-(N-morpho)-ethanesulfonic acid and 0.5M NaCl in deionized water, pH 6.0)), mixed SAMs were incubated in activation buffer (200 mM EDC and 100 mM NHS in MES buffer) for 25 min. Substrates were rinsed twice with deionized water. Excess liquid was removed by applying a stream of N_2 for approximately 5 s. Following activation of the surface, subtractive contact printing (Coyer et al., 2007) was used to produce patterns of FN as described below.

Nanotemplate Fabrication

Subtractive contact printing was used to produce micron- and nanoscale patterns of FN. High-resolution nanotemplates were produced using electron-beam lithography. Silicon wafers (4”) were spin-coated with resist ZEP520A at 5000 RPM for 60s followed by a postbaking at 180 °C for 120 s. The ZEP resist was exposed in an JEOL JBX-9300FS Electron-Beam Lithography System, developed in amyl acetate for 120 s, immersed in isopropanol for 1 min, and blown dry under a stream of N_2. The ZEP pattern was transferred into the silicon substrate using an STS ICP Standard Oxide Etcher. The ZEP resist was removed by immersion in n-methyl pyrrolidinone (NMP, 1165 Remover) at 80 °C for 30 min, 1 min sonication in NMP, acetone and isopropanol wash, and blown dry under a stream of N_2.

Subtractive Contact Printing

PDMS planar elastomers were polymerized using Sylgard 184 prepolymers (Dow Corning, Midland, MI) at a ratio of 10:1 (base polymer:curing agent). PDMS was cured at 60 ºC overnight in untreated polystyrene dishes. Cured PDMS was cut into 30 × 30 mm^2 square flat stamps. The elastomers were cleaned by sonication in a 1:3 solution of isopropanol:deionized water for 5–10 min, rinsed using deionized water, rinsed using ethanol, and blown dry under a stream of N_2. Elastomers were pre-stamped on clean glass coverslips to remove unreacted PDMS. The side of the elastomer that was in contact with the polystyrene dish was inked with 800 μL of FN solution (100 μg/mL in PBS) for 30 min at room temperature. Elastomers inked with proteins were rinsed using PBS and deionized water. Excess liquid was removed by applying a stream of N_2 for approximately 30 s. Silicon substrates and nanotemplates were cleaned and treated in an oxygen plasma (Plasma Preen II-862, Plasmatic Systems Inc, North Brunswick, NJ) for 3 min. Proteins on homogenously inked elastomers were removed in selected areas by bringing the elastomers into contact with the nanotemplate for 15 s. The protein patterns were transferred from the elastomers to SAMs-coated 25 mm diameter glass coverslips using a 30 s printing step. Intimate contact between the elastomer and the nanotemplate/substrate was achieved after placing the elastomer on the nanotemplate/substrate by applying a slight pressure with tweezers. Non-adhesive areas were then blocked by incubating coverslips in 0.1% heat denatured BSA for 30 min. Finally, substrates were incubated for 2 h in DPBS to elute loosely adsorbed proteins.

Activity of Tethered FN

The biological activity of printed patterns of FN was evaluated using antibodies specific to FN binding domains. We previously demonstrated that the HFN7.1 monoclonal antibody specific for the integrin binding domain behaves as a receptor-mimetic antibody and its binding to immobilized fibronectin is predictive of cell adhesion

activity (Keselowsky et al., 2003). Substrates prepared by subtractive contact printing were treated with either HFN7.1 (1:100) or polyclonal human FN antibody (anti-hFN; 1:200) diluted in blocking buffer for 1 hour at 37°C. Primary antibodies were visualized using AlexaFluor 488- and 555- conjugated secondary antibodies (anti-rabbit IgG, anti-mouse IgG; 1:200) diluted in blocking buffer for 1 hour at 37°C. Images were captured using a Nikon Eclipse E400 fluorescence microscope and ImagePro Plus image acquisition software.

Cell Seeding and Focal Adhesion Staining

FN conjugated to Alexa Fluor 555 fluorphore was used to visualize patterns of printed protein. In order to leave free primary amines on FN for tethering to mixed SAMS, a ratio of 25:1 w/w of FN to amine-reactive Alexa Fluor 555 succinimidyl ester was used in the reaction. Cells were seeded on patterned substrates at 235 cells/ mm^2 in DMEM supplemented with 10% newborn calf serum (NCS). For visualization of focal adhesions, cells were extracted in cytoskeleton buffer (0.5% Triton X-100 in 50 mM NaCl, 150 mM sucrose, 3 mM $MgCl_2$, 20 g/ml aprotinin, 1 g/ml leupeptin, 1 mM PMSF, 50 mM Tris, pH 6) for 10 min to remove membrane and soluble cytoskeletal components. Extracted cells were fixed in cold formaldehyde (3.7% in DPBS) for 5 min, blocked in blocking buffer (5% goat serum in DPBS) for 1 hour, and incubated with primary antibody (anti-vinculin 1:125 dilution) diluted in blocking buffer for 1 hour at 37°C. Primary antibodies were visualized using AlexaFluor 488-conjugated secondary antibodies (anti-rabbit IgG 1:200 dilution) diluted in blocking buffer for 1 hour at 37°C. Images were captured using a Nikon Eclipse E400 fluorescence microscope and ImagePro Plus image acquisition software.

Results

Tethering Patterns of Proteins by Printing onto Activated Surfaces

Patterns of proteins were directly immobilized by covalent tethering onto surfaces presenting mixed SAMs of alkanethiols using a modified version of contact printing . Details of the method are shown in Fig 4.1. Gold-coated substrates were incubated overnight in a mixed solution of alkanethiols terminated with either tri(ethylene glycol) (EG_3) or carboxylic acid (EG_6-COOH) (Fig 4.1A). Before printing, active *N*-hydroxysuccinimidyl (NHS) esters were generated from the carboxylic acid groups of the EG_6-COOH alkanethiol by NHS/EDC chemistry. Next, a protein pattern is produced on an elastomer by first adsorbing a uniform layer of protein from solution and then completing a contact and release step to a template (Fig 4.1B). The resulting pattern on the elastomer mirrors the recessed pattern on the template. To transfer the protein pattern to the final substrate, a contact and release step is completed between the elastomer and the substrate (Fig 4.1C). Active NHS esters on the surface couple to amine groups on the protein. All steps from activation through printing were completed in less than 45 minutes to avoid incomplete immobilization due to inactivation of the NHS esters. After printing, a protein-resistant background was produced by incubating substrates in bovine serum albumin (BSA) which binds unreacted NHS-esters.

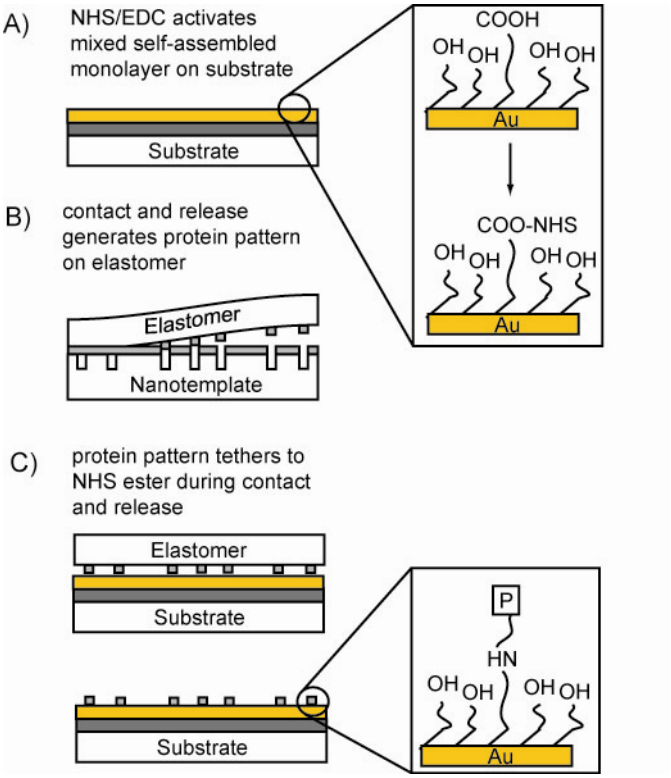

Figure 4.1. Printing strategy for direct covalent immobilization of protein patterns to mixed SAMs.

Biological Activity of Patterned Proteins

Patterns of the cell adhesion protein fibronectin were produced to demonstrate the ability of the technique to immobilize proteins in controlled geometries while maintaining protein activity. Arrays of circular regions (20 μm in diameter) with a repeat spacing of 75μm (Fig 4.2) were patterned using a template produced using photolithography. A complete array was printed across a 25 mm diameter coverslip in one stamping step using a 30 × 30 mm^2 elastomer and equivalent template area.

Activity of the tethered FN was verified using the FN-specific HFN7.1 monoclonal antibody that is receptor-mimetic. Immunofluorescence images show an array of circular regions matching the FN pattern. This result indicates that protein is not denatured during printing and tethering and that the central integrin receptor-binding domain of FN is active in the final configuration. Uniform FN distribution is demonstrated by low variation in the signal intensity across the entire array as well as within circles. A fragment of FN (10× smaller than full-length FN) was also printed and tethered to mixed SAMs showing that various protein sizes are supported by this technique. The background region between circle regions remained devoid of antibody indicating that high contrast patterns are produced by the patterning technique and that the non-fouling background effectively resists protein adsorption. Taken together, these results verify that protein activity is maintained during patterning and immobilization and that the non-patterned areas are resistant to protein adsorption.

Multi-scale Patterns with Nanoscale Features

Complex patterns of proteins with spacing and sizes varying across multiple length scales are desirable for studies of biological processes whose functionality requires coordination across the same scales. In order to demonstrate these capabilities, patterns of proteins were produced in which the pattern geometry includes feature dimensions at both micro- and nanometer length scales. Templates consisting of micron- and nano-scale

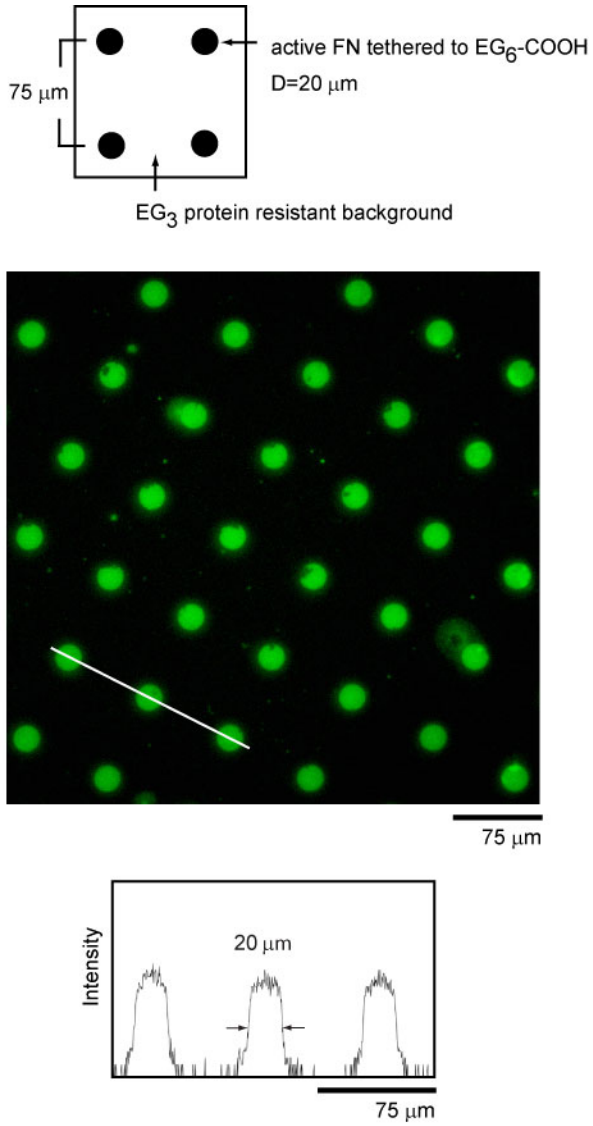

Figure 4.2.Micron patterns of FN remain active during printing as demonstrated by binding of a receptor mimetic antibody.

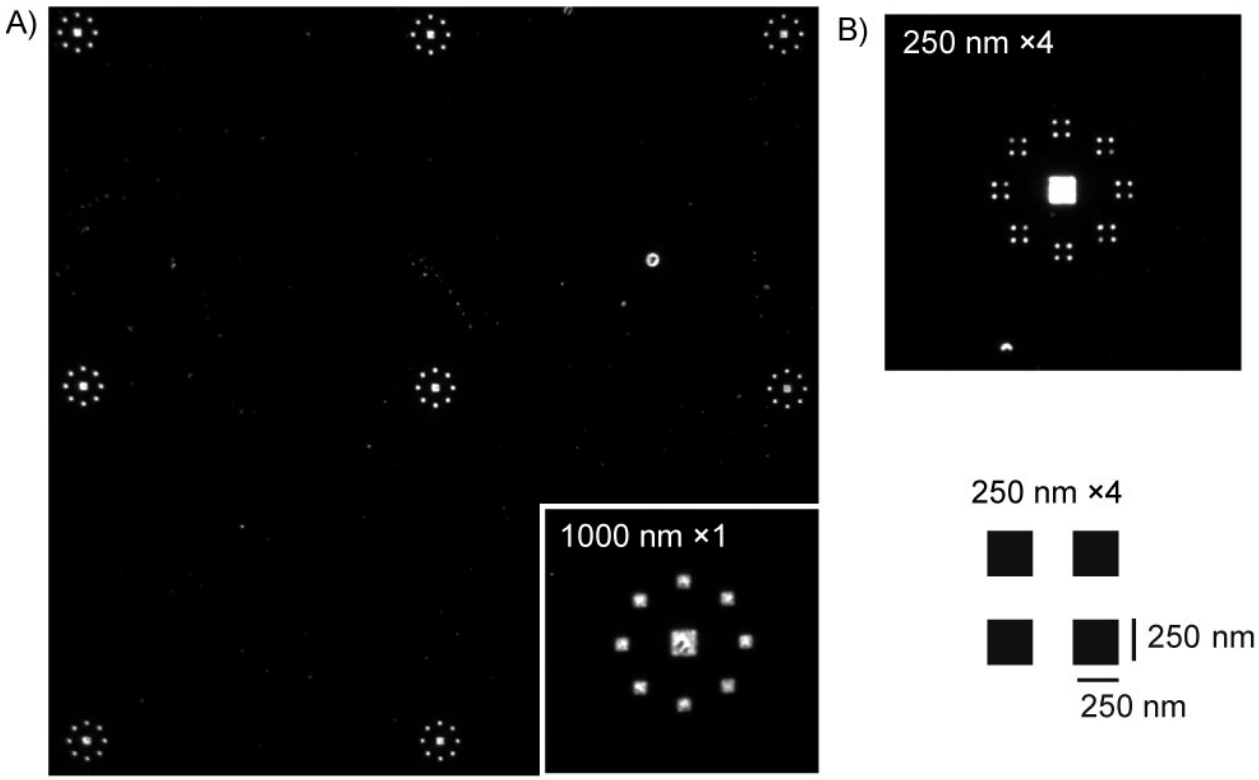

Figure 4.3. Micro- and nano-scale patterns with various geometries are produced with high contrast.

features were fabricated using e-beam lithography. FN patterns printed to mixed-SAM substrates were treated with FN-specific polyclonal antibodies and fluorescent secondary antibodies in order to visualize by immunofluorescence. Features measuring as small as several hundred nanometers were simultaneously patterned and printed with micron feature sizes of $2 \times 2\ \mu m^2$ (center square) (Fig 4.3C). Spacing ranging from 100 μm between patterns (Fig 4.3A) to several hundred nanometers between individual features in a cluster of four (Fig 4.3C) was achieved. High-contrast patterns and features with uniform dimensions and protein staining were maintained across all size scales.

Controlled Cell Adhesion on Mixed-SAMs

Covalent immobilization of proteins and a protein-resistant background of alkanethiols were used to ensure robust arrays of protein that could maintain a controlled adhesive interface during extended periods of cell culture. We verified that proteins were tethered to the carboxylic acid-terminated alkanethiol and that the mixed-SAM background would resist cell adhesion by plating cells on substrates with various alkanethiol treatments. Several surface conditions were evaluated to confirm that fibronectin was immobilized via NHS/EDC activation of the carboxylic acid-terminated alkanethiol (Table 4.1). NIH3T3 cells were plated on mixed-SAM substrates (EG_3+ EG_6-COOH) after activating and printing a uniform FN layer (non-patterned) (Fig 4.4A). Confluent populations of spread cells displayed the typical fibroblastic morphology. Cell adhesion was not supported when mixed-SAM substrates were not activated with NHS/EDC (Fig 4.4B), indicating that without active NHS-esters protein is not tethered to the substrate during printing. Similarly, activated mixed-SAMs surfaces did not support cell adhesion when FN was not printed (Fig 4.4C). These results confirm that mixed-SAMs are protein-resistant and non-adhesive after quenching unreacted NHS ester-groups with BSA. Surfaces coated with EG_3 alone and printed with FN (Fig 4.4D) exhibited background levels of cell adhesion to the same extent as control surfaces with

Table 4.1. Conditions tested to verify cell adhesion to SAM surfaces through immobilized FN.

SAM	EG_6-COOH:EG_3	NHS/EDC	Printed FN	Cell Morphology	Figure
EG_3 + EG_6-COOH	1:100	+	+	spread, fibroblastic	4.4A
EG_3 + EG_6-COOH	1:100	-	+	no spreading, limited balling up	4.4B
EG_3 + EG_6-COOH	1:100	+	-	no spreading	4.4C
EG_3	NA	NA	+	no adhesion	4.4D
EG_3	NA	NA	-	no adhesion	4.4E

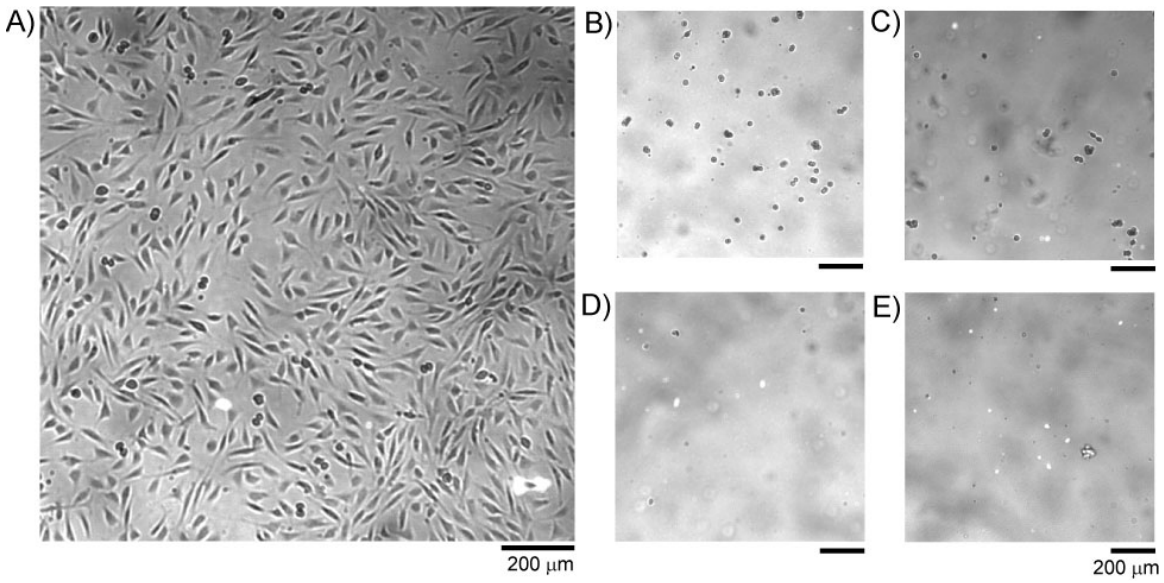

Figure 4.4. Cell adhesion supported by FN (non-patterned) printed to activated surface of mixed SAM.

EG_3 and no FN printing (Fig 4.4E). These results confirm that immobilization of protein is prevented, either from printing or from solution, on EG_3 SAMs. These results confirm that protein tethering occurs through carboxylic acid-terminated alkanethiols that have been activated by NHS/EDC chemistry. Further, the non-adhesive character of mixed SAMs including >95% tri(ethylene glycol)-terminated alkanethiols is maintained during printing and is able to resist deposition of protein from solution and/or cells. Taken together, these results demonstrate that printing to mixed-SAMs is applicable to cell studies that require the ability to support or prevent cell adhesion.

Controlled Spatial Arrangement of Focal Adhesions

Our patterning technique was also shown to be a useful approach to controlling cellular processes by using FN patterns to control the formation of focal adhesions in adherent cells. Focal adhesions are integrin-mediated adhesive junctions between cells and extracellular matrix components whose structural and signaling roles are critical in various functionalities including generation of adhesion strength (Geiger et al., 2009; Zamir and Geiger, 2001). Vinculin is a structural component of focal adhesions that has been highly studied as a central regulator of cell adhesion strength (Chen et al., 2005; Galbraith et al., 2002; Gallant et al., 2005). Using standard immunofluorescence techniques, we visualized the localization of vinculin in response to patterns of FN. Vinculin staining of cells spread on non-patterned FN shows areas of high intensity at sites of vinculin localization (Fig 4.5A), indicating the formation of elongated focal adhesions that are typical of spread cells. Patterns of FN were then used to limit vinculin localization and focal adhesion formation to defined regions. Circular patterns (10 μm diameter) of FN supported adhesion of one cell per island (Fig 4.5B). Vinculin localized to focal adhesion structures that were constrained to the adhesive region. Intense signal at the edge of the patterns shows preferential localization to the edge of the circle. As well, punctate and elongated complexes are visible throughout the interior region. These results

are in agreement with previous work that demonstrated comparable focal adhesion formation on surfaces produced by micropatterning alkanethiols and coated with adsorbed FN (Gallant et al., 2005). In order to control focal adhesion formation, patterns were designed with spatial arrangement of the adhesive region. Patterns with dimensions of 1×1 μm^2 were arrayed around an outside diameter of 10 μm that limits adhesion to one cell per island (Fig 4.5B). Vinculin staining shows preferentially localization of focal adhesions to the eight regions at the edge of the pattern. These results demonstrate that focal adhesion formation can be controlled with high precision by modulating the geometry of the adhesive region.

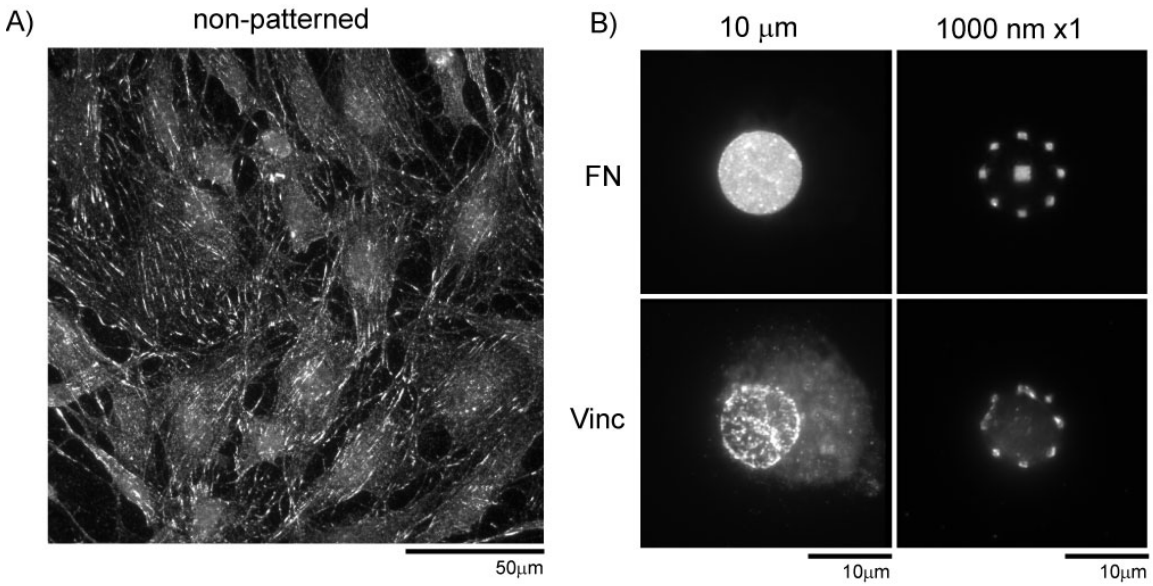

Figure 4.5. Focal adhesion (vinculin) formation on FN patterns.

Discussion

We present a facile and cost-effective printing strategy for surface modification that directly immobilizes high-resolution patterns of proteins by covalent tethering to surfaces. A variation of contact printing is used to simply and efficiently achieve pattern dimensions ranging from micro- to nano-scale. Tethering directly from a stamp to a mixed self-assembled monolayer provides an easy approach to producing patterns of covalently immobilized proteins surrounded by protein-resistant background. The high-throughput and multi-length scale characteristics of this technique make it readily-accessible to researchers across a variety of fields including studies of basic biology and biotechnological applications.

Control over the composition and organization of patterns of proteins is critical when designing responses in biotechnology application and systematically analyzing biological systems. In this method, the subtractive patterning technique extends the flexibility of contact printing methods to provide the user with control over various spatial parameters with high-resolution and fidelity. Complex patterns can be produced in which feature dimensions spanning multiple length scales from microns to hundreds of nanometers are combined in the same pattern. Various geometries were easily produced including squares, circles, and arrays with well-defined spatial arrangements. E-beam lithography was used in this study for template fabrication, but any method that can make nanostructured templates can be used such as nanoimprint techniques or colloidal lithography. The use of flat elastomers for printing makes possible large spacing between features that is not limited by stamp stability. By using subtraction of proteins from the elastomer to create patterns, high-resolution features can be produced. Previous work has used the subtractive patterning technique to produce sub-100 nm pattern sizes (Coyer et al., 2007) while similar techniques have achieved arrays of single molecules (Bernard et al., 2001). Further, the subtractive patterning technique can be used to pattern multiple

proteins simultaneously with intrinsic self-alignment (Coyer et al., 2007). Backfilling with a biologically-relevant protein or completing repeat inking and subtraction steps produces surfaces with controlled organization of multiple proteins that can be used to direct protein-protein interactions or generate complex chemical signals that mimic in vivo environments.

The activity and organization of immobilized proteins is an important characteristic of engineered bioactive surfaces. In this work, protein activity was verified using antibody binding and cell adhesion experiments. The activity of the central integrin receptor-binding region of fibronectin was maintained through all steps of the process thereby demonstrating that the protein was not denatured during the printing process and that the tethered protein is in a conformation/orientation that supports cell adhesion. The density of tethered protein is affected by two criteria: 1) adsorption of a monolayer of protein to the elastomer from solution, and 2) transfer efficienty of the protein layer to the final substrate. Proteins adsorb onto the hydrophobic elastomers in monolayers and transfer at a very high efficiency from the elastomer to more hydrophobic surfaces (Tan et al., 2002). This suggests that over a certain threshold changes to the protein concentration of the inking solution will not produce changes to the final tethered density. Under that threshold, protein adsorption to the stamp is determined by the concentration of inking solution and the time of inking and may not reach a steady-state condition. Varying the ratio of carboxylic-terminated alkanethiols changes the number of NHS-esters available for coupling to amines on proteins, presumably modifying the density of tethered proteins on the surface. Since most proteins meet the requirements of the subtractive patterning technique and have primary amines available for tethering, this strategy is expected to be applicable to a variety of proteins given proper alkanethiol ratios and inking concentrations. Examples include fragments of molecules such as fibronectin and antibodies both of which have been patterned using the subtractive technique. Combined, these characteristics make the combination of printing and

tethering to mixed-SAMs a powerful technique in which bioactive surfaces can be produced with characteristics that are tailored to a wide variety of applications.

One such application is biological systems where control over cellular environments is desirable for medical applications and fundamental science studies. This technique is relevant to biological studies since it provides a robust non-adhesive background, maintains protein activity, and is high-throughput. Non-fouling backgrounds resisted protein adsorption from solution and from deposition by cells over extended culture periods. High-throughput sample production is made possible by patterning and printing steps that take less than 30 seconds each and use of a template that is reusable after plasma-etching. The applicability of this technique to studies of cellular processes was demonstrated by controlling formation of focal adhesions in adherent cells using printed patterns of the adhesion protein fibronectin. Focal adhesions are known to be critical in cell functions including adhesion, proliferation, and migration (Geiger et al., 2009). By controlling the spatial arrangement and size of focal adhesions, specific cellular responses may be achieved. In these experiments, cells seeded on surfaces of non-patterned tethered FN took on a spread fibroblastic morphology and formed focal adhesions typical of cells on culture dishes. Using FN patterns on a protein-resistant background, the adhesive region for individual cells was constrained. Focal adhesion formation in response to patterned surfaces was visualized by immunofluorescence staining for the structural component vinculin. Using this approach, we achieved control over the spatial arrangement and size of focal adhesions by modulating the organization of the adhesive regions. By modifying the size and spacing of FN regions in a circular array, the size of focal adhesions was limited and the spacing between individual focal adhesions was defined. These results demonstrate the unique capabilities for studies of biological form and function that are achieved with the subtractive patterning technique. By controlling the various parameters that define the spatial arrangement of the adhesive interface, the individual effect of each parameter on functional outcomes can be

elucidated. Cell arrays consisting of patterns with dimensions at both micro- and nanometer length scales would be useful in studies of cell adhesion and tissue remodeling. In addition, by using the multi-protein capabilities of the subtractive patterning technique, this strategy can be used to study cell functionality that results from coordinated responses to multiple proteins such as neuron signaling or differentiation.

Conclusion

This work introduces a strategy for direct tethering of patterns of proteins with micro- and nanometer resolution to surfaces coated with mixed-SAMs of alkanethiols. Printing proteins to activated surfaces of mixed-SAMs provides a straightforward approach for covalently immobilizing proteins in user-defined patterns. Various pattern geometries are produced that combine dimensions at both micro- and nanometer length scales. Using the subtractive patterning technique, pattern sizes of several hundred nanometers are produced across large patterned areas with high contrast and high uniformity. Protein activity is maintained during tethering to carboxylic acid-terminated alkanethiols mixed-SAMS by coupling of amines to NHS-esters. Arrays of cells are produced by constraining adhesion by patterning the adhesion protein fibronectin in a non-adhesive background. Applicability to biological studies is demonstrated by controlling focal adhesion formation of adherent cells by varying the geometry of FN patterns. This technique provides a flexible and easy method for producing patterns of proteins in which the size and spatial arrangement of features can be tuned to the needs of applications in microfluidics, biomaterial functionalization, and fundamental biology studies.

CHAPTER 5

NANOSCALE GEOMETRY OF THE ADHESIVE INTERFACE MODULATES INTEGRIN RECRUITMENT AND CELL ADHESION

Summary

Cell adhesion to extracellular matrices (ECM) is critical to many cellular processes including differentiation, proliferation, migration, and apoptosis. Although significant progress has been made in identifying molecules involved in adhesion, the mechanisms that regulate the generation of strong adhesive forces remain poorly understood. Specifically, the role of nanoscale geometry of the adhesive interface in integrin recruitment and adhesion forces remains elusive due to limitations in the techniques available for engineering cell adhesion environments. Using a novel experimental approach, we determined the role of nanoscale geometry (adhesion area, spacing, and clustering) in the recruitment of integrins into clusters and the functional implications to adhesion strength. Results showed that the area over which integrin recruitment occurred and the quantity of bound integrin varied with pattern geometry according to the adhesion area size and location. Below a threshold adhesion area, the frequency of integrin recruitment events decreased significantly. Adhesion strength was shown to vary with area of individual adhesion points but not with total adhesion area. A relationship between adhesion strength and integrin recruitment was established in which variations in adhesion strength correlated with the level of adhesion area occupancy. Below the threshold area, nanoscale patterns were unable to participate in generation of strong adhesive forces. These results provide new insights on the role of nanoscale geometry of the adhesive interface in modulating adhesive forces and integrin recruitment.

Introduction

Cell adhesion to the extracellular matrix provides spatial and chemical cues that determine cell functionality and fate. Integrin-mediated cell-ECM adhesion is central to cell survival, migration, differentiation, and proliferation (Danen and Sonnenberg, 2003; De Arcangelis and Georges-Labouesse, 2000). Adhesions between cells and the extracellular matrix ligands are responsible for providing mechanical and biochemical signals that drive cell function. Sensing of complex geometries through adhesive structures produces biochemical and mechanical signals in cells that are transmitted through focal adhesions and cytoskeletal networks to produce functional responses such as differentiation (Geiger et al., 2009; Vogel and Sheetz, 2006). While significant contributions have been made determining the components involved in adhesive contacts and signaling interactions, the roles of nanoscale spatial geometry in cell adhesion, mechanosensing, and mechanotransduction are still being uncovered.

Adhesion is a multi-step process in which integrin receptors bind to extracellular matrix ligands followed by clustering of integrins which triggers recruitment of signaling and structural proteins to form focal adhesions. Integrins are extracellular receptors on the cell surface that bind to the extracellular matrix protein fibronectin (FN) and promote a variety of cell processes including adhesion and migration (Hynes, 2002). Bound receptors rapidly associate with the actin cytoskeleton and cluster together to form focal adhesions, discrete supramolecular complexes that contain structural and signaling proteins such as vinculin, talin, tensin, FAK, and paxilin (Geiger et al., 2001). The organization of adhesion ligands regulates adhesive responses. A spacing between ligands of the adhesive domain RGD of 440 nm was required for cell spreading and 140 nm for focal adhesion assembly (Massia and Hubbell, 1991). Spatz and coworkers used block co-polymer micelle lithography to show that integrin spacing below 73 nm is required for mature integrin adhesion, cell spreading, and focal adhesion assembly (Arnold et al., 2004; Cavalcanti-adam et al., 2007). Recently, initial integrin binding was

shown to require a spacing of 40 nm between FN molecules (Roca-Cusachs et al., 2009). These results indicate the importance of spatial distribution of adhesion ligands in adhesion functions. Focal contact formations ranging in size are well established in migrating cells where leading edges have highly dynamic binding events (Giannone et al., 2007; Ponti et al., 2004). The highly variable nature of focal adhesion geometry generates balance in migrating cells between adhesion and contraction (Gupton and Waterman-Storer, 2006). Distinct focal adhesions exist at the leading edge compared to the trailing end of migrating cells thereby producing mechanical characteristics that match the adhesion requirements at each location (Munevar et al., 2001). The range of sizes of focal contacts appears to be a critical parameter that differentiates the functionality of these structures.

McClay and Erickson proposed the widely accepted model for adhesion strength in which a two-step process occurs consisting of initial integrin-ligand binding followed by rapid strengthening (Lotz et al., 1989). Adhesion strengthening comes from (i) increases in the cell-substrate contact area (spreading), (ii) recruitment of receptors to anchoring sites (integrin clustering), and (iii) interactions with cytoskeletal elements that combine to make adhesive structures that enhance force distribution by stiffening of the local membrane (focal adhesion assembly). Subsequent studies using various experimental approaches support roles for these mechanisms in adhesion strengthening. Strengthening of integrin-cytoskeleton linkages was shown to occur in response to a force applied using fibronectin-coated beads and an optical trap (Choquet et al., 1997). Atomic force microscopy measurements demonstrated that integrin-ligand bond lifetimes are prolonged by application of force in a behavior called catch bonds (Kong et al., 2009). Analyses with elastic substrates demonstrated that focal adhesions act as strong anchorage points to the ECM and are involved in generation of forces in migrating cells (Balaban et al., 2001; Beningo et al., 2001; Tan et al., 2003). Micropatterned surfaces of FN were used in combination with the spinning disk assay to demonstrate that adhesive

area strongly modulates integrin binding and focal adhesion assembly (Gallant et al., 2005). A relationship was established between increases in adhesion strength and available area. Adhesion strengthening results found that focal adhesion assembly only contributes 20-30% of adhesion strength at steady state. These studies provide an understanding of the molecular events involved in adhesive forces as well as the role of micrometer adhesion area in adhesion strengthening. However, the contribution of submicron adhesion areas to modulation of adhesion strength through integrin recruitment and focal adhesion assembly has not been elucidated. For example, the area required for sufficient recruitment of integrins into clusters and focal adhesion formation to support strengthening of adhesive bonds has not been determined. Furthermore, the implications of quantity and positioning of integrin clusters and focal adhesions to adhesion strength has not been assessed. This information is needed to generate a complete understanding of the regulation of mechanical interactions between the cell and the ECM.

We investigated the role of nanoscale size, spacing, and clustering in recruitment and clustering of integrins and generation of adhesion strength by systematically varying the geometry of the adhesive interface. We elucidated the roles of total adhesion area, number of adhesion sites, and island size in the recruitment and clustering of bound integrins. A minimum adhesion area was determined below which the frequency of integrin recruitment to nanoscale adhesion regions drops significantly. The importance of these nanoscale criteria on cell functionality was demonstrated by determining the role of each characteristic in the generation of adhesion strength. Adhesion force was determined to be highly dependent on the size of individual adhesion sites independent of the total adhesion area. Below the threshold size established from integrin recruitment analyses, nanoscale adhesion areas did not significantly contribute to adhesion strength. A relationship between adhesion strength and integrin recruitment was established in which

the number of adhesion regions with bound integrin plays a dominant role over the level of integrin clustering.

Materials and Methods

Cells and Reagents

NIH3T3 fibroblasts (American Type Culture Collection, Manassas, VA) were cultured in DMEM (Invitrogen, Carlsbad, CA) supplemented with 10% newborn calf serum (NCS) (HyClone, Logan, UT) and 1% penicillin-streptomycin (Invitrogen, Carlsbad, CA). Cell culture reagents, including human plasma FN and Dulbecco's phosphate-buffered saline (PBS), were purchased from Invitrogen (Carlsbad, CA). Albumin from bovine serum (BSA) was purchased from Sigma-Aldrich (St. Louis, MO). Antibodies against α5 integrin (ab1921, Millipore, Billerica, MA), and human FN (anti-hFN polyclonal antibody, Sigma Aldrich) were used for immunostaining. AlexaFluor 488- and 555-conjugated secondary antibodies and Alexa Fluor 555 succinimidyl ester were purchased from Invitrogen (Carlsbad, CA). Cross-linker 3,3 dithiobis(sulfosuccinimidylpropionate) (DTSSP) was purchased from Pierce Chemical (Rockford, IL). Poly(dimethylsiloxane) (PDMS) elastomer and curing agent (Sylgard 184) were produced by Dow Corning (Midland, MI). ZEP520A was purchased from Zeon Chemicals (Tokyo, Japan). Amyl acetate was produced by Mallinckrodt Baker (Phillipsburg, NJ), and n-methyl pyrrolidinone (NMP, 1165 Remover) was obtained from MicroChem (Newton, MA). Tri(ethylene glycol)-terminated alkanethiol ($HS\text{-}(CH_2)_{11}\text{–}(OCH_2CH_2)_3\text{–}OH$; EG_3) and carboxylic acid-terminated alkanethiol ($HS\text{-}(CH_2)_{11}\text{–}(OCH_2CH_2)_6\text{–}OCH_2\text{–}COOH$; EG_6-COOH) were purchased from ProChimia Surfaces (Sopot, Poland). Peptide tethering reagents, N-hydroxysuccinimide (NHS) and N-(3-dimethylaminopropyl)-N'-ethylcarbodiimide hydrochloride (EDC) were obtained from

Sigma-Aldrich (St. Louis, MO). 2-(N-morpho)-ethanesulfonic acid was purchased from Sigma-Aldrich (St. Louis, MO).

Monolayer Surface Preparation

Self-assembled monolayers (SAMs) of alkanethiols on gold were used to present anchoring groups for covalent immobilization of FN within a non-fouling background. Surfaces of mixed SAMs were prepared using tri(ethylene glycol)-terminated alkanethiol (EG_3) and carboxylic acid-terminated alkanethiol (EG_6-COOH). Gold-coated substrates were prepared by sequential deposition of titanium (100 Å) and gold (200 Å) films via an electron beam evaporator (Thermionics Laboratories, Hayward, CA, 2×10-6 Torr, 1 Å /s) onto clean 25 mm-diameter glass coverslips (Bellco Glass, Vineland, NJ). Mixed SAM surfaces were prepared on substrates by immersing in a mixed solution of EG_3/EG_6-COOH thiols (100 parts EG_3 to one part EG_6-COOH, 1.0 mM final concentration in 200 proof ethanol) overnight in untreated polystyrene dishes with a nitrogen cap and sealed with parafilm. Following washing in ethanol for 15 min, twice in deionized water, and MES buffer (0.1M 2-(N-morpho)-ethanesulfonic acid and 0.5M NaCl in deionized water, pH 6.0)), mixed SAMs were incubated in activation buffer (200 mM EDC and 100 mM NHS in MES buffer) for 25 min. Substrates were rinsed twice with deionized water. Excess liquid was removed by applying a stream of N_2 for approximately 5 s. Following activation of the surface, subtractive contact printing (Coyer et al., 2007) was used to produce patterns of FN as described below.

Nanotemplate Fabrication and Subtractive Contact Printing

Subtractive contact printing was used to produce micron- and nanoscale patterns of FN. High-resolution nanotemplates were produced using electron-beam lithography. Silicon wafers (4”) were spin-coated with resist ZEP520A at 5000 RPM for 60s followed by a postbaking at 180 °C for 120 s. The ZEP resist was exposed in a JEOL JBX-9300FS

Electron-Beam Lithography System, developed in amyl acetate for 120 s, immersed in isopropanol for 1 min, and blown dry under a stream of N_2. The ZEP pattern was transferred into the silicon substrate using an STS ICP Standard Oxide Etcher. The ZEP resist was removed by immersion in n-methyl pyrrolidinone (NMP, 1165 Remover) at 80 °C for 30 min, 1 min sonication in NMP, acetone and isopropanol wash, and blown dry under a stream of N_2.

PDMS planar elastomers were polymerized using Sylgard 184 prepolymers (Dow Corning, Midland, MI) at a ratio of 10:1 (base polymer:curing agent). PDMS was cured at 60 ºC overnight in untreated polystyrene dishes. Cured PDMS was cut into 30 × 30 mm^2 square flat stamps. The elastomers were cleaned by sonication in a 1:3 solution of isopropanol:deionized water for 5–10 min, rinsed using deionized water, rinsed using ethanol, and blown dry under a stream of N_2. Elastomers were pre-stamped on clean glass coverslips to remove unreacted PDMS. The side of the elastomer that was in contact with the polystyrene dish was inked with 800 μL of FN solution (100 μg/mL in PBS) for 30 min at room temperature. Elastomers inked with proteins were rinsed using PBS and deionized water. Excess liquid was removed by applying a stream of N_2 for approximately 30 s. Silicon substrates and nanotemplates were cleaned and treated in an oxygen plasma (Plasma Preen II-862, Plasmatic Systems Inc, North Brunswick, NJ) for 3 min. Proteins on homogenously inked elastomers were removed in selected areas by bringing the elastomers into contact with the nanotemplate for 15 s. The protein patterns were transferred from the elastomers to SAMs-coated 25 mm diameter glass coverslips using a 30 s printing step. Intimate contact between the elastomer and the nanotemplate/substrate was achieved after placing the elastomer on the nanotemplate/substrate by applying a slight pressure with tweezers. Non-adhesive areas were then blocked by incubating coverslips in 0.1% heat denatured BSA for 30 min. Finally, substrates were incubated for 2 h in PBS to elute loosely adsorbed proteins.

Cell Seeding and Integrin Cross-linking

FN conjugated to Alexa Fluor 555 was used to visualize patterns of printed protein. In order to leave free primary amines on FN for tethering to mixed SAMS, a ratio of 25:1 w/w of FN to amine-reactive Alexa Fluor 555 succinimidyl ester was used in the reaction. Cells were seeded on patterned substrates at 235 cells/ mm^2 in DMEM supplemented with 10% newborn calf serum (NCS).

Bound integrins were visualized using a cross-linking and extraction method (Garcia 1999, Keselowsky Garcia 2005). Cells patterned on substrates were incubated in DTSSP (1.0 mM) for 30 min to cross-link integrins to their bound ligand. DTSSP was then quenched using 50 mM Tris followed by extraction of uncross-linked components of the cell with 0.1% SDS supplemented with protease inhibitors (16.7 μg/ml phenylmethylsulfonyl fluoride (PMSF), 10 μg/ml leupeptin, 10 μg/ml aprotinin). After extraction, samples were fixed in cold paraformaldehyde (3.7% in DPBS) for 5 min, blocked in blocking buffer (5% goat serum in PBS) for 30 min, and incubated with primary antibody (anti-α5 integrin, 5 μg/ml) diluted in blocking buffer for 1 hour at 37°C. Primary antibodies were visualized using AlexaFluor 488-conjugated secondary antibodies (anti-rabbit IgG, 10 μg/ml) diluted in blocking buffer for 1 hour at 37°C. Images were captured using a Nikon Eclipse E400 fluorescence microscope and ImagePro Plus image acquisition software. Heat map images were produced by averaging individual images for a given condition using ImagePro Plus.

Statistics

Results were analyzed using one-way ANOVA and Tukey's post-hoc test for pairwise comparisons. Statistical comparisons for pad occupancy were completed using Kruskal-Wallis nonparametric tests followed by pairwise comparisons adjusted by multiplying the p-value by the number of comparisons. All statistical analysis was completed using SYSTAT 11.0.

Results

Cell Adhesion Arrays on Patterns of FN with Nanoscale Geometry

Patterns of FN consisting of features with a range of nanoscale geometries were produced using a modified version of contact printing to directly immobilize proteins by covalent tethering onto surfaces presenting mixed SAMs of alkanethiols. Details of the method have previously been reported (Coyer et al., 2007). Briefly, gold-coated 25-mm diameter glass substrates were coated with a mixed self-assembled monolayer of alkanethiols terminated with either tri(ethylene glycol) (EG_3) or carboxylic acid (EG_6-COOH). The subtractive patterning technique (Coyer et al., 2007) was used to pattern FN into features with dimensions ranging from 2 μm to several hundred nanometers. Upon printing to the substrate, FN was tethered to EG_6-COOH terminated alkanethiols that were activated to NHS esters. Patterns were surrounded by a protein-resistant background consisting of EG_3-terminated alkanethiols and quenched EG_6-COOH terminated alkanethiols. Cells seeded on the arrays are limited to one cell per pattern and adhesion was constrained to the adhesion region presented by the protein pattern (Fig 5.1B). Spreading in between the patterns is prevented by the non-fouling background. Patterns consist of a center pad (2×2 μm^2) surrounded by an evenly-spaced array of eight adhesion pads at a diameter of 10 μm (Fig 5.1C). This pattern design was implemented after initial patterns of a single pad did not support cell adhesion. This configuration provides sufficient total area to support adhesion while maintaining nanoscale adhesion features. Two pad orientations are present in each pattern, one with the pad edge aligned at 90° to the center of the pattern, the other rotated 45°. The adhesion pads are made up of one, two, four, or nine adhesion islands. The designed edge length of the islands ranges from 1000 nm to 250 nm.

Patterned substrates were shown to maintain the original pattern dimensions and resist FN deposition from cells (Fig 5.2). FN labeled with a fluorophore (FN 555) was

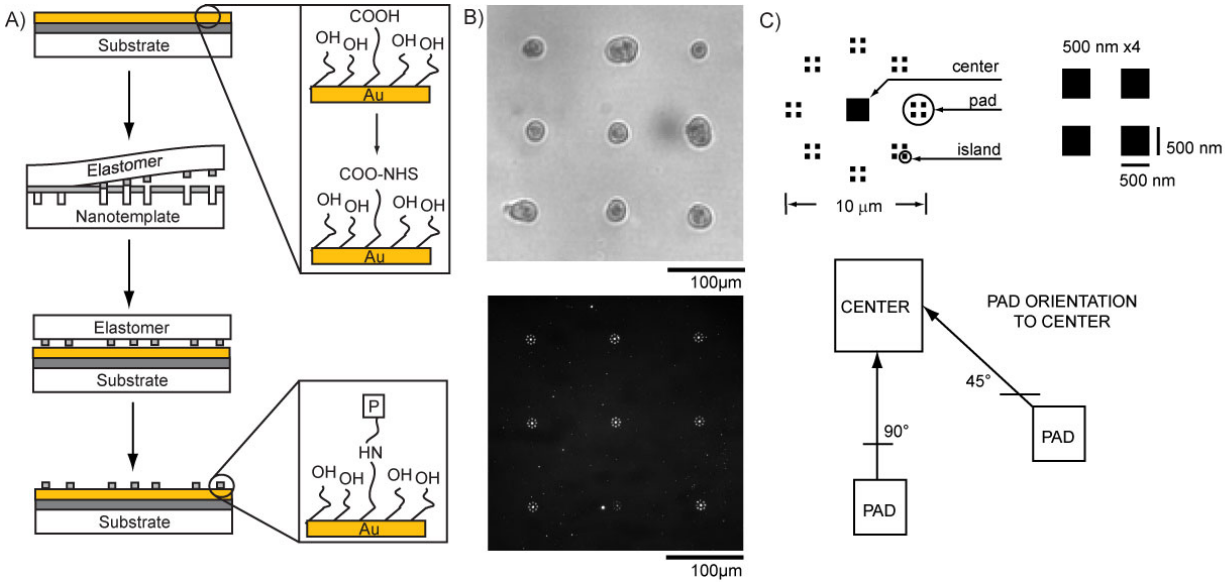

Figure 5.1. Immobilization of the adhesion protein fibronectin into nanoscale patterns with defined geometry produces single-cell adhesion arrays.

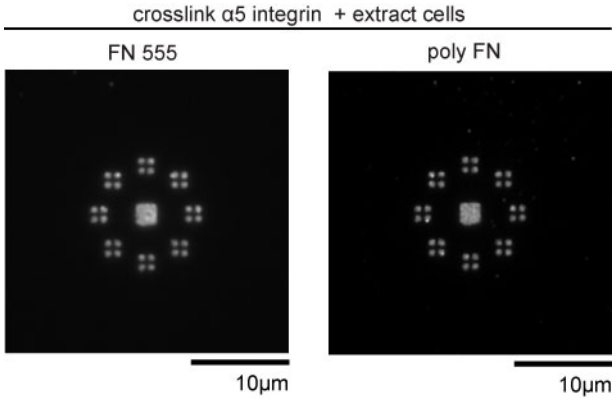

Figure 5.2. FN is constrained to patterned regions and background resists protein deposition from cells.

used to visualize printed patterns by fluorescence microscopy. Cells were seeded overnight on the patterns in the presence of serum. Bound integrins were cross-linked to the underlying FN using sulfo-DTSSP (Garcia et al., 1999; Keselowsky and Garcia, 2005) and uncross-linked cellular components were extracted with detergent. Immunostaining for printed and cell-deposited FN demonstrated that printed patterns of FN maintain high-fidelity and resist reorganization by cells.

Integrin Localization is Controlled by Nanoscale Geometry of the Adhesion Interface

Integrin recruitment for cells adhering to nanopatterned substrates was analyzed by immunostaining to determine how the nanoscale geometry of the adhesion interface modulates cell adhesion. The cross-linking/extraction method (Garcia et al., 1999; Keselowsky and Garcia, 2005) was used to covalently cross-link bound integrins to FN using the cell-impermeable bifunctional reagent sulfo-DTSSP. After detergent extraction of uncross-linked cellular components, immunostaining for α5 integrin was performed. We previously demonstrated that this technique provides specific staining of bound integrin and shows equivalent localization of α5β1 integrin to focal adhesions as conventional immunostaining (Garcia et al., 1999; Keselowsky and Garcia, 2005), indicating that the cross-linking/extraction method does not alter integrin distribution. In addition, an advantage of this technique is that it removes non-specific nuclear staining that can impede visualization of integrins on nanopatterns. Previous antibody-blocking experiments demonstrated that adhesion in this cell model is mediated by α5β1 integrin-FN interactions without significant contributions to adhesion strength from other receptors and / or extracellular ligands (Gallant et al., 2005; Keselowsky et al., 2003). Recruitment of α5 integrin (green) varied in response to changes in size and geometry of adhesive regions of FN (red) (Fig 5.3). Integrin clustering localized to adhesive pads presenting FN islands. In order to determine the frequency of integrin recruitment events to adhesion regions in a large cell population, stacked “heat map” images of α5 integrin

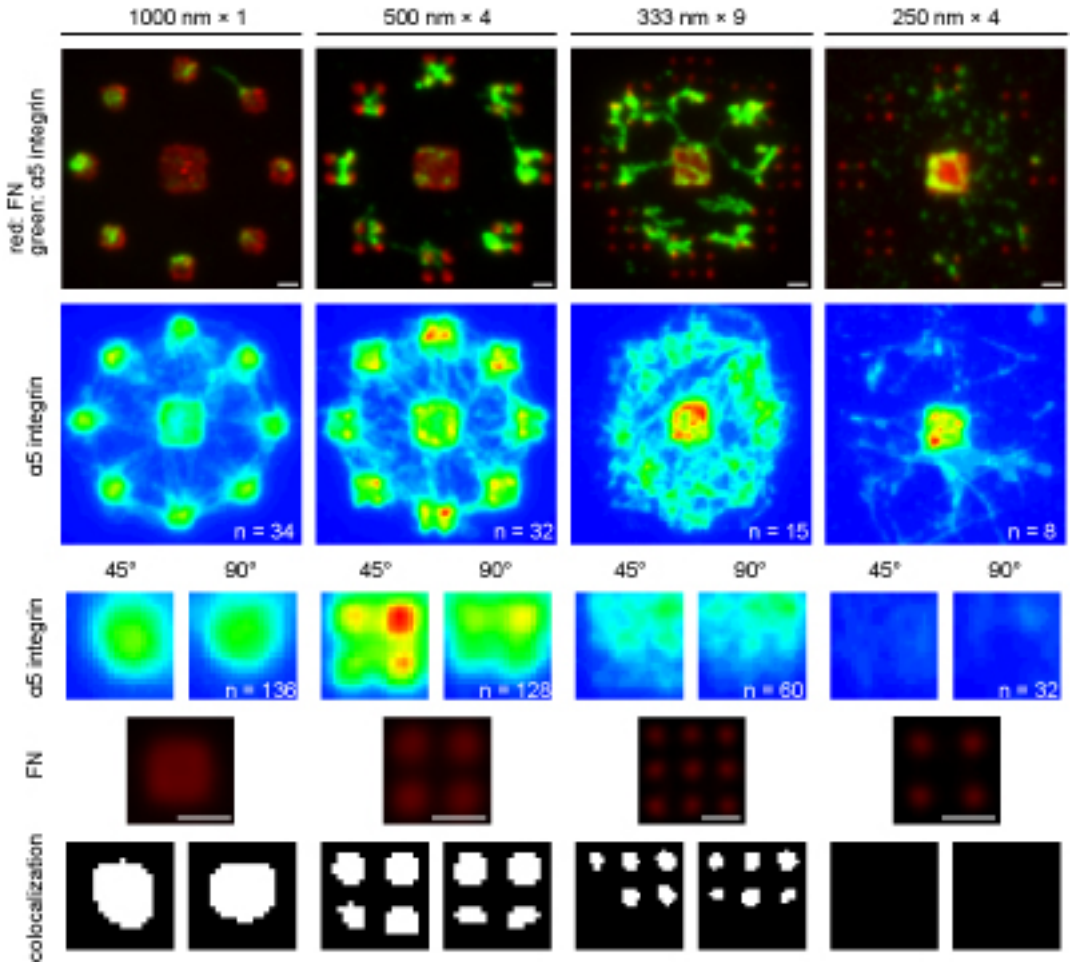

Figure 5.3. Localization of bound integrin depends on the geometry of the adhesive interface. The size and orientation of adhesive regions directs integrin clustering. Scale bars 1 μm.

recruitment were produced by averaging individual images of integrin staining in cells on patterns. Average images are used to filter out signal from low frequency events ("noise") and provide information about the location of the most common integrin binding events. Three patterns were designed with the same total area (12 μm^2) but in different area splitting configurations of 1000 nm × 1, 500 nm × 4, and 333 nm × 9. A smaller total area (6 μm^2) was achieved with the pattern configuration of 250 nm × 4. On 1000 nm × 1 patterns, high intensity areas in close proximity to the location of adhesion pads indicate high levels of integrin recruitment. Low intensity signal between the center and adhesion pads indicates low frequency integrin recruitment. Similar localization occurs on 500 nm × 4 patterns with increased intensity concentrated on the pads around the periphery. On 333 nm × 9 patterns, integrin recruitment becomes more diffuse and the level of bound integrin decreases. In contrast, the signal intensity increases at the center pad indicating increased recruitment of integrins to this location compared with previous patterns. The heat map of the 250 nm × 4 pattern indicates a further decrease in integrin recruitment throughout the interior and increased levels of recruitment at the center pad. Note that on all patterns integrin recruitment does not occur on all available areas in the adhesion region. Interestingly, preferential recruitment occurs at islands closer to the center pad. These results demonstrate that the nanoscale geometry of the adhesive interface directs the recruitment of bound integrins into clusters. Regions of high density recruitment form in response to the size and geometry of features on the interface. An adhesion area-dependent transition occurs from integrin localization to adhesive regions to no localization at a threshold size between 333 nm and 250 nm.

By changing the orientation of the adhesion pad, the presentation of the pad relative to the center of the adherent cell is altered. The role of pad orientation in integrin recruitment was analyzed using heat map images produced by averaging all pad locations of the same orientation (45° vs. 90°). In addition, colocalization analysis was used to compare the location of integrin to FN patterns. This analysis produces an image in

which the white region indicates the area at which both integrin and FN signal is present. Comparing integrin recruitment for both 45° and 90° pad orientations on 1000 nm × 1 patterns indicates differences in the localization of recruited integrin. On pads with a 45° orientation, integrin preferentially recruits to the corner of the adhesion pad. In contrast, pads with a 90° orientation have integrins localization that is centered at the edge of the adhesion pad. Similar variation in localization is seen on 500 nm × 4 patterns. Interestingly, the area of highest integrin recruitment occurs on the 45° pad orientation in the same region as the island that is closest to the center of the pattern. More recruitment of integrin occurs here than on the pad with 90° orientation. Less integrin recruitment occurs at the two islands that are equidistant from the center of the pattern. The island furthest from the center has the lowest intensity. Recruitment decreases on the 333 nm × 9 pattern. Again, intensity correlates to orientation to the center of the pattern with the highest intensity colocalization to the islands that are closest to the center of the pattern. At the islands farthest from the center, recruitment levels are only slightly above background. When the pattern geometry is decreased to 250 nm × 4, minimal integrin recruitment occurs at all island locations. These results demonstrate roles for pattern geometry and orientation in modulating cell adhesion through recruitment of integrins. The extent of integrin clustering was determined by the island size, the number of islands, and the distance of the islands from the center of the pattern. As the size of adhesion islands decreases, integrin recruitment is hampered until reaching a pattern size that is too small to support integrin clustering.

Frequency of Integrin Occupancy Varies with Pattern Geometry

It was evident from examining multiple images that the number of adhesion pads occupied by integrin receptors was dependent on the adhesion pad geometric configuration. In order to evaluate pad occupancy, individual images with positive integrin staining for the center area (indicating a cell) were categorized by the number of

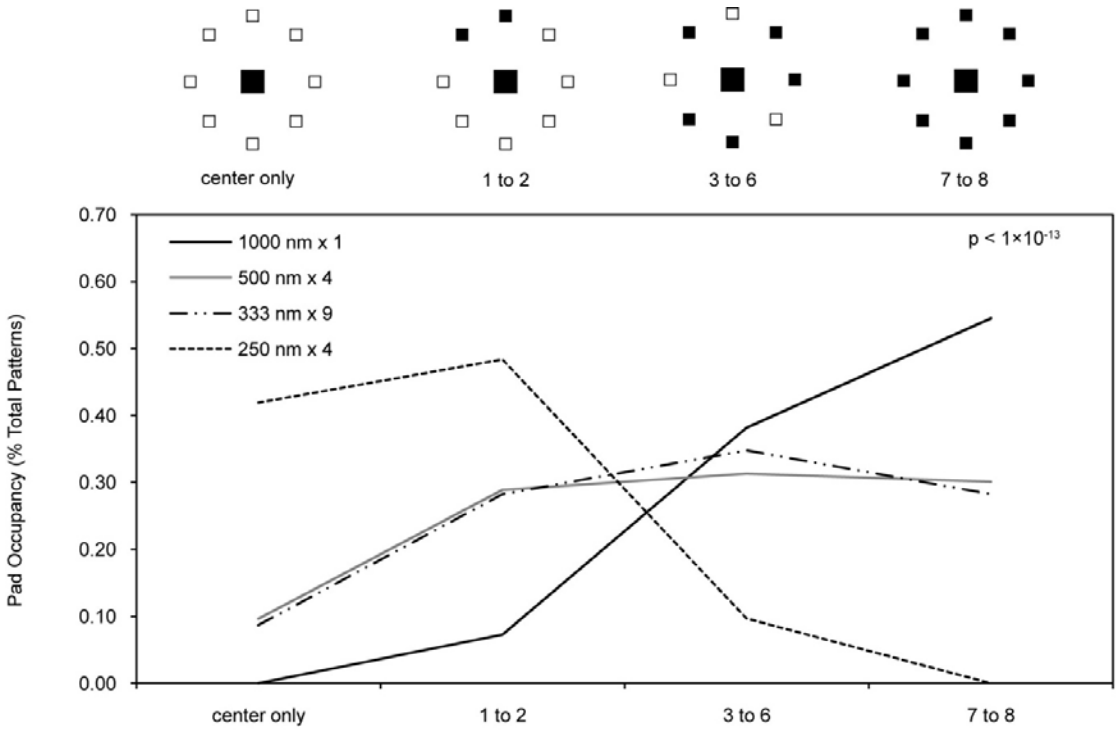

Figure 5.4. The extent of integrin localization to adhesive regions is affected by the adhesive interface geometry. Kruskal-Wallis: 1000 nm × 1 > 500 nm × 4 = 333 nm × 9 > 250 nm × 4 ($p < 0.05$).

pads with integrin staining and normalized by the total number of patterns counted. The results are displayed as a frequency polygon (Fig 5.4). Cells on 1000 nm × 1 patterns predominantly occupied three or more pads with over half of the locations showing pad occupancy on all adhesive pads. In contrast, cells on 250 nm × 9 patterns showed low pad occupancy with over 90% of locations having two or less pads occupied. Patterns 500 nm × 4 and 333 nm × 9 generated pad occupancies that were equally distributed from partial to full occupancy. These results indicate a range of adhesion that occurs on patterns with nanoscale geometries. Larger adhesion patterns provide the highest level of pad occupancy and therefore a greater extent of adhesion. Decreased adhesion occurs with decreased pattern size. However, no difference in pad occupancy occurs between the 500 nm and 333 nm pattern sizes. This analysis revealed a threshold below which pattern sizes are too small to support integrin recruitment and therefore inefficient pad occupancy occurs.

Role of Cell Contractility on Integrin Recruitment to Nanoscale Patterns

In order to determine the effect of contractile forces on adhesion to nanopatterns, integrin recruitment was analyzed in cells after treatment with the contractility inhibitor Y-27632 (10 μM) (Fig 5.5). Y-27632 is a specific inhibitor of Rho-kinase that has been shown to reduce contractility and focal adhesion assembly (Dumbauld et al., 2010; Narumiya et al., 2000; Zhong et al., 1997). We previously showed that this inhibitor dose effectively reduces contractility in NIH3T3 fibroblasts adhering of FN micropatterns (Dumbauld et al., 2010). Pad occupancy by integrins was determined by categorizing the number of pads with integrin staining. Cells treated with inhibitor showed no difference in pad occupancy compared to control cells. In both groups, a majority of pattern locations had integrin staining on 1 to 6 pads, but few patterns had integrin recruitment on all pads. This result indicates that inhibition of contractile forces does not affect the ability of cells to cluster integrins on nanoscale adhesion patterns. The effect of

contractile forces on integrin recruitment was also analyzed using heat map averages of integrin staining for samples with and without inhibitor treatment. In control cells, preferential recruitment is indicated by high intensity at peripheral adhesion regions, consistent with the previous analysis (Fig. 5.3). Cells treated with inhibitor exhibited a decrease in integrin recruitment at periphery locations compared to control patterns. Interestingly, intensity levels at the center pad decrease as well from control to inhibitor conditions. These results indicate that cells with inhibited contractile forces are still able to recruit integrins to adhesive contacts in a similar response as control cells. However, a decrease in the levels of nano-scale integrin recruitment and clustering occurs due to an inhibition of contractile forces. Analysis of the effect of pad orientation on integrin recruitment is achieved by a heat map average image of all pads with the same orientation. Decreased integrin recruitment occurs at both 45° and 90° pad orientation with inhibitor treatment. Note that the preferential localization of integrins to adhesion islands that are closest to the center of the pattern occurs independent of contractility conditions. However, the higher maximum intensity that occurs in the 45° orientation compared to 90° of control cells does not occur after contractility is inhibited. Taken together, these results indicate that cell contractility is not required for integrin recruitment to adhesion regions. However, the extent of integrin clustering at the nanoscale is dependent on contractility. Further, the role of orientation is maintained to the extent that integrin recruitment occurs preferentially at islands closer to the center of the cell body, but the extent of integrin clustering is diminished.

Nanoscale Adhesive Geometry Regulates Adhesive Forces

Adhesion strength on nanoscale patterns was quantified in order to assess the functional dependence of cell adhesion on nanoscale geometry of the adhesion interface. The spinning disk assay has been used to quantify modulation of adhesion strength in response to changes in adhesion area (Gallant et al., 2005). Adhesion strength was

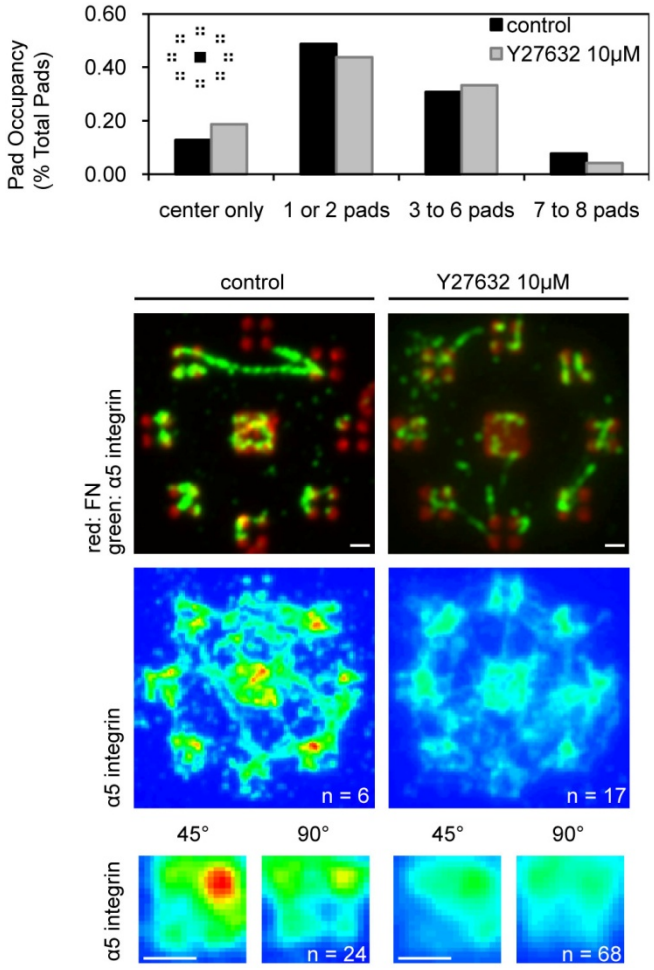

Figure 5.5. Varying the contraction forces in cells on nanopatterns did not change integrin occupancy of adhesion pads compared to control cells. However, decreased integrin recruitment occurred as shown in heat map averaging images. Scale bars 1 μm.

measured on various nanoscale patterns. For comparison, the upper-bound adhesion strength was determined using patterns of 10 μm diameter circles, while the lower-bound adhesion strength achieved as nanopattern size approaches zero was determined using patterns consisting of a center pad with no peripheral pads (Fig 5.6). Adhesion strength on nanoscale patterns varies between the maximum adhesion achieved on the 10 μm circle and the minimum that occurs on the pattern with the center pad only. As pattern features are decreased from micrometer dimensions to nanoscale features, adhesion strength decreases significantly. A further decrease in adhesion strength occurs when the adhesion area is split into nanoscale patterns presenting 1, 4 and 9 islands (all three patterns have the same total pad area). This result indicates that nanoscale pattern geometry modulates adhesion strength. A similar indication of the importance of geometry can be seen between the 10 μm circle and the 1000 nm × 1 pattern where a decrease in total adhesion area of 6.5-fold results in only a 1.3-fold decrease in adhesion strength. Combined these results demonstrate that nanoscale geometry of the adhesive interface is a critical component in the generation of adhesive forces.

Modulation of Adhesion Strength through Nanoscale Geometry

There are several characteristics of adhesive interface geometry that could be responsible for variations in adhesion strength on nanoscale patterns. The role of total adhesion area, spacing between adhesion points, and size of individual adhesion points at nanoscale dimensions has yet to be determined. Adhesion strength was analyzed as a function of each of these characteristics in order to uncover their roles in generation of adhesive force.

The total pad area is the sum of the adhesion areas within each of the eight pad regions arrayed around the periphery. By changing the island size and the number of islands per pad, patterns with various total pad areas were produced. Furthermore, patterns were produced in which the same total pad area is arranged into different

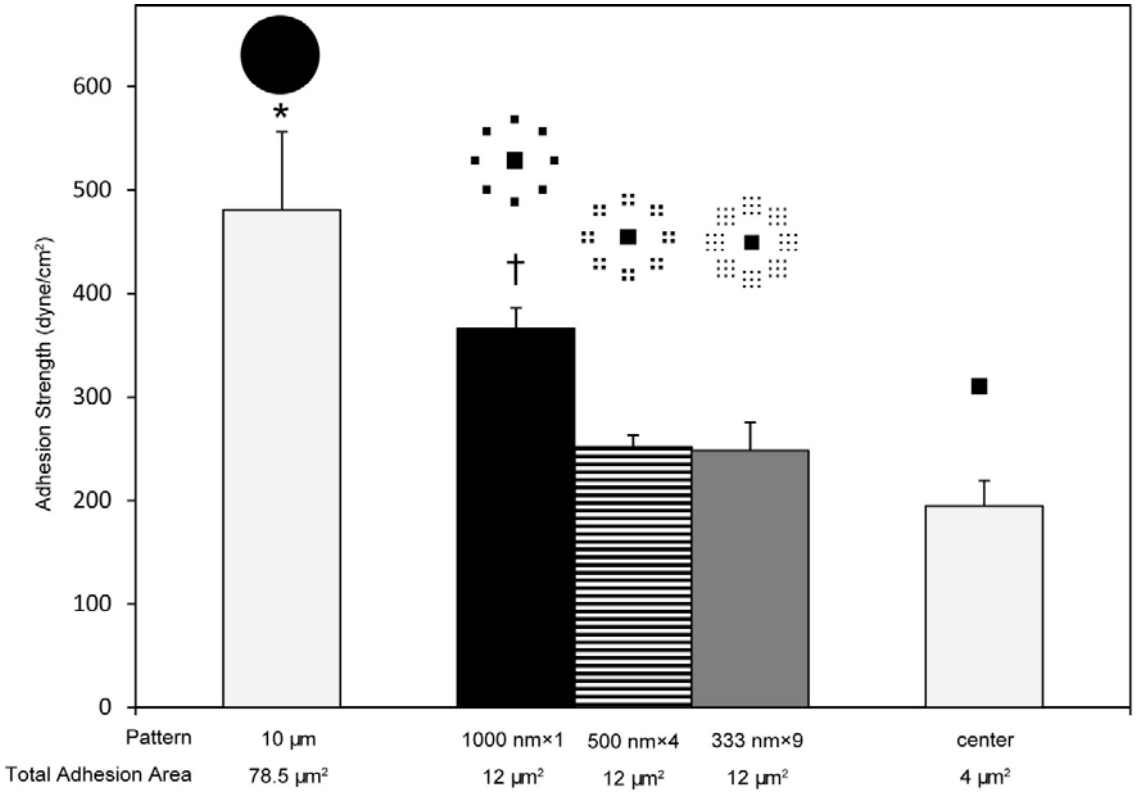

Figure 5.6. Cell adhesion strength on patterns with nanoscale geometries ranges between bounds of full adhesion region and center only. ANOVA: * 10 μm > all other patterns ($p < 0.002$); † 1000 nm × 1 > 500 nm × 4, 333 nm × 9, center ($p < 0.01$)

geometries. Adhesion strength was analyzed as a function of these characteristics (Fig 5.7). As expected, a decrease in total pad area results in decreased adhesion strength as shown for pattern sizes 1000 nm to 500 nm with one island per pad. A similar trend is seen for patterns with four and nine islands per pad. Importantly, differences in adhesion strength occur when the total pad area is organized in different geometries as seen for three patterns each having the same total area of 12 μm^2. As the pad area is divided from one pad into four and nine islands per pad, the adhesion strength decreases significantly. The same trend is seen at a smaller total pad area of 2 μm^2 when one island with edge dimensions of 500 nm is split into four islands of dimension 250 nm. These results reveal a role for nano-scale area splitting in regulating adhesion strength where the same total adhesion area can produce a range of adhesion strengths based on the geometry of the presented area. Decreasing the size of the individual adhesion regions alters the generation of adhesive force independent of the total pad area. Further, this characteristic is shown to be effective across a range of sizes from 1000 to 250 nm.

Spacing between adhesion regions is another characteristic of the adhesive interface that we investigated as a modulator of adhesion strength (Fig 5.8). Using patterns with island sizes of 250 nm, the adhesion strength was determined for island spacings of 0.75 μm and 1.25 μm. No difference in adhesion strength occurred at the two spacings. These results indicate that spacing between adhesion regions at nanoscale dimensions is not responsible for modulation of adhesion strength.

The dependence of adhesion strength on the nanoscale area of individual adhesive points was determined by analyzing adhesion strength as a function of area of a single island (Fig 5.9). As island area increases, the adhesive force that can be generated increases. The nonlinear relationship between cell strength and island area can be described by a logarithmic fit (grey line). This functional dependence indicates a decreasing dependence of adhesion strength on island area as pattern size increases. Two patterns have an island area of 0.25 μm^2 (500 nm × 1 and 500 nm × 4) but a different

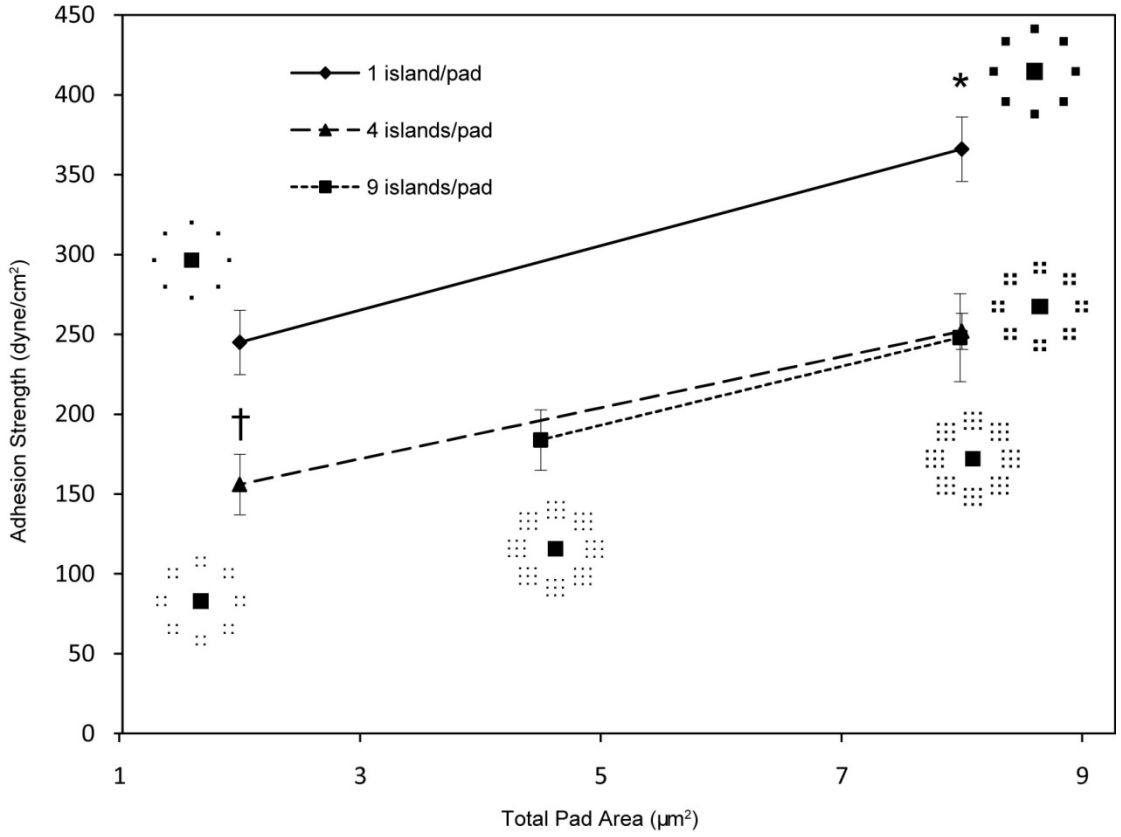

Figure 5.7. Adhesion strength is modulated by total pad area and number of islands within a pad. Adhesion strength decreases with decreasing pad area and with area splitting. ANOVA: * 1000 nm × 1 > all other patterns ($p < 0.003$); † 500 nm × 4 > 250 nm × 4 ($p < 0.01$); ‡ 500 nm × 1 > 250 nm × 4 ($p < 0.01$).

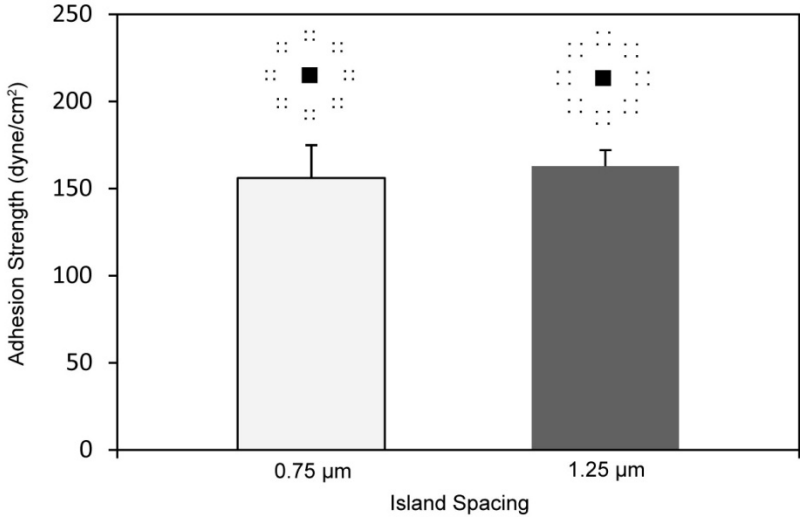

Figure 5.8. Adhesion strength modulation by spacing between adhesion islands.

number of islands per pad and total pad area. Interestingly, no difference in adhesion strength is measured on these patterns. A similar trend is seen for islands with dimension of 250 nm where no difference in adhesion strength is measured for all four adhesion patterns. These results indicate that at nanometer length scales, adhesion strength is determined by the area of the adhesion island independent of the number of islands per pad. This suggests that at nanometer length scales the size of individual adhesion points available to adherent cells plays a significant role in modulation of adhesion strength.

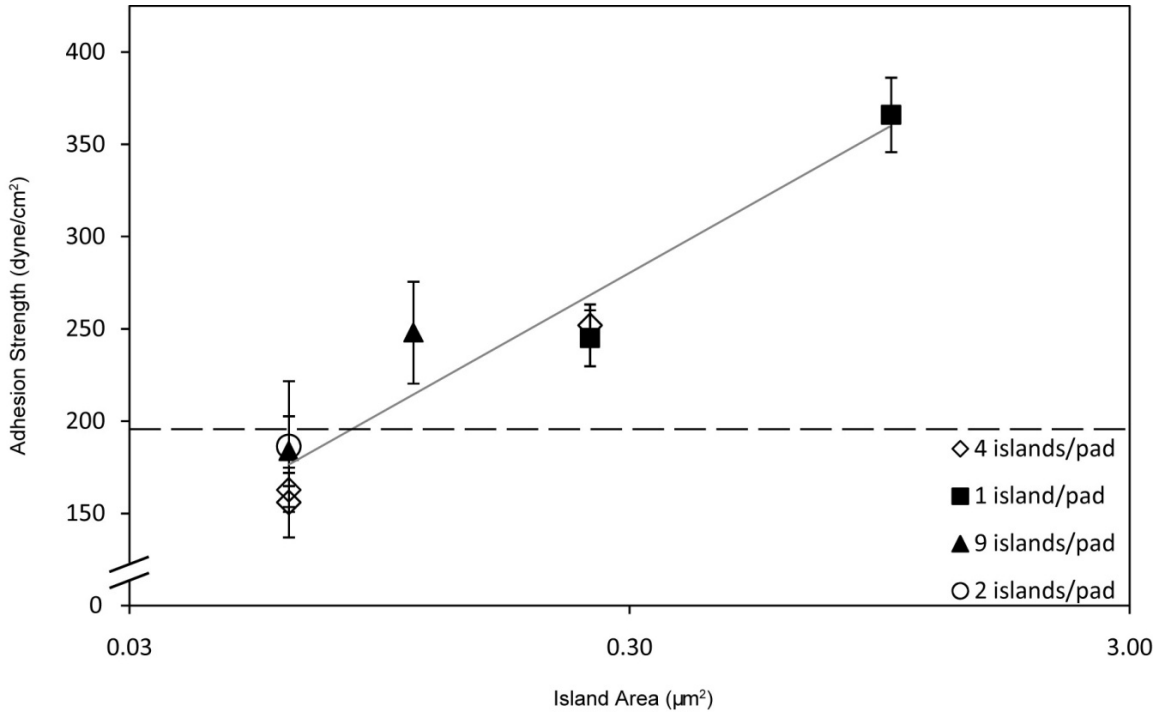

Figure 5.9. Adhesion strength decreases with island area independent of the number of islands per pad. A logarithmic fit (grey line, strength = 65.4 ln(area) + 350, $R^2 = 0.92$) describes the cell strength-island area relationship. The dashed line is adhesion strength to center pad only 194 dyne/cm^2 (st dev +/- 48).

Discussion

We analyzed the adhesive responses of cells to nanoscale geometry of the adhesive interface by combining a high-resolution technique for producing nanoscale patterns of proteins with biochemical analysis and a quantitative adhesion assay. Engineered substrates were used to vary the size, spacing, and number of adhesive areas in order to systematically assess the contributions of each to recruitment of bound integrin and generation of adhesive force. The geometry of the adhesion patterns were motivated by a range of observed focal adhesion sizes between 0.25 and 10 μm^2 (Balaban et al., 2001; Ballestrem et al., 2001; Goffin et al., 2006; Kato and Mrksich, 2004; Nobes and Hall, 1995) as well as previous experiments with areas of 0.1 μm^2 (Lehnert et al., 2004). This approach expands on other adhesion analysis approaches by combining controlled regulation of adhesive regions at nanoscale sizes with a robust assay for quantifying adhesion strength. The work presented herein provides new insights on how integrin recruitment is directed by nanoscale geometry of adhesive regions and the functional outcomes on cell adhesion strength.

Integrin recruitment on nanoscale patterns showed a range of localization characteristics that were directed by the geometry of the adhesion pattern. Nanoscale geometry was shown to induce changes to the area over which integrin recruitment occured, the level of integrin recruitment within a cluster, preferential locations for clustering of integrins, and the area of integrin clusters. The area over which integrin recruitment occurred was shown to depend on the size of individual adhesion regions. For larger pattern sizes of 1000 nm and 500 nm, integrin recruitment occurred across the entire pattern. As pattern size decreased to 333 nm, integrin recruitment events were less likely to happen at the furthest pattern locations, showing preferential binding to islands that were closer to the center of the cell. Below 333 nm, a threshold value was crossed under which integrin recruitment to nanoscale patterns diminished significantly. Small

punctate formations can be seen in individual images of integrin recruitment, but they do not occur with high frequency at any of the adhesion pads. These results agree with previous studies which determined that cells were able to adhere to and spread on adhesion regions of 0.25 μm^2 (equivalent to 500 × 500 nm^2) and larger, but that adhesion with no spreading occurred on 0.1 μm^2 (equivalent to 316 × 316 nm^2 patterns) (Lehnert 2004). Our studies expand on previous work by determining the minimum area threshold for integrin clustering to exist between 333 × 333 nm^2 (0.11 μm^2) and 250 × 250 nm^2 (0.06 μm^2). Below this threshold, integrin recruitment is limited to small punctate binding events. Our results agree with recent studies that use fibronectin-coated magnetic beads to show that initial integrin binding requires a spacing of 40 nm between FN molecules (Roca-Cusachs et al., 2009), a spacing smaller than that required for robust integrin binding and focal adhesion assembly. Previous studies of robust binding requirements have been done on surfaces with uniform distribution of adhesive ligands and determined a spacing between ligands of 140 nm or 73 nm to be required for robust integrin binding and focal adhesion assembly (Arnold et al., 2004; Cavalcanti-adam et al., 2007; Massia and Hubbell, 1991). In contrast to our system, these surfaces support cell spreading. The ability of cells to spread on the surface may affect the requirements for integrin binding and focal adhesion assembly. In our system, integrin binding is separated from cell spreading effects, thereby determining area requirements for integrin binding independent of cell spreading effects.

The level of integrin clustering was also shown to be regulated by pattern geometry. Higher levels of clustering occurred on an adhesion area of 500 × 500 nm^2 than on an adhesion area of 1000 × 1000 nm^2. Note that these patterns have the same total pad area meaning that the same amount of ligand is available for integrin binding. Therefore, the quantity of integrin being recruited to the surface is increased. Within the 500 × 500 nm^2 pad, the level of clustering was highest on the island positioned closest to the center of the pattern (45° orientation). A decrease in integrin clustering occurred

when the orientation of the pad was 90° where two islands were equidistant from the pattern center. Combined, these results suggest a hierarchy of criteria for integrin clustering to nanoscale adhesive regions that includes proximity to the center of the pattern and pattern area. At the optimal location and pattern area, elevated levels of integrin clustering occurs as seen in 500 nm × 4 patterns. As pattern geometry varies from the optimal size and location, decreased integrin clustering occurs. This occurs on 1000 nm × 1 patterns where levels of integrin clustering decreased compared to 500 nm × 4 patterns. As pattern size decreases on patterns of 333 nm × 9 and 250 nm × 4, the level of integrin clustering that can be supported decreases, independent of island location. The numerous combinations of area and location that can occur provides the wide range of integrin clustering responses that are required to produce complex and versatile adhesion functionalities. This behavior may be driven by differences in the formations of actin filaments that occur and the resulting force that is applied. Contractile forces in cells have been shown to play an important role in the activation of focal adhesion components and formation of mature focal adhesions (Riveline et al., 2001). One explanation is that patterns of 500 nm × 4 may support a more robust network of actin than 1000 nm × 1 which produces larger forces. Another explanation is that the network may be more concentrated on the 500 nm islands. This would explain the difference in integrin level between pad orientations for the 500 nm × 4 patterns. In the 45° orientation, bound actin is concentrated at the island closest to the pattern center. In the 90° orientation, actin binding is distributed between two islands instead of one, thereby decreasing the force that can be applied.

In order to determine whether contractile forces are involved in integrin recruitment to nanoscale adhesion patterns, integrin recruitment was assessed in cells treated with the ROCK inhibitor Y-27632 on 500 nm × 4 patterns. Pad occupancy in cells with inhibited contractility showed no differences compared to control cells. This indicates that the area of bound integrin is not affected by ROCK inhibition. However,

the level of integrin clustering decreased in cells treated with inhibitor. Heat map images showed a decrease in the level of integrin clustering that occurred after inhibitor treatment. At all island locations and both 90° and 45° orientations, the level of integrin recruitment decreased significantly compared to control samples. These results suggest that while contraction forces are not required for integrin recruitment to the adhesive interface, they are required for clustering of integrins above a base level. By inhibiting actin formation, cytoskeletal forces decrease which results in a decrease in the level of integrin recruitment. These results agree with previous studies that link enhancement of integrin function to application of force (Astrof et al., 2006; Friedland et al., 2009). Recent atomic force microscopy studies have demonstrated the catch bond behavior of integrin-FN bonds where applied force prolongs bond lifetime (Kong et al., 2009), These results could explain our observations about integrin recruitment where applied forces would cause a decrease in the dissocation rate of bound integrin thereby increasing the amount of integrin localized to the nanopatterns at a given time. As applied force increases at islands that are closer to the center of the pattern, the dissociation rate decreases resulting in an increase in the level of integrin recruitment.

In order to understand the functional implications of integrin recruitment on nanoscale patterns, we analyzed adhesion strength using a quantitative adhesion assay. We demonstrate that adhesion strength varies with nanoscale geometry as total pad area, island number, and island area are modulated. When total pad area was decreased (constant number of islands per pad) adhesion strength decreased. Small changes in pattern size resulted in significant decreases in adhesion strength. This is in agreement with previous work that showed a strong dependence of adhesion strength on adhesive area (Gallant et al., 2005). Our studies also uncovered the role of area splitting in adhesion strengthening. When total pad area was kept constant but individual islands were broken into multiple islands of smaller dimensions, adhesion strength decreased. This area splitting effect occurred at pattern dimensions of both 1000 nm and 500 nm

indicating a range of sizes over which this effect can occur. Combined, these results indicate that cues other than total area are present in the nanoscale geometry of the adhesion interface and are responsible for regulating adhesion strength. The impact of these cues is not limited to a specific size but instead plays a role in adhesion areas that are equivalent to both large mature focal adhesions as well as small early-stage integrin-ligand bindings. Further analysis of adhesion strengthening and nanoscale characteristics uncovered a relationship between nanoscale area of individual adhesion points and adhesion strengthening. Not only did increased island area produce an increase in adhesion strength but it also showed a dominant role over the number of islands in a cluster. Patterns with the same island area but a different number of islands per pad exhibited no differences in adhesion strength.

The integrin recruitment results we collected for pad occupancy and level of integrin clustering explain the functional differences in adhesion strength. The low adhesion strength for patterns of 250 nm dimension can be explained by the lack of integrin recruitment that occurs. These patterns are below a threshold dimension and so integrin recruitment is limited to low frequency formations. Without integrin clusters, these adhesion areas do not generate adhesive forces. Adhesion strength values drop to levels that are similar to lower-bound levels achieved on patterns with no nanoscale features (Fig 5.9, dashed line, center pad only).

Interestingly, no differences in adhesion strength are observed between 333 nm × 9 and 500 nm × 4 patterns. Integrin recruitment on these patterns was equal in terms of pad occupancy, but different in terms of the level of integrin clustering. One explanation for the similar adhesion strengths for the 333 nm × 9 and 500 nm × 4 patterns is that pad occupancy has a stronger influence on adhesion strength than the level of integrin clustering within the pads. This suggests that adhesion strength is determined by the number of pads with integrin recruitment and binding, but not the quantity of integrins in a cluster. Increased pad occupancy produces increased adhesion strength, which is seen

with the 1000 nm × 1 pattern. Analysis of heat map images of the 333 nm × 9 and 500 nm × 4 patterns show a similar area over which integrin recruitment occurs above threshold (colocalization area).These results suggest that above a threshold level, an increase in the level of integrin clustering does not produce changes in adhesion strength.

Another interesting result is that equal adhesion strengths occur on 500 nm × 4 and 500 nm × 1 patterns. While similar pad occupancies can explain the similar adhesion strengths, the area over which integrin recruitment occurs varies from 1 μm^2 to 0.25 μm^2. This indicates that no difference in adhesion strength occurs when island size is maintained but total available area changes. This result can be explained by a model from Gallant and Garcia which uses mechanical equilibrium analysis to calculate the forces that are produced by adhesive structures to resist detachment force. The model predicts the force exerted by an adhesive unit at the edge of a detaching cell is constant on all adhesion patterns. Further analysis that considers the roles of integrin binding and focal adhesion assembly in the adhesive unit predicts that an adhesive unit of 200 nm can support the same detachment force as a larger conventional focal adhesion (Gallant and Garcia, 2007). This indicates that a range of adhesive unit sizes can produce similar adhesion forces. In our experimental results, the difference in area between the cluster that forms on the 500 nm × 4 pattern and the cluster on the 500 nm × 1 pattern is a similar area difference between a conventional focal adhesion and the 200 nm unit studied in the model. Our results present experimental evidence validating this theoretical prediction.

Taken together, these results suggest that adhesion strength is regulated by the pad occupancy which describes the number of locations where integrin clusters have formed. The level of clustering within the pad does not strongly modulate the adhesion strength as long as it is above a threshold value for robust integrin formations. The area of integrin clusters was determined to not correlate with adhesion strength for cluster areas of 0.25 μm^2 to1 μm^2. These results agree with previous findings that showed no correlation existing between force and focal adhesion size for focal adhesion smaller than

1 μm^2 (Tan et al., 2003). Interestingly, the force-size relationship does occur for areas above 1 μm^2 (Balaban et al., 2001).

Conclusion

We have shown that integrin recruitment and adhesion strength are directed by geometry of the adhesive interface at nanoscale sizes between individual molecules and supramolecular complexes. A unique experimental approach was used to analyze localization of bound integrin and quantify adhesion strength while systematically varying the area, spacing, and clustering of adhesion areas. Integrin recruitment was shown to respond to changes in the size, clustering, and orientation of adhesion regions. Increased levels of integrin binding occurred on adhesion areas whose size and position suggest increased force application from actin filaments. Below a threshold pattern area between 333 × 333 nm^2 (0.11 μm^2) and 250 × 250 nm^2 (0.06 μm^2), integrin recruitment switches from robust integrin clusters to low frequency formations. Adhesion strength was shown to be modulated by nanoscale geometry of the adhesion area. A relationship was established between adhesion strength and area of individual adhesion islands, independent of the total available adhesion area. Patterns with adhesion areas below the threshold were unable to generate adhesion strength. Adhesion strength is seen to vary with integrin pad occupancy and not with the level of integrin clustering at adhesion regions. Adhesion strength was shown to be independent of area of integrin clusters for areas between 0.25 μm^2 and 1 μm^2. These results provide new insights on the role of nanoscale geometry in the generation of adhesive forces through integrin recruitment.

CHAPTER 6

SUMMARY OF CONCLUSIONS

Although significant progress has been made in identifying the molecules that are involved in cell adhesion and their interactions, the mechanisms that dictate the generation of strong adhesive forces remain poorly understood. Specifically, the role of nanoscale geometry of the adhesive interface in integrin recruitment and adhesion forces remains elusive due to limitations in the techniques available for engineering cell adhesion environments. Systematic analysis of the role of nanoscale geometry of the adhesive interface in modulating integrin recruitment and adhesion strength promises to expand our understanding of cell adhesion, extend our ability to engineer materials with controlled adhesion, and enhance the design of treatments for adhesion-related diseases.

The first goal of this project was to develop an experimental technique capable of producing nanoscale patterns of proteins on surfaces for cell adhesion arrays. Many approaches have been pursued for patterning proteins on surfaces with high resolution, but limitations caused by significant time requirements, small patterning area, and challenging techniques have prevented wide-spread application to studies of biological systems. These limitations were overcome by developing a new experimental platform. First, we developed the subtractive pattering technique which achieves high resolution patterns of proteins. Next, we combined the subtractive patterning technique with mixed-self-assembled monolayers to produce arrays of single cells on controlled areas of adhesion surrounded by non-adhesive background.

The subtractive patterning technique combines the advantages of virtually any high-resolution lithographic method and microcontact printing by transferring a pattern of proteins from a nanotemplate to a substrate using a planar elastomer as the transfer vehicle. Results demonstrate that this method is capable of producing protein pattern

sizes as small as 90nm with high contrast and high reproducibility as well as micron size patterns. Spacing between geometries ranging from 1 to 100 μm was achieved. Patterns of lines, linelets, and clusters of squares were produced, each with resolution as low as hundreds of nanometers. The only requirement for this method is to use a nanotemplate and final substrate having a higher work of adhesion for water than the elastomer. Many surfaces that are less hydrophobic than the elastomer can be used for this purpose. There are several important benefits to this technique. First, the technique meets the needs of biological experiments including high-throughput sample production, use outside of a cleanroom environment, and patterning over large area. Second, a variety of complex architectures of multiple proteins can be created. This includes a simple approach for co-aligning proteins into complementary patterns. The flexibility of this technique enables a multitude of variations in the size, spacing, and orientation of the patterns of proteins by simple changes in the procedure. Combined, these capabilities make the subtractive patterning technique well-suited for a variety of applications including studies of biological systems.

In order to use the subtractive patterning technique for cell adhesion experiments, a robust immobilization strategy was required that maintained the original geometry of the protein patterns under extended cell culture conditions. The objective of our next study was to develop a method for producing cell adhesion arrays that constrain adhesion to nanoscale patterns of protein that are surrounded by a non-fouling background. Out of several approaches that were attempted, the use of surfaces coated with mixed self-assembled monolayers was selected for the robust nature of the protein-resistant background and the ability to tether proteins directly to components of the mixed self-assembled monolayer. A mixed self-assembled monolayer was used which consists of carboxylic acid- and tri(ethylene glycol)-terminated alkanethiols that form highly-organized monolayers on gold-coated substrates. We demonstrated that proteins patterned by the subtractive patterning technique transfer from the elastomer and tether to the

mixed self-assembled monolayer. Tethering of the protein occurs between primary amines on the protein and the COOH-end groups of the carboxylic acid-terminated alkanethiols which are activated to NHS-esters. This approach provides several benefits for cell adhesion studies. Tethering of proteins provides a covalent bond between proteins and the surface which resists desorption of the protein or rearrangement by adherent cells. Backgrounds composed of tri(ethylene glycol)-terminated alkanethiols resist protein adsorption and cell adhesion, thereby constraining cell adhesion only to the areas of patterned protein. This technique is facile, cost-effective, and high-throughput which makes it easy to incorporate into the repertoire of biological experimental techniques. The use of the subtractive patterning technique enables a wide variety of pattern geometries including multi-length scale patterns with features that have dimensions at both nano- and micro-meter length scales. This is especially useful for studying biologically systems where functionality often involves coordination between components with sizes at both length scales. Overall, the combination of subtractive patterning and mixed self-assembled monolayers provides a facile approach to producing cell adhesion arrays where the nanoscale geometry of the adhesive interface can be modulated across a wide variety of sizes, spacing, and clusters making it highly applicable to cell adhesion studies.

In our next study, we verified that the activity of the adhesion protein fibronectin was maintained during the process of sample production. Using a receptor-mimetic antibody and cell seeding, we determined that the activity of the central integrin receptor-binding region of fibronectin was maintained throughout the process, that the protein was not denatured during subtractive patterning, and that the final conformation/orientation of the tethered protein supports cell adhesion. Since the same steps are completed for multi-protein patterns, we presume that all proteins will maintain activity during this process.

The applicability of this technique to studies of cellular processes was first demonstrated by directing formation of focal adhesions in adherent cells. Cells seeded on

samples prepared using our technique with uniform layers of non-patterned FN took on a spread fibroblastic morphology and formed focal adhesions typical of cells on culture dishes. Using FN patterns on a protein-resistant background, focal adhesion formation in adherent cells was constrained to the patterned region. By varying the pattern geometry, we directed the location and size of focal adhesions. These results demonstrate the unique capabilities achieved through this experimental platform for studies of biological form and function in which the spatial arrangement of the adhesive interface is engineered with nanoscale resolution to produce specific biological responses.

The second goal of this project was to analyze the recruitment of integrins into clusters in response to nanoscale geometry of the adhesive interface (adhesion area, spacing, and clustering) and determine the functional implications by quantifying variations in adhesion strength. Integrin recruitment was assessed using two metrics: 1) pad occupancy, which is defined as the number of adhesion pad locations that have integrin recruitment, and 2) integrin clustering characteristics, which includes the quantity of integrins that are recruited to a cluster, the localization of integrins within a cluster, and the area of the cluster. Pad occupancy provides information about the overall integrin binding across the interface between cell and substrate. The integrin clustering characteristics provide information about the geometry within individual clusters and how this relates to adhesion area geometry. Using patterns consisting of adhesion islands with dimensions ranging from 250 nm to 1000 nm in clusters of one, two, four, or nine islands, we determined that nanoscale geometry regulates integrin recruitment. Results showed that the pad occupancy and the integrin cluster characteristics varied according to the adhesion area size and location. A threshold area was determined between 333 × 333 nm^2 (0.11 μm^2) and 250 × 250 nm^2 (0.06 μm^2) below which integrin recruitment switched from robust integrin clusters to initial integrin bonds that were punctuate and occurred with low frequency. This threshold establishes a limit under which integrin binding is inhibited. Above that threshold, integrin recruitment transitioned through three

stages that correlated with increases in island area. In the first stage which correlates to an adhesion area of 0.11 μm^2, integrin binding was supported by the available area, the level of integrin recruitment was low, and the pad occupancy was evenly distributed between low, medium, and full occupancy. In the second stage which correlates to an adhesion area of 0.25 μm^2, integrin binding was also supported, the level of integrin recruitment increased significantly to maximum values seen for any patterns, and pad occupancy was the same as the first stage. In the third stage which correlates to an adhesion area of 1 μm^2, integrin binding was supported, the maximum level of integrin recruitment was higher than the first stage but lower than the second stage, and pad occupancy was most often full. These results demonstrate a range in integrin response that occurs with variation of the adhesion area and location. The numerous combinations of area and location that can occur provides the wide range of integrin recruitment responses that are required to produce complex and versatile adhesion functionalities. Furthermore, we suggest that this behavior is driven by differences in the actin networks that form which in turn varies the cytoskeletal forces that are applied.

The cytoskeleton plays an important role in generation of forces that are known to affect adhesive function such as integrin binding and focal adhesion formation. In order to assess the role of cytoskeletal forces in integrin recruitment to nanoscale patterns, we used an inhibitor of Rho-kinase that has been shown to reduce contractility and focal adhesion assembly. Comparing integrin recruitment in cells treated with inhibitor to control cells we demonstrated that integrins are still recruited to adhesive contacts after contractile forces are inhibited. However, a decrease in the level of integrin recruitment occurs where the quantity of bound integrin decreases across the entire pattern and within individual clusters. These results suggest that while contraction forces are not required for integrin recruitment to the adhesive interface, they are required for clustering of integrins above a base level. We suggest that the decrease in integrin recruitment is related to force-dependent function of integrins in which application of force decreases

the dissocation rate of bound integrin thereby increasing the amount of integrin localized to a nanopattern at a given time.

The third goal of this project was to determine the functional implications of nanoscale geometry of the adhesive interface by quantifying the adhesion strength of cells on patterns. The spinning disk assay provided a robust technique for measuring adhesion strengths on various geometries that could then be compared to determine the effect of geometry on adhesion strength. Analysis of adhesion strength on various patterns uncovered several unexpected roles for nanoscale geometry in modulation of adhesion strength. The importance of nanoscale area was determined by results showing that adhesion strength decreased with a decrease in total pad area. Adhesion strength was also shown to depend on area splitting. When total pad area was kept constant but adhesive pads were broken down into multiple islands of smaller dimensions, adhesion strength decreased. This area splitting effect occurred at pattern dimensions of both 1000 nm and 500 nm indicating a range of sizes over which this effect can occur. In another set of experiments, no differences in adhesion strength occurred with changes to the space between adhesion islands. Further analysis determined a relationship between adhesion strength and the size of individual adhesion islands independent of the number of islands per pad. No difference in adhesion strength occurred on patterns of 500 nm × 4 and 500 nm × 1. Combined with results from integrin recruitment analysis, these results suggest that pad occupancy plays a dominant role in generation of adhesion strength and that a integrin clusters with sizes ranging between 0.25 um^2 to1 um^2 can produce similar adhesion forces.

The adhesion strengthening response to nanoscale geometry correlates to the integrin recruitment results for pad occupancy and level of integrin recruitment. Below a threshold area, integrin recruitment is limited to low frequency punctuate formations. Without mature clusters of integrin, these adhesion areas are not able to support adhesion strengthening. Above the threshold, the adhesion strength increases and is similar across

several patterns with island areas of 0.11 μm^2 and 0.25 μm^2. Although differences in the level of integrin recruitment occur between these two adhesion areas, this does not result in a change in adhesion strength. Adhesion strength is determined by the area of the integrin clusters that form on these patterns. Previous modeling efforts have shown that adhesion units with areas similar to the integrin cluster areas produce similar adhesion forces independent of their area. An increase in adhesion strengthening does occur when the island area is increased to 1 μm^2. This increase in adhesion strength from patterns with the same total area but smaller individual islands correlates to differences in the pad occupancy. The highest adhesion strength correlates to the pattern with the highest pad occupancy. The patterns with island areas of 0.11 μm^2 and 0.25 μm^2 have similar adhesion strengths and similar pad occupancy results. These results demonstrate that adhesion strength is regulated by the ability of nanoscale geometries to support integrin clustering over the entire adhesion area. Combined, these results demonstrate that adhesion strength is modulated by the number of adhesion pads with integrin clustering. The level of clustering within the pad does not modulate the adhesion strength as long as it is above a threshold value for mature integrin formations. Furthermore, we determined that integrin clusters with areas between 0.25 um^2 and 1 um^2 support similar levels of adhesion strengthening.

In conclusion, this thesis project analyzes the role of nanoscale geometry of the adhesive interface in regulating integrin recruitment to adhesive contacts and modulating cell adhesion strengthening to ECM. The following outcomes were achieved by completing the three specific aims previously outline. First, we developed a strategy for producing robust patterns of tethered proteins with nanoscale resolution in a non-fouling background. This technique meets the requirements for cell adhesion studies of high-throughput production, large pattern areas, and high fidelity under extended cell culture conditions. Second, we established the relationship between various stages of integrin clustering from initial punctuate formations to mature integrin formations and the

nanoscale geometry of the adhesive interface. A threshold area was determined above which mature integrin formation could occur. Third, we determined that adhesion strength is modulated by the size of individual adhesion islands and the area splitting of adhesion pads into several smaller areas. We determined that adhesion strengthening correlates to integrin pad occupancy but not to the quantity of integrin that is recruited to a cluster. As a whole, this project provides new insights on the role of size and location of clusters of recruited integrin in the modulation of adhesion strength in response to nanoscale geometry of the adhesive interface.

CHAPTER 7

FUTURE CONSIDERATIONS

An important area to focus future studies is the role of focal adhesions in adhesion strengthening responses to nanoscale geometry of the adhesive interface. Focal contact formations ranging in size are well established in migrating cells where leading edges have highly dynamic binding events (Giannone et al., 2007; Ponti et al., 2004). The highly variable nature of focal adhesion geometry generates balance in migrating cells between adhesion and contraction (Gupton and Waterman-Storer, 2006). Distinct focal adhesions exist at the leading edge compared to the trailing end of migrating cells thereby producing mechanical characteristics that match the adhesion requirements at each location (Munevar et al., 2001). The range of sizes of focal contacts appears to be a critical parameter that differentiates the functionality of these structures. The experimental system introduced in this project could be used to direct the size and location of focal adhesions in order to identify different categories of adhesive contacts and to determine the role of adhesion area, spacing, and clustering on focal adhesion formation. Furthermore, a correlation could be made between focal adhesion spatial geometry and the generation of adhesive forces. Specifically, the relationship between focal adhesion area and adhesion strengthening at submicron sizes could be established.

Another characteristic of focal adhesions that plays a critical role in cell function is the recruitment and interaction of adhesion protein components. By combining the experimental platform developed in this project with immunostaining, the localization of specific components to adhesive structures that form on nanoscale geometries could be elucidated. Structural and signaling proteins (talin, vinculin, FAK, tensin) have been investigated for their role in regulating adhesive functions. Talin acts as a mechanical linkage between integrins and the cytoskeleton (Giannone et al., 2007; Jiang et al., 2003) and is the final step in integrin activation (Tadokoro et al., 2003). Vinculin forms a

ternary complex with β_1 integrin and talin which is involved in focal adhesion dynamics and composition (Cohen et al., 2006). Importantly, vinculin has been shown to be involved in the generation of adhesive forces (Galbraith et al., 2002; Gallant et al., 2005). FAK and tensin have been heavily studied in their interactions with integrins and other focal adhesion components. Aggregation of integrins into clusters induced recruitment of FAK and tensin but not other focal adhesion components while integrin occupancy and aggregation together were required for recruitment of all focal adhesion components and formation of robust focal adhesions (Miyamoto et al., 1995a; Miyamoto et al., 1995b). The goal of future studies should be to analyze how the composition of focal adhesions varies in response to the nanoscale geometry of the adhesive interface. Using immunostaining techniques for vinculin, talin, tensin, and phospho-FAK, focal adhesion formation can be visualized and colocalization analysis with integrins and FN patterns can be completed. These experiments will determine whether differences in the composition of focal adhesions occur with variation of focal adhesion size. Furthermore, it will be determined which focal adhesion components must be recruited to adhesive contacts in order to support the generation of adhesion strength.

It is also important to dissect the mechanisms involved in integrin-cytoskeleton interactions that are involved in adhesion strengthening responses. The role of specific adhesive elements can be evaluated using transgenic systems. An inducible system that expresses wild-type and mutant derivatives of the adhesive elements can be used to re-express proteins in cells that lack endogenous expression. A retroviral system has been used to express wild-type and mutant vinculins in vinculin-null cells. Cells re-expressing eGFP-vinculin have been visualized by live-cell microscopy where functional activity of vinculin was shown by localization to focal adhesions. Similar systems are available for expression of wild-type integrin and integrins with mutations to domains that have been shown to be critical for binding of other focal adhesion components. By combining this system with the nanopatterning techniques developed in this project, the mechanistic

roles of integrin and vinculin in adhesive responses to nanogeometries could be elucidated. Adhesion analysis on nanopatterned cells re-expressing vinculin mutants could be used to determine whether vinculin plays a role in the modulating adhesion strength in response to nanoscale geometry. This sytem could be combined with plasmids expressing mutations of other adhesion elements (talin, FAK) to determine which molecules and molecular interactions are required for regulating focal adhesion formation on nanopatterns and generation of adhesion strength. Further information about adhesive responses to nanogeometries could be achieved by completing live-cell microscopy on cells re-expressing adhesion components with fluorophore tags. These studies could determine the time-dependence of recruitment of adhesion components during maturation of focal adhesions from initial bindings to mature adhesive contacts. Combined, these studies would provide insight on the specific biomolecular interactions that are occurring during the response to nanoscale geometries and the functional dependence of various components.

The combined analysis of focal adhesions using systematic variation of their spatial characteristics, immunostaining of the components involved, and transgenic manipulation of adhesion proteins will provide valuable information about the role size, composition and molecular mechanisms play in cells sensing cues from adhesive interface geometry and translating them into functional outcomes.

Another area of interest for future experiments is using controlled design of multi-protein environments to produce desired cellular responses or examine the functional dependence on spatial arrangement of proteins. The cellular microenvironment is comprised of a wide range of biomolecules that present complex chemical and physical cues. The ability to control multiple signals being generated from several components simultaneously is desired to gain additional control over complex cell functions such as mechonsensing and mechanotransduction. Studies have shown the opportunities available in patterning multiple proteins in order to control cellular function. Patterns of lamin and

collagen were used to produce different levels of adhesion and spreading of myoblasts (Mei et al., 2008). Spatial control over adhesion of hepatocytes and fibroblasts was achieved through controlled patterning of collagen and PEG layers (Hui and Bhatia, 2007). The importance of spatial organization of T cell receptors (TCRs) and leukocyte function-associated antigen-1 (LFA-1) in immunological synapse formation was elucidated by geometrically constraining the location of their respective ligands (Mossman et al., 2005). The subtractive patterning technique provides several unique opportunities for patterning of multiple proteins. First, arrays of multiple proteins can be produced where the density of cells as well as the extent of their cell-cell interactions can be controlled. The patterning technique introduced here extends previous studies that were limited in the size of the patterns as well as the number of proteins that could easily be achieved. Second, multi-protein patterns would be useful for studying the antagonistic and synergistic effects of various biologically relevant molecules. The dependence of these effects on relative area and proximity could be determined by varying the geometries of the patterns of each protein separately. The effect of these proteins on various cellular processes could be determined including adhesion strength and intracellular signaling. Overall, engineer surfaces with a wide range of spatial and biochemical cues can provide extensive control over biological responses which would be useful in applications that include axon guidance and stem cell differentiation.

APPENDIX A

LARGE-SCALE ARRAYS OF ALIGNED SINGLE VIRUSES

Summary

The fabrication of single virus arrays is demonstrated using direct printing of unmodified anti-M13 bacteriophage antibodies onto silicon with nanometer resolution, widely variable feature pitch, and flow alignment of the viruses. Organization of virus-based systems into functional, addressable arrays has many technological applications including microarray technology and bottom-up nanoassemblies.

Introduction

Many self-assembly schemes based on those found in biological systems have been demonstrated for the organization of inorganic and biological materials on the nanometer scale. Extending these examples into practical use relies on the ability to hierarchically organize them over arbitrary length scales. Achieving this level of control, however, has been hindered by the incompatibility of biological materials with current processing methods. Efforts for bridging this gap have mostly focused either on nonspecific chemical modification of surfaces, alteration of the naturally occurring system, or a combination thereof. The desire exists to develop general biocompatible processes for the organization of unmodified biological systems that capitalize on the numerous highly specific interactions commonly found in nature including DNA, antibodies, and protein complexes. To this end, the fabrication of single-virus arrays is herein demonstrated using the direct printing of unmodified anti-M13 bacteriophage

* Modified from Solis, D.J., Coyer, S.R., Garcia, A.J., Delamarche, E. Large-Scale Arrays of Aligned Single Viruses. *Adv. Mater.* **22**, 110-114 (2009). D.J.S. and S.R.C. contributed equally to this work.

antibodies on silicon with nanometer resolution and widely variable feature pitch. The ntersection of biology and technology has provided many unique solutions to challenges in both fields. Technological advances have allowed biological systems to be studied with ever-increasing detail and reproducibility. Alternately, biologically inspired approaches have shown great promise for the self-assembly and directed assembly of materials on the nanometer scale. The filamentous M13 bacteriophage virus has exhibited a tremendous capacity for incorporating biological (Petrenko et al., 1996) and inorganic materials (including metallic,(Souza et al., 2006) magnetic, and semi-conducting materials (Mao et al., 2004)) into its self-assembled, genetically modifiable architecture. Macroscopic organization of M13 bacteriophages has been achieved using liquid crystalline behavior,(Lee et al., 2002) phase separation phenomena,(Nam et al., 2006) and virus-membrane complexes (Yang et al., 2004) to create materials of high uniformity and element density. Nevertheless, these methods are not applicable for the fabrication of addressable arrays of single elements.

Materials and Methods

Preparation of Nanotemplates

High-resolution nanotemplates were produced using electron-beam lithography. PMMA-resist-coated silicon wafers were exposed in an e-LiNE electron-beam lithography system (voltage: 20 kV, aperture: 10 mm, beam current: 29 pA) (Raith GmbH, Dortmund, Germany), developed in a solution of MIBK:isopropanol at a 1:3 ratio for 30 s, immersed in isopropanol for 1 min, and blow-dried under a stream of N2. The PMMA pattern was transferred into the silicon substrate using a low-etch-rate reactive ion etcher in a balanced process that used SF6 as a precursor for the etching and C4F8 for the passivation of the sidewalls (Alcatel Vacuum Technology France, Annecy, France), which lasted for 25 s.

Protein Inking of Planar Elastomers

Sylgard (Dow Corning, Midland, MI) 184 PDMS elastomers were cured at 60 °C for at least 24 h in Petri dishes. The side of the elastomer that was in contact with the Petri dish was inked with ~100mL of antibody solution for 45 min. Anti-fd Bacteriophage (B7786, Sigma, St. Louis, MO) was used at a concentration of 0.1mg mL^{-1} in phosphate-buffered saline (PBS) (A7906, Sigma). After inking, elastomers were rinsed using PBS and deionized water and blow-dried under a stream of N2 for ~30 s.

Subtraction and Printing of Proteins

Details of the subtractive printing technique have been previously published [14]. Briefly, clean silicon substrates and nanotemplates were treated with oxygen plasma at 200W for 60 s (Technics Plasma 100-E, Florence, KY). Proteins on homogenously inked elastomers were removed in selected areas by bringing the elastomers into contact with the nanotemplate for 15 s, followed by manual release. The protein patterns were transferred from the elastomers to the final substrates using a 30-second-long printing step. Intimate contact between the elastomer and the nanotemplate/substrate occurred after placing the elastomer on the nanotemplate/substrate by hand and applying a slight pressure with tweezers. Before reuse, the nanotemplates were cleaned of organic material by repeating the treatment with oxygen plasma.

Visualization

AFM images were obtained using a Nanoscope Dimension 3000 (Digital Instruments, Santa Barbara, CA) operated in tapping mode using standard silicon cantilevers (174–191 kHz, Nanosensors, Neuchatel, Switzerland). AFM images were planarized, displayed, and analyzed using NanoScope 6.12r1 software.

Phage Preparation

M13 bacteriophage stock (New England Biolabs) was amplified in the host bacteria E.coli (ER2738 NEB) using standard phage methods [25]. Briefly, phage stock (1×10^{12}

pfu mL^{-1}) was added to a 1:100 dilution of an overnight culture of bacteria and incubated with shaking at 37 °C for 5.5 h. Phages were separated from bacteria via centrifugation and concentrated by polyethylene glycol/NaCl precipitation overnight at 4 °C, followed by centrifugation. Dialysis of the resulting phage was used to remove excess salts and ensure a correct pH.

Sample Preparation

5mL of phage stock in TBST, Tris-Buffered Saline (TBS) plus 0.1% Tween-20 (Sigma–Aldrich) was incubated under gentle agitation (without using convective flow) with the subtractively printed substrates for 1 h, followed by gentle but thorough washing using TBST, TBS, water (18.2 MØ) and dried with compressed nitrogen. Samples were placed in a vacuum desiccator overnight prior to AFM analysis. In some experiments, viruses were aligned by rinsing in one direction after the immobilization step and before drying the sample.

Results

Methods for patterning viruses, including chemical linkers,(Cheung et al., 2003) nucleic acid hybridization,(Yi et al., 2005) and metal ions (Vega et al., 2005; Vega et al., 2007) have been demonstrated, but often face a tradeoff between specificity and generality of the approach. The use of highly specific antibody interactions, however, has remained relatively unexplored.(Suh et al., 2006) This has mainly been due to the gross loss of antibody activity during sample preparation and processing.(Kusnezow and Hoheisel, 2002) Soft-lithographic methods, such as microcontact printing, have been successful in maintaining biomolecular activities (Bernard et al., 1998) but remain challenged by the vast range of length scales on which biological interactions occur: proteins and viruses (nanometer), cells (micrometer), and tissue (millimeter). This limitation in feature size and pitch is due to the mechanical properties of the elastomeric materials used in the printing of proteins, mainly poly(dimethylsiloxane) (PDMS). To

overcome this limitation, a subtractive printing technique has recently been developed as a versatile method for the patterned transfer of antibodies from solution to substrate through a series of step-wise reductions in nonspecific hydrophobic interactions (Fig. A.1).(Coyer et al., 2007) This method benefits from the use of a featureless elastomer enabling feature sizes, pitches, and total patterned areas that are independent of its mechanical properties (Von Philipsborn et al., 2006) Therefore, these parameters are defined by the lithographic process used in fabricating the template master (Fig. A.1b). A judicious choice of substrate and elastomeric materials allows for the direct transfer of biological material without the need for chemical modification of either the substrate or the biological system. Herein, we apply the subtractive contact printing technique for the nanometer-scale patterning of antibodies with micrometer pitch to capture individual M13 bacteriophages. Further, we explore the effects of both the solution parameters and antibody feature size for the optimization of phage-pattern interactions.

The complexity of biological systems creates large interdependencies on pH, ionic valency and strength, and concentration,which can greatly complicate the driving forces governing immobilization of biological entities to surfaces.(Kumagai et al., 2006) M13 bacteriophage solutions undergo radical physical transformations under minor solution variations due to the filamentous structure (880nm × 6 nm) and large negative surface charge density (SCD, σ) of the virus, which is a known function of pH ($\sigma_{M13} = 1e^{-}256^{-1}\ A^{-2}$ for pH≥7; for comparison, $\sigma_{DNA} = 1e^{-}106^{-1}\ A^{-2}$).(Butler et al., 2003; Zimmermann et al., 1986) Therefore, solution conditions were optimized for the binding of M13 bacteriophage to macroscopic antibody patterns (2μm × 2μm features) to decouple these effects when studying the impact of the feature size. Maintaining a large negative SCD during phage binding was necessary to minimize

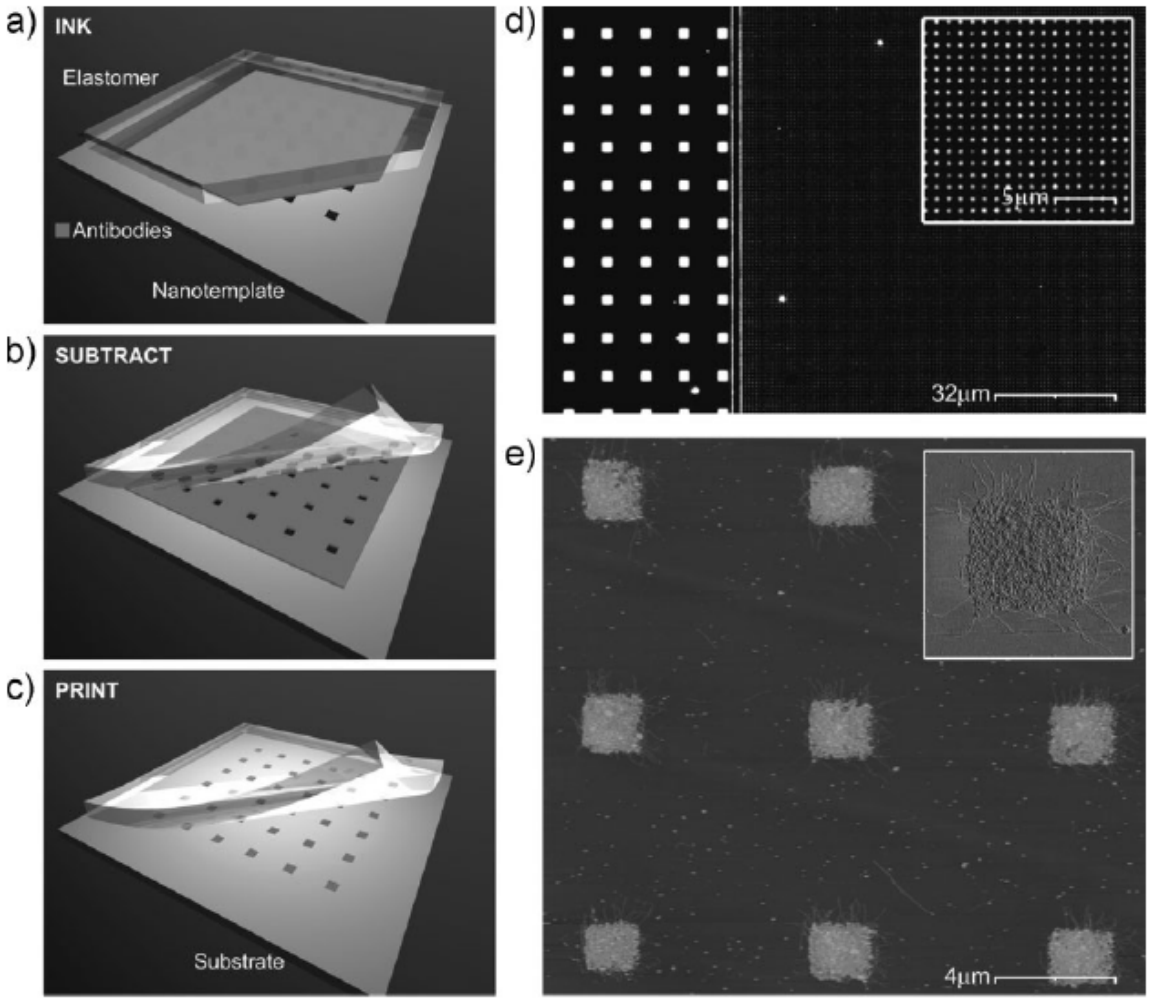

Figure A.1. Subtractive printing of antibodies for producing virus arrays. a) Inking of antibody monolayer from solution to a hydrophobic PDMS elastomeric surface. b) Subtraction of unwanted antibodies from the elastomer using a fabricated silicon nanotemplate. c) Printing of the resulting antibody pattern onto a blank substrate. d) Fluorescence microscope image of patterned fluorescently-tagged antibodies, with the inset showing high-density nanoscale features. e) AFM images revealing the immobilization of phage to 2-mm islands of anti-fd bacteriophage antibodies with minimal background.

multiple-site occupancy and nonspecific background binding by increasing phage–phage and phage–silicon electrostatic repulsion, as silicon also has a negative SCD under standard buffer conditions ($1e^{-}2381^{-1}$ A^{-2}).(Kumagai et al., 2006) Reduction of the ionic strength of the buffered phage solutions by 50% (<75mM NaCl) was used to minimize charge-screening effects. Optimization of the binding conditions resulted incomplete coverage of the patterned antibody, with only minimal nonspecific background binding to the substrate. Importantly, for the given system, where a repulsive electrostatic interaction exists between the phage and the substrate, there was no need for surface passivation.

Achieving single-element arrays requires controlling both the antibody feature size and the binding kinetics. Although reducing the solution concentration of phage can be used to statistically achieve single-element site occupancy, this approach is limited by the binding affinity of the capture antibody. The lower detection limit of the printed anti-M13 bacteriophage capture antibody was determined using patterns with average feature sizes of 240nm × 240 nm, and was consistent with the supplierrecommended working dilution of 10^7 plaque forming units (pfu) mL^{-1}. Phage solutions in the range of 10^7 to 10^9 pfu mL^{-1} incubated with the antibody patterns produced individual, well separated immobilized phages with increasing site occupancy and pattern coverage (Fig. A.2). At phage concentrations above 10^9 pfu mL^{-1}, local changes in the binding statistics were observed and are suggestive of large inhomogeneities in the phage solution. At the highest concentrations studied (10^{10} –10^{11} pfu mL^{-1}), changes in the interactions resulted in phage bundling and the creation of star-like patterns.

Understanding the interactions between the bacteriophage protein coat and the patterned antibody is necessary for achieving single site occupancy. On the 2μm × 2μm macroscopic patterns, atomic force microscopy (AFM) analyses revealed two bacteriophage binding conformations, in which either complete immobilization of the protein coat or localization to the feature edge occurs. Decreasing the feature size below

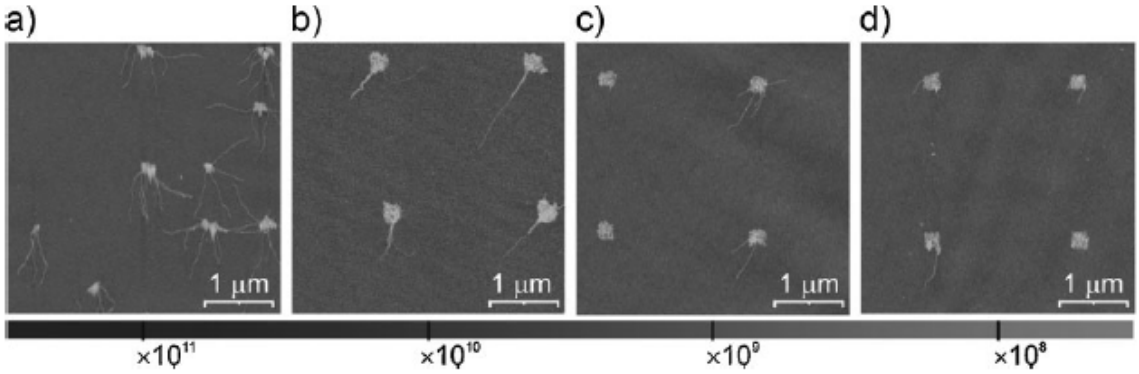

Figure A.2. Activity of printed antibody and optimization of solution conditions for arraying phages. The phage concentration (denoted in pfu mL^{-1} below the images) is one determinant of the formed arrays as revealed by these AFM images. For 240nm × 240nm antibody islands and decreasing concentrations, arrays evolve from a) star-like patterns of multiple phage per site, to b) phage bundling, wherein individual phages bind and then bundle, c) single and multiple phages per site with high occupancy rate, and d) single-phage occupancy with lower site-occupancy level.

~625nm promoted the predominantly edge-binding regime as a result of the physical size and persistence length of the M13 bacteriophage (the commonly reported value is 2.2 μm, with recent reports suggesting an even shorter length of 1.2μm (Khalil et al., 2007). The extension of the phage off of the antibody feature increases the repulsive electrostatic phage–silicon interaction, driving the majority of the protein coat into solution. Patterns having average antibody features of 240nm × 240 nm, 200nm × 200 nm, and 90nm × 90nm were incubated with a phage solution of 109 pfu mL^{-1} at a pH and ionic strength as previously optimized. Antibody patterns having average feature sizes of 240nm × 240nm had a majority of sites occupied by two or more phages (this was found to be easily manipulable by minor changes in solution conditions). Reduction of the antibody feature size to 200nm × 200nm achieved arrays with 42% single site occupancy and high coverage with a greater degree of reproducibility than the larger patterns had. However, a number of sites having two or more phages (21%) still remained. Further reduction of the antibody feature size to 90nm × 90nm achieved complete single site occupancy at the cost of low coverage (20%). At these dimensions, the low occupancy probably originates from the detachment of the phage-bound antibodies during sample washing.

The high aspect ratio of the M13 bacteriophage provides a sufficiently large hydrodynamic coefficient of drag for alignment in fluid flows.(Takeuchi et al., 1996) Given the extent of the phage coat in solution for the nanoscale features, control over the direction of arrayed phage was achievable by using flow alignment. This enabled a four-fold increase in the density of the arrayed phage by decreasing the interfeature spacing from 2.5 to 1.0 μm (Fig. A.3). Multiple fields with antibody islands having a size of 200nm × 200nm and with an area of 0.25 mm^2 were patterned in one step on silicon substrates. These fields can be repeated over a total area of 30mm × 30mm using reasonable (24 h or less) electron-beam writing times. Given a 1mm pitch between islands and an average phage occupancy per island of 42%, at least 3×10^5 phages can be arrayed per mm^2 of substrate. In practice, a phage library having a concentration of 10^9

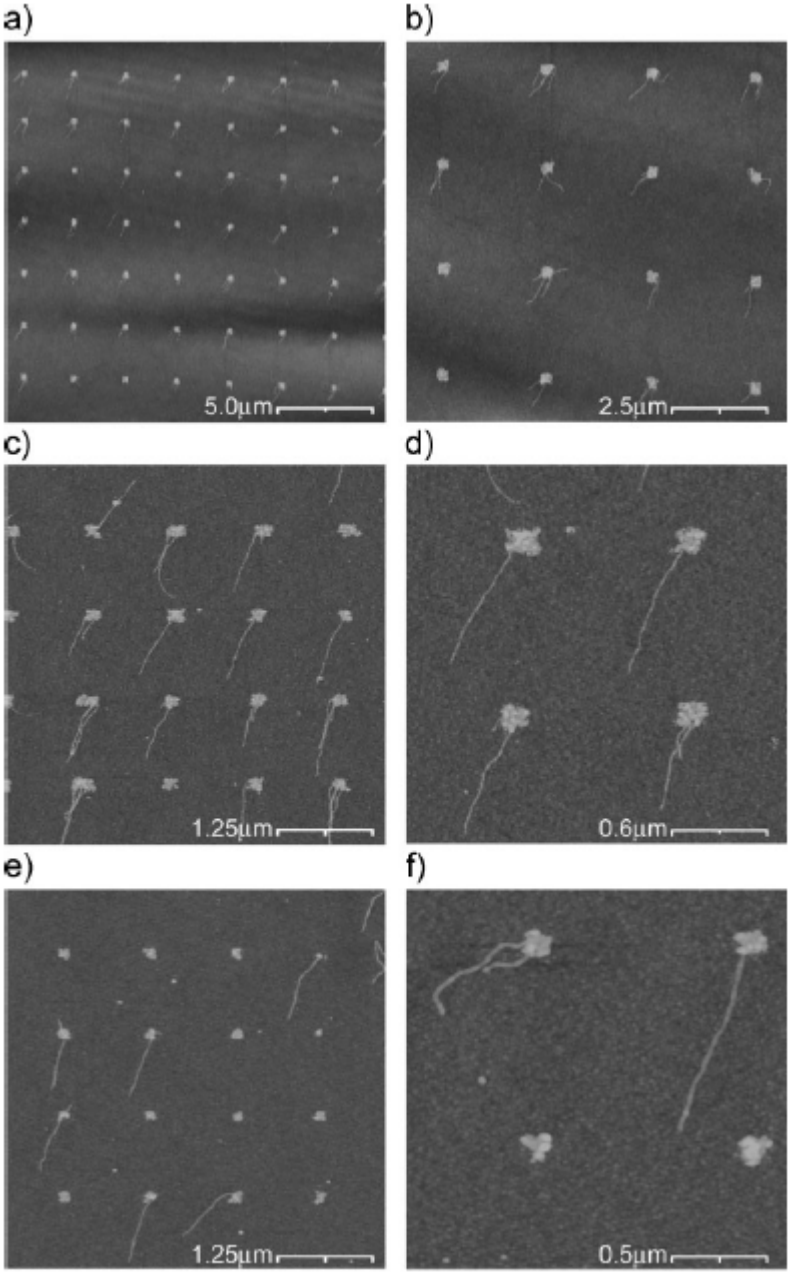

Figure A.3. Influence of the size of antibody islands on the virus arrays as assessed using AFM. Feature sizes are 240nm × 240nm (a,b), 200nm × 200nm (c,d), and 90nm × 90nm (e,f).

pfu mL^{-1} can easily be made to a volume of 100mL, which is sufficient to incubate several cm^2 of substrate. The maximum size of an array is therefore not limited by the antibody patterning or phage assembly steps. Observation of extensive bending of the phage in the liquid flow implies a strong antibody–protein binding and suggests a possible means of studying the persistence length of filamentous systems. Increasing the phage density and alignment to prefabricated structures for the creation of more complex architectures can therefore be realized using the combination of subtractive printing and flow alignment.

We extended the previous experiments, which aimed at identifying parameters responsible for nonspecific phage deposition, phage bundling, and island occupancy, in order to refine the conditions for which at least one phage is present per island, (Fig. A.4). Islands (n=114) with a lateral size of ~250nm were analyzed using atomic force microscopy (AFM) and a strong reduction in the chance of having at least one phage per island was observed only when the concentration decreased below 5×10^9 pfu mL^{-1}. In comparison, 100-nm islands (n=299) had a strongly reduced fractional occupancy: the fractional occupancy was only 59% at a starting concentration of 5×10^{10} pfu mL^{-1} and diminished to 18% and 3% for phage concentrations of respectively 5×10^9 and 5×10^8 pfu mL^{-1}. Two sets of conditions may therefore be used for arraying phages. If single phage arrays are desired, they should be arrayed on a 100-nm antibody island at a concentration of 5×10^{10} pfu mL^{-1}. If arrays with very high density are desired and multiple island occupancy is unimportant, for example, if identical phages must be arrayed, then 250-nm islands and a phage concentration of 5×10^{10} pfu mL^{-1} should be selected.

Using nanoscale patterns of antibodies directed against a phage coat protein, as it was done here, provides a general strategy for arraying phages irrespectively of their biological diversity: identical phages or different phages forming a library can be arrayed in the same way. The arrayed phages may subsequently be exposed to ligands of interest

and phage–ligand interactions may be identified using simple surface fluorescence assays. Organization of biological systems into functional, addressable arrays has many technological applications, including microarray technology and bottom-up nanoassemblies.(Nam et al., 2008) Beyond the technical implications, addressable arrays of individual biological components have the potential to elucidate the intricate relationships between spatial organization and resulting functionality in biological systems. Macroscopic cellular activities such as proliferation, migration, and differentiation all rely on interactions with elements whose size and organization are defined at the nanoscale. Extending the understanding of these processes from the ensemble to the molecular level will enable more advanced diagnostics and therapeutics.

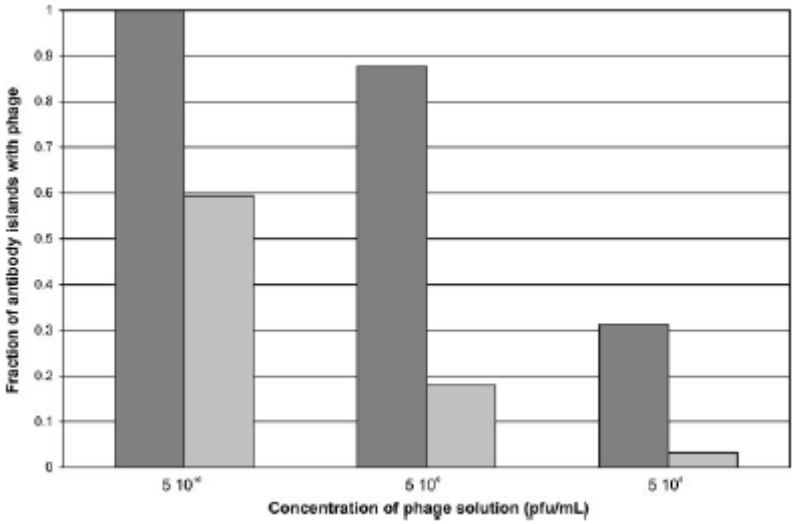

Figure A.4. Fraction of antibody islands having at least one phage as a function of the concentration of phages in solution and island size. Darkand light-grey histograms, respectively, correspond to square islands of approximately 250 and 100 nm in lateral dimension.

Discussion and Conclusion

Using nanoscale patterns of antibodies directed against a phage coat protein, as it was done here, provides a general strategy for arraying phages irrespectively of their biological diversity: identical phages or different phages forming a library can be arrayed in the same way. The arrayed phages may subsequently be exposed to ligands of interest and phage–ligand interactions may be identified using simple surface fluorescence assays. Organization of biological systems into functional, addressable arrays has many technological applications, including microarray technology and bottom-up nanoassemblies.(Nam et al., 2008) Beyond the technical implications, addressable arrays of individual biological components have the potential to elucidate the intricate relationships between spatial organization and resulting functionality in biological systems.Macroscopic cellular activities such as proliferation, migration, and differentiation all rely on interactions with elements whose size and organization are defined at the nanoscale. Extending the understanding of these processes from the ensemble to the molecular level will enable more advanced diagnostics and therapeutics.

APPENDIX B

POLY(DIMETHYLSILOXANE) ELASTOMERS WITH TETHERED PEPTIDE LIGANDS FOR CELL ADHESION STUDIES

Summary

Poly(dimethylsiloxane) (PDMS) is the choice of material for a wide range of bio- and non-biological applications because of its chemical inertness, non-toxicity, ease of handling, and commercial availability. However, PDMS exhibits uncontrolled interactions with biological components (proteins, cells) and it has proven difficult to functionalize to present bioactive ligands. We present a facile strategy for functional surface modification of PDMS using commercial reagents to engineer polymer brushes of oligo(ethylene glycol) methacrylate that prevent cell adhesion and can be functionalized to display bioadhesive ligands. The polymer brushes resist biofouling and prevent cell adhesion, and bioadhesive peptides can be tethered either uniformly or constrained to micropatterned domains using standard peptide chemistry approaches. This approach is relevant to various biomedical and biotechnological applications.

Introduction

Mechanochemical interactions of cells with their surrounding matrix provide forces and signaling cues regulating cell fate and processes such as survival, cell cycle progression and the expression of differentiated phenotypes (Geiger et al., 2009; Vogel and Sheetz, 2006; Vogel and Sheetz, 2009). Cell adhesion to extracellular matrix components, including fibronectin (FN), collagen, and laminin, is primarily mediated by the integrin family of transmembrane receptors (Hynes, 2002).

* Modified from Wu, Y., Coyer, S.R., Garcia, A.J., Ma, H. Poly(dimethylsiloxane) Elastomers with Tethered Peptide Ligands for Cell Adhesion Studies. *Acta Biomterialia.* Article in press (2010).

Following ligand binding, integrins cluster together and promote the assembly of supramolecular complexes containing signaling and structural components that coordinate mechanotransduction pathways (Zaidel-Bar et al., 2007). Adhesive interactions have been exploited in various biomedical and biotechnological applications to control cell and tissue responses (Garcia, 2005; Langer and Tirrell, 2004; Lutolf and Hubbell, 2005). These strategies have principally focused on presenting bioadhesive proteins or oligopeptides derived from extracellular matrix proteins to target integrin receptors in order to direct cell adhesive responses. Moreover, recent evidence indicates that the mechanical properties of the surrounding matrix (e.g., elastic modulus) significantly contribute to mechanotransduction events in diverse cellular processes including stem cell commitment, cell differentiation, and transformation (Engler et al., 2006; Isenberg et al., 2009; Khatiwala et al., 2009; Paszek et al., 2005).

Synthetic and natural materials, including poly(acrylamide) and poly(ethylene glycol) gels, alginate, and agarose, have been used to engineer substrates with defined mechanical properties that are functionalized with bioadhesive ligands to direct adhesion (Boontheekul et al., 2007; Dillon et al., 1998; Greenfield et al., 2009; Guarnieri et al., 2007; Kandow et al., 2007; Lutolf and Hubbell, 2003; Peyton et al., 2006; Wang et al., 2001). Nevertheless, these materials present limitations related to processability, range of mechanical properties (modulus, strain to failure, duty cycle), and compatibility with other materials that hinder their broad applicability in other fields such as MEMs and microfluidics. In contrast, poly(dimethylsiloxane) (PDMS) is the choice of material for a wide range of bio- and non-biological applications because of its chemical inertness, non-toxicity, ease of handling, and commercial availability (El-Ali et al., 2006; Psaltis et al., 2006; Whitesides, 2006). However, PDMS exhibits uncontrolled interactions with biological components (proteins, cells) and it has proven difficult to functionalize to present bioactive ligands. To address these limitations, we developed a facile strategy for functional surface modification of PDMS using commercial reagents to generate an

initiator-integrated PDMS (iPDMS) which is amenable to surface-initiated polymerization (Wu et al., 2007). In the present work, we engineered polymer brushes of oligo(ethylene glycol) methacrylate that prevent cell adhesion and can be functionalized to display bioadhesive ligands.

Materials and Methods

Reagents and Cells

The vinyl-terminated initiator was purchased from HRBio (Beijing, China). Sylgard 184 was obtained from Dow Corning. Oligo(ethylene glycol) methacrylate (Mn = 526, OEGMA526) and other chemicals were purchased from Aldrich and used as received. Human plasma FN, cell culture reagents, rhodamine-phalloidin, and AlexaFluor-conjugated antibodies were purchased from Invitrogen (Carlsbad, CA). Monoclonal antibody against vinculin (clone V284) was obtained from Millipore (Billerica, MA). NIH3T3 fibroblasts (American Type Culture Collection, Manassas, VA) were cultured in Dulbecco's modified Eagle medium supplemented with 10% fetal calf serum (Hyclone Laboratories, Logan, UT) and penicillin-streptomycin. Cells were sub-cultured every two-three days using standard techniques.

Preparation of iPDMS and Polymer Brushes

Sylgard 184 was used as the model elastomer. To prepare regular PDMS substrates, the viscous base (component A) and the curing agent (component B) were mixed well (10:1 ratio by weight) and cured at 80 C for 2 h. To prepare iPDMS, a third component (component C), the vinyl terminated initiator, was mixed well with the base and curing agent, and cured as described for PDMS. The component C reacts with hydrosilane hydrogens in the presence of Pt catalyst, and is covalently integrated into the highly cross-linked three-dimensional network (Wu et al., 2007).

Surface-initiated atom transfer radical polymerization with OEGMA526 was carried out as previously described (Wu et al., 2007). Briefly, the reaction mixture was prepared by thoroughly mixing two parts. Part 1 was a transparent, pale-blue solution, prepared by adding a specified amount of CuCl2/2,2'-bipyridine (Bipy) (1:2 mole ratio) and a fixed amount of monomer to 5 mL MilliQ-water. Part 2 was a colorless solution, prepared by adding a specified amount of ascorbic acid to 5 mL MilliQ-water. After both solutions were deoxygenated, two parts were mixed together under nitrogen. The mixture was further deoxygenated and the resulting mixture was red in color due to the reduction of deactivator Cu(II)/Bipy complex to activator Cu(I)/Bipy complex. The mixture had a molar ratio of OEGMA526/HEMA/CuCl2/Bipy/AscA =20/200/1/2/1, with a feed of 2.76 mM CuCl2. This mixture was then transferred to cover the iPDMS sample under nitrogen atmosphere and surface-initiated polymerization was initiated and continued for 30 min at 25 °C. The polymerization was stopped when iPDMS was removed from the solution. The iPDMS sheets after SIP were first incubated in an aqueous solution of 1 M bromoacetic acid and 2 M sodium hydroxide for overnight to generate terminal carboxyl groups. Samples were thoroughly rinsed with methanol, milliQ-water, and dried under flowing nitrogen before further treatment.

Polymer brushes were characterized by goniometry and X-ray photoelectron spectroscopy (XPS). Static water contact angles were measured on a Dataphysics OCA20 contact angle system (Filderstadt, Germany) at room temperature. XPS was carried out using monochromatic Al Ká X-rays (1486.7 eV) in an AXIS Ultra instrument (Kratos Analytical, UK). The X-ray source was 2 mm nominal X-ray spot size operating at 15 kV and 12 mA for both survey and high-resolution spectra. Survey spectra (0-1100 eV) were recorded at 160 eV pass energy with an energy step of 1.0 eV, and a dwell time of 200 ms. High-resolution spectra were recorded at 40 eV pass energy with an energy step of 0.1 eV and a dwell time of 500 ms with a typical average of 3 scans. All peaks were referenced to C1s (CHx) at 285 eV in the survey scan spectra and C1s (CHx) at

284.8 eV in the deconvoluted high resolution C 1s spectra. All data were collected and analyzed using software provided by the manufacturer.

Biofunctionalization and Cell Adhesion Studies

Human plasma FN was tethered to polymer brushes using standard peptide chemistry as previously described (Petrie et al., 2006). Briefly, following extensive washing in 70% ethanol and ultrapure H_2O, samples were incubated in 2.0 mM EDC and 5.0 mM NHS in 0.1 M 2-(N-morpho)ethanesulfonic acid and 0.5 M NaCl (pH 6.0). FN solution (20 ìg/mL in PBS) was then incubated on the activated supports for 30 min and unreacted surface NHS esters then quenched in 20 mM glycine. For micropatterning experiments, PDMS stamps with desired features were inked with FN solution (100 ìg/mL) and stamped onto activated substrates for 30 sec.

Cells were detached (0.05% trypsin) from culture dishes, resuspended in serum-containing media, and plated onto PDMS samples. Cells were allowed to adhere and spread in the presence of 10% serum. On the next day, cells were permeabilized in cytoskeleton buffer with protease inhibitors (0.5% Triton X-100 in 50 mM NaCl, 150 mM sucrose, 3 mM $MgCl_2$, 20 ìg/mL aprotinin, 1 ìg/mL leupeptin, 1 mM PMSF, 50 mM Tris, pH 6) for 10 min and fixed in 3.7% formaldehyde for 5 min. After blocking in 5% FBS, samples were incubated in primary antibodies against vinculin, washed, incubated in AlexaFluor488-conjugated antibodies, rhodamine-phalloidin, and Hoechst dye. Images of adherent cells were obtained using a 60X objective using a Nikon TE-300 microscope (Melville, NY) equipped with a Spot RT camera (Diagnostic Instruments, Sterling Heights, MI).

Results

In the present study, we expand on a facile strategy for functional surface modification of PDMS using commercial reagents to engineer polymer brushes of oligo(ethylene glycol) methacrylate that prevent cell adhesion and can be functionalized to display bioadhesive ligands. This strategy is outlined in Figure 1.

Commercially available PDMS typically consists of two parts: a viscous base and a curing agent, which are mixed at a 10:1 ratio by weight to form PDMS elastomer via a curing process. The main component of the base is a poly(dimethyl-methylvinylsiloxane) prepolymer (component A). It also contains a small amount of platinum (Pt) metal complex as catalyst dissolved in the main component. The curing agent contains a mixture of vinyl-endcapped PDMS precursors and poly(dimethyl-methylhydrogenosiloxane) precursors as cross-linkers (component B). Upon mixing together base and curing agents, the vinyl groups and the hydrosilane hydrogens undergo a hydrosilylation reaction in the presence of Pt catalyst, which results in highly cross-linked three-dimensional networks. The mechanical properties of the elastomer can be altered by varying the A:B ratio. We previously showed that a vinyl-terminated initiator (component C) could compete with vinyl-endcapped PDMS precursors in the hydrosilylation reaction during the curing process, and thus the vinyl-terminated initiator could be integrated in situ into the PDMS networks to generate iPDMS (step 1, Fig. 1) (Wu et al., 2007). We examined different A:B:C ratios and settled on 10:1:0.5 as the mixture cured as regular PDMS and exhibited no significant differences in mechanical properties (Young's modulus 2.12 MPa (PDMS) vs. 2.05 MPa (iPDMS)) or hydrophobocity (water contact angle 112° (PDMS) vs. 114° (iPDMS)).

We carried out surface-initiated polymerization of OEGMA brushes on iPDMS as previously described (Wu et al.) (step 2, Fig. 1). XPS analysis confirmed successful polymerization on iPDMS as demonstrated by the disappearance of the Br peak and characteristic spectra for OEGMA at the C1s peak (Ma et al., 2006) (Figure 2).

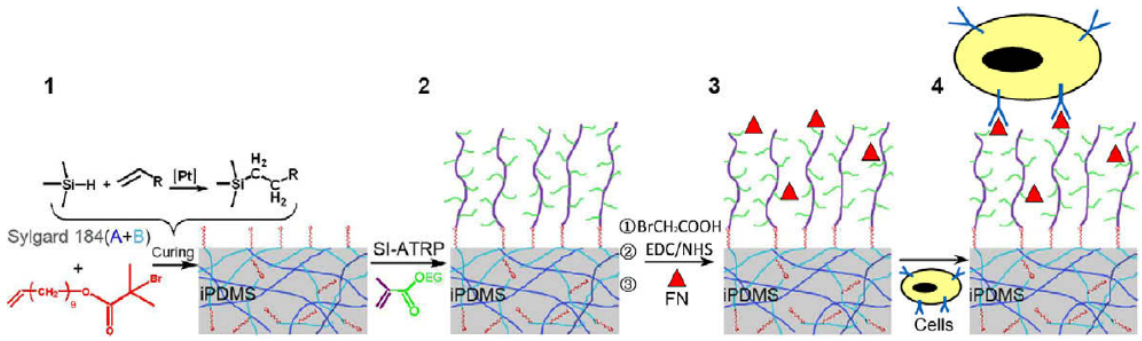

Figure B.1. Schematic of PDMS surface modification to present bioadhesive ligands within non-fouling polymer brushes. 1. Generation of initiator-integrated PDMS (iPDMS). 2. Surface initiated polymerization of oligo(ethylene glycol)methyl methacrylate brushes on PDMS. 3. Tethering of bioadhesive ligand (fibronectin, FN) via EDC/NHS chemistry. 4. Cell adhesion to functionalized surfaces.

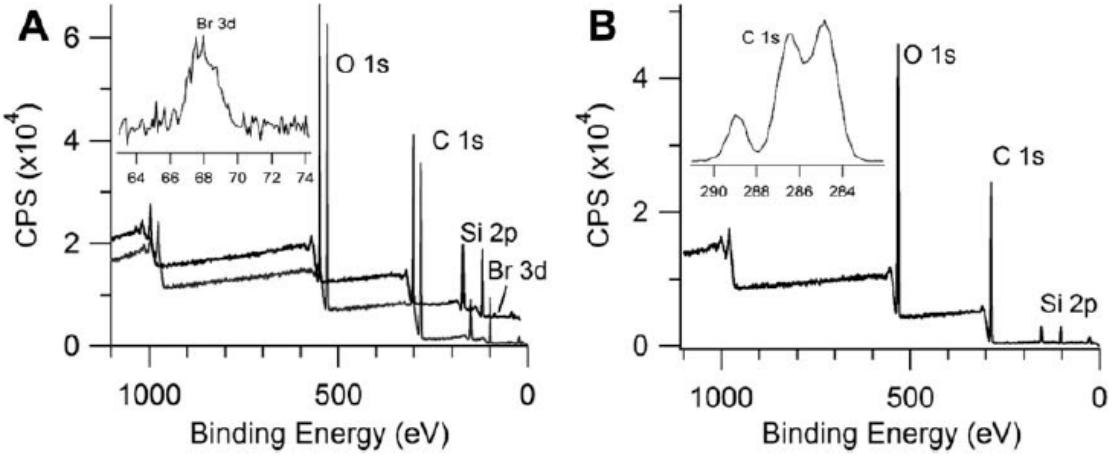

Figure B.2. XPS spectra of functionalized PDMS. A. Spectra for PDMS (black) and iPDMS (gray). Inset shows Br 3d narrow spectrum for iPDMS. B. Spectrum for iPDMS following surface-initiated polymerization showing characteristic bands for OEGMA. Inset shows C1s narrow scan.

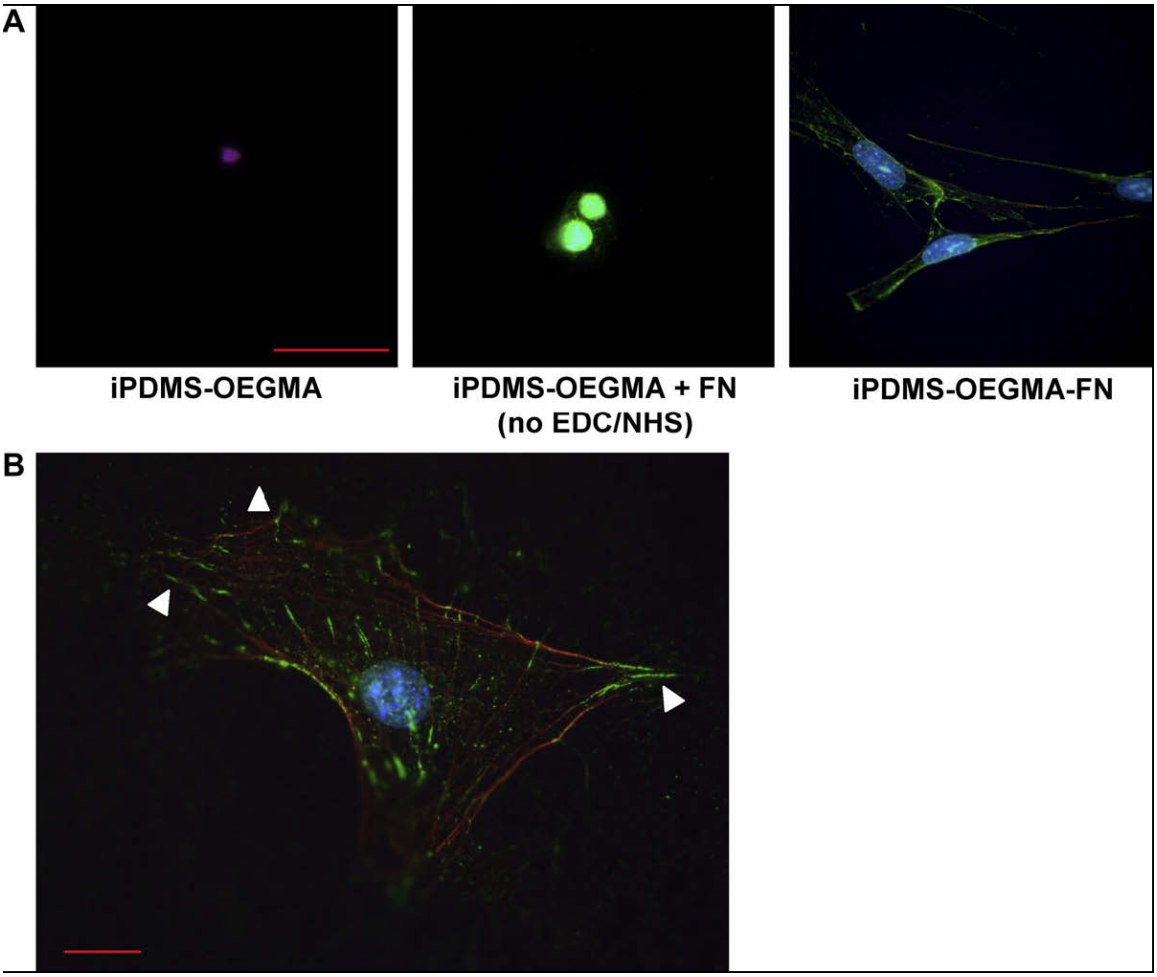

Figure B.3. Cell adhesion to functionalized PDMS in the presence of 10% serum. Immunofluorescence staining for vinculin (green), actin (red) and DNA (blue). A. PDMS presenting polymer brushes functionalized with FN support cell adhesion and spreading (iPDMS-OEGMA-FN) whereas as unfunctionalized brushes (iPDMS-OEGMA) or brushes exposed to FN in the absence of tethering reagents (iPDMS-OEGMA + FN) display minimal cell adhesion. Scale bar 50 μm. B. Cells on PDMS presenting polymer brushes functionalized with FN exhibit prominent actin stress fibers and vinculin-containing focal adhesions. Scale bar 20 μm.

Significant reductions in water contact angle (114° (pre) vs. 57° (post)) following polymerization also showed successful surface modification.

We next functionalized iPDMS substrates presenting polymer brushes with human plasma fibronectin as a model bioadhesive ligand. Fibronectin was tethered onto the brushes using standard EDC/NHS chemistry (step 3, Fig. 1) and the resulting bioactivity was analyzed via cell adhesion and spreading studies (step 4, Fig. 1). Figure 3A presents images of cells cultured overnight on substrates in the presence of 10% serum. As expected, unfunctionalized brushes (iPDMS-OEGMA) supported extremely low levels of cell adhesion and the few cells that attached remained round. iPDMS substrates presenting polymer brushes that were exposed to fibronectin without EDC/NHS activation also exhibited minimal levels of cell adhesion and spreading. These results confirm the non-fouling character of the OEGMA brushes, even in the presence of high concentrations of fibronectin. In contrast, substrates that were incubated to fibronectin following EDC/NHS activation supported high levels of cell adhesion and spreading. Furthermore, cells adhering to these functionalized support displayed prominent actin fibers and vinculin-containing focal adhesions (Figure 3B). Control substrates that were activated in EDC/NHS but incubated in non-adhesive serum albumin instead of fibronectin exhibited minimal cell adhesion and spreading.

As a final demonstration of our ability to functionalize PDMS elastomers with bioadhesive ligands, lanes of fibronectin were microcontact printed onto PDMS samples presenting EDC/NHS-activated polymer brushes (Figure 4). Cells adhered and spread on the micropatterned lanes of fibronectin but remained constrained to the micropatterned domains. Varying the width (5 vs. 50 ìm) of the fibronectin stamp resulted in differences in the number of cells, extent of spreading and focal adhesion assembly per fibronectin lane. These results demonstrate spatial control over the presentation of bioadhesive ligands on non-fouling PDMS elastomers.

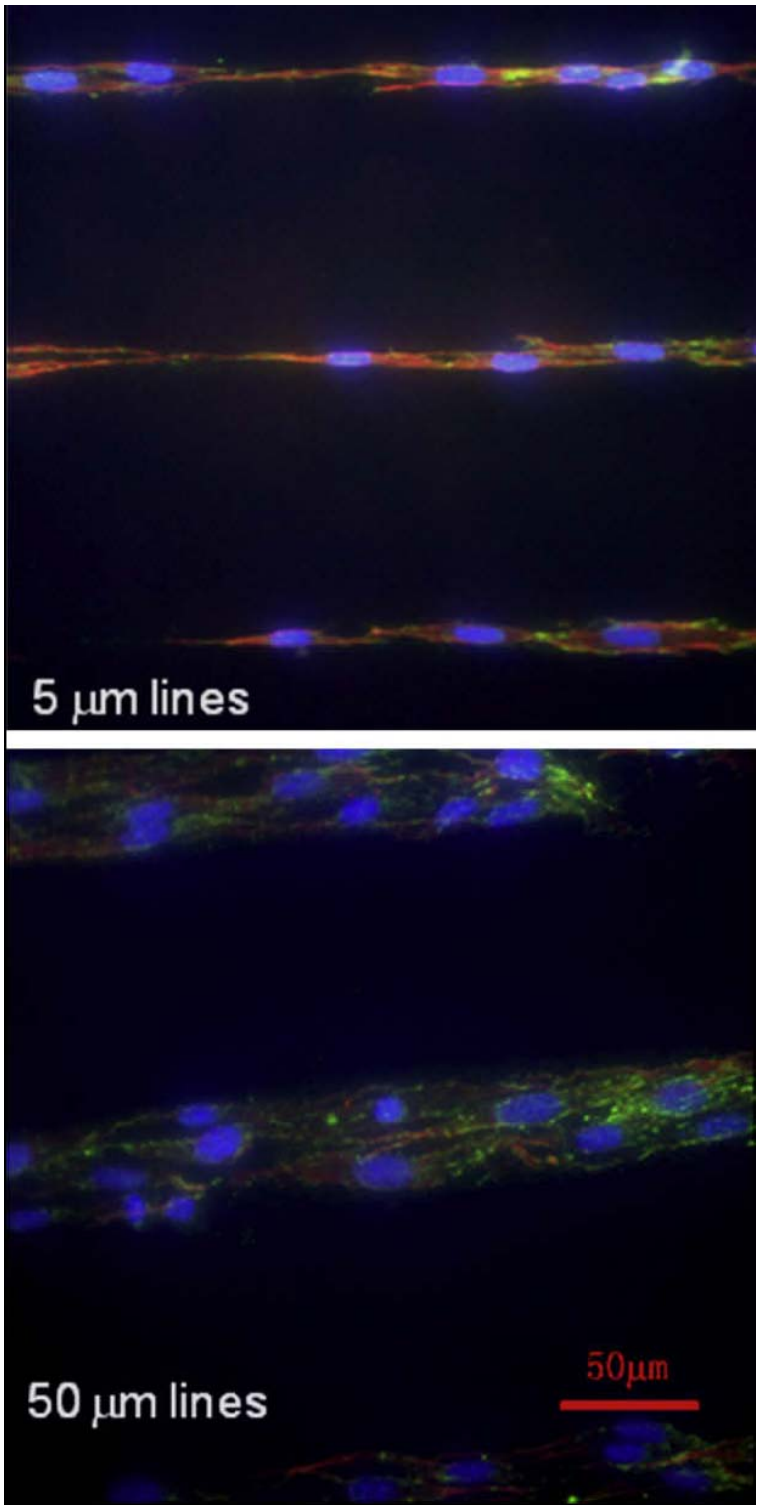

Figure B.4. Cell patterning on PDMS presenting polymer brushes functionalized with FN for 5 and 50 μm width lanes.

Discussion

We expand a strategy for functional surface modification of PDMS using commercial reagents to engineer polymer brushes of oligo(ethylene glycol) methacrylate that prevent cell adhesion and can be functionalized to display bioadhesive ligands. The polymer brushes resist biofouling and prevent cell adhesion, and bioadhesive peptides can be tethered either uniformly or constrained to micropatterned domains using standard peptide chemistry approaches. We expect that this technique will be relevant to numerous bio-MEMS and microfluidics applications as well as fundamental studies of mechanotransduction.

Cell adhesion studies demonstrated that the tethered fibronectin retained full biological activity as evidenced by robust actin cytoskeleton and focal adhesion assembly. Because this approach uses the standard EDC/NHS tethering chemistry, we expect that this technique will be applicable to other peptides and proteins, including growth factors, as well as other molecules presenting primary amines. Whereas the density of tethered ligand was not determined in the present study, we have previously shown that this parameter can be easily controlled by varying the solution concentration of the biomolecule (Petrie et al., 2006; Petrie et al., 2009).

Recent efforts have focused on tethering bioactive factors onto PDMS substrata and demonstrated successful coupling and bioactivity (Klenkler et al., 2008; Klenkler and Sheardown, 2006; Seo et al., 2008). These approaches rely on generating co-polymers with PDMS or multi-step modifications of plasma-treated PDMS. In contrast, the present work shows a more facile and flexible approach that does not alter the mechanical properties of the underlying PDMS support. Furthermore, because there are no intermediate functionalization steps for the biomolecules, the current tethering approach has the flexibility to tether multiple ligands either simultaneously or sequentially without purification steps (Petrie et al., 2009).

Conclusion

We validate a strategy for functional surface modification of PDMS using commercial reagents to engineer polymer brushes of oligo(ethylene glycol) methacrylate that prevent cell adhesion and can be functionalized to display bioadhesive ligands. The polymer brushes resist biofouling and prevent cell adhesion, and bioadhesive peptides can be tethered either uniformly or constrained to micropatterned domains using standard peptide chemistry approaches. As such, this approach is relevant to various biomedical and biotechnological applications.

REFERENCES

Anderson, D.G., Burdick, J.A., and Langer, R. (2004). Materials science - Smart biomaterials. *Science* **305**, 1923-1924.

Anderson, J.M., Bonfield, T.L., and Ziats, N.P. (1990). Protein Adsorption and Cellular Adhesion and Activation on Biomedical Polymers. *International Journal of Artificial Organs* **13**, 375-382.

Arnold, M., Cavalcanti-adam, E.A., Glass, R., Blummel, J., Eck, W., Kantlehner, M., Kessler, H., and Spatz, J.P. (2004). Activation of integrin function by nanopatterned adhesive interfaces. *ChemPhysChem* **5**, 383-388.

Arnold, M., Hirschfeld-Warneken, V.C., Lohmuller, T., Heil, P., Blummel, J., Cavalcanti-Adam, E.A., Lopez-Garcia, M., Walther, P., Kessler, H., Geiger, B., *et al.* (2008). Induction of cell polarization and migration by a gradient of nanoscale variations in adhesive ligand spacing. *Nano Letters* **8**, 2063-2069.

Astrof, N.S., Salas, A., Shimaoka, M., Chen, J.F., and Springer, T.A. (2006). Importance of force linkage in mechanochemistry of adhesion receptors. *Biochemistry* **45**, 15020-15028.

Balaban, N.Q., Schwarz, U.S., Riveline, D., Goichberg, P., Tzur, G., Sabanay, I., Mahalu, D., Safran, S., Bershadsky, A., Addadi, L., *et al.* (2001). Force and focal adhesion assembly: a close relationship studied using elastic micropatterned substrates. *Nature Cell Biology* **3**, 466-472.

Ballestrem, C., Hinz, B., Imhof, B.A., and Wehrle-Haller, B. (2001). Marching at the front and dragging behind: differential alpha-V beta 3-integrin turnover regulates focal adhesion behavior. *Journal of Cell Biology* **155**, 1319-1332.

Beningo, K.A., Dembo, M., Kaverina, I., Small, J.V., and Wang, Y.L. (2001). Nascent focal adhesions are responsible for the generation of strong propulsive forces in migrating fibroblasts. *Journal of Cell Biology* **153**, 881-887.

Bernard, A., Delamarche, E., Schmid, H., Michel, B., Bosshard, H.R., and Biebuyck, H. (1998). Printing patterns of proteins. *Langmuir* **14**, 2225-2229.

Bernard, A., Fitzli, D., Sonderegger, P., Delamarche, E., Michel, B., Bosshard, H.R., and Biebuyck, H. (2001). Affinity capture of proteins from solution and their dissociation by contact printing. *Nature Biotechnology* **19**, 866-869.

Bietsch, A., and Michel, B. (2000). Conformal contact and pattern stability of stamps used for soft lithography. *Journal of Applied Physics* **88**, 4310-4318.

Blank, K., Mai, T., Gilbert, I., Schiffmann, S., Rankl, J., Zivin, R., Tackney, C., Nicolaus, T., Spinnler, K., Oesterhelt, F., *et al.* (2003). A force-based protein biochip. *Proceedings of the National Academy of Sciences of the United States of America* **100**, 11356-11360.

Boontheekul, T., Hill, E.E., Kong, H.J., and Mooney, D.J. (2007). Regulating myoblast phenotype through controlled gel stiffness and degradation. *Tissue Eng* **13**, 1431-1442.

Butler, J.C., Angelini, T., Tang, J.X., and Wong, G.C.L. (2003). Ion multivalence and like-charge polyelectrolyte attraction. *Physical Review Letters* **91**.

Capadona, J.R., Petrie, T.A., Fears, K.R., Latour, R.A., Collard, D.M., and Garcia, A.S.J. (2005). Surface-nucleated assembly of fibrillar extracellular matrices. *Advanced Materials* **17**, 2604-2608.

Chen, C.S., Mrksich, M., Huang, S., Whitesides, G.M., and Ingber, D.E. (1997). Geometric control of cell life and death. *Science* **276**, 1425-1428.

Chen, C.S., Tan, J., and Tien, J. (2004). Mechanotransduction at cell-matrix and cell-cell contacts. *Annual Review of Biomedical Engineering* **6**, 275-302.

Cheung, C.L., Camarero, J.A., Woods, B.W., Lin, T.W., Johnson, J.E., and De Yoreo, J.J. (2003). Fabrication of assembled virus nanostructures on templates of chemoselective linkers formed by scanning probe nanolithography. *Journal of the American Chemical Society* **125**, 6848-6849.

Chicurel, M.E., Chen, C.S., and Ingber, D.E. (1998). Cellular control lies in the balance of forces. *Current Opinion in Cell Biology* **10**, 232-239.

Choquet, D., Felsenfeld, D.P., and Sheetz, M.P. (1997). Extracellular matrix rigidity causes strengthening of integrin-cytoskeleton linkages. *Cell* **88**, 39-48.

Christman, K.L., Enriquez-Rios, V.D., and Maynard, H.D. (2006). Nanopatterning proteins and peptides. *Soft Matter* **2**, 928-939.

Cohen, D.M., Kutscher, B., Chen, H., Murphy, D.B., and Craig, S.W. (2006). A conformational switch in vinculin drives formation and dynamics of a talin-vinculin complex at focal adhesions. *Journal of Biological Chemistry* **281**, 16006-16015.

Cornell, B.A., BraachMaksvytis, V.L.B., King, L.G., Osman, P.D.J., Raguse, B., Wieczorek, L., and Pace, R.J. (1997). A biosensor that uses ion-channel switches. *Nature* **387**, 580-583.

Coussen, F., Choquet, D., Sheetz, M.P., and Erickson, H.P. (2002). Trimers of the fibronectin cell adhesion domain localize to actin filament bundles and undergo rearward translocation. *Journal of Cell Science* **115**, 2581-2590.

Coyer, S.R., Garcia, A.J., and Delamarche, E. (2007). Facile preparation of complex protein architectures with sub-100-nm resolution on surfaces. *Angewandte Chemie-International Edition* **46**, 6837-6840.

De Arcangelis, A., and Georges-Labouesse, E. (2000). Integrin and ECM functions - roles in vertebrate development. *Trends in Genetics* **16**, 389-395.

Dembo, M., Torney, D.C., Saxman, K., and Hammer, D. (1988). THE REACTION-LIMITED KINETICS OF MEMBRANE-TO-SURFACE ADHESION AND DETACHMENT. *Proceedings of the Royal Society of London Series B-Biological Sciences* **234**, 55-83.

Demers, L.M., Ginger, D.S., Park, S.J., Li, Z., Chung, S.W., and Mirkin, C.A. (2002). Direct patterning of modified oligonucleotides on metals and insulators by dip-pen nanolithography. *Science* **296**, 1836-1838.

Dillon, G.P., Yu, X., Sridharan, A., Ranieri, J.P., and Bellamkonda, R.V. (1998). The influence of physical structure and charge on neurite extension in a 3D hydrogel scaffold. *J Biomater Sci Polym Ed* **9**, 1049-1069.

Dugina, V., Fontao, L., Chaponnier, C., Vasiliev, J., and Gabbiani, G. (2001). Focal adhesion features during myofibroblastic differentiation are controlled by intracellular and extracellular factors. *Journal of Cell Science* **114**, 3285-3296.

Dumbauld, D.W., Michael, K.E., Hanks, S.K., and García, A.J. (2010a). Focal adhesion kinase-dependent regulation of adhesive forces involves vinculin recruitment to focal adhesions. *Biology of the Cell* **102**, 203-213.

Dumbauld, D.W., Shin, H., Gallant, N.D., Michael, K.E., Radhakrishna, H., and García, A.J. (2010b). Contractility modulates cell adhesion strengthening through focal adhesion kinase and assembly of vinculin-containing focal adhesions. *Journal of Cellular Physiology* **223**, 746-756.

El-Ali, J., Sorger, P.K., and Jensen, K.F. (2006). Cells on chips. *Nature* **442**, 403-411.

Engler, A.J., Sen, S., Sweeney, H.L., and Discher, D.E. (2006). Matrix elasticity directs stem cell lineage specification. *Cell* **126**, 677-689.

Evans, E.A. (1985). DETAILED MECHANICS OF MEMBRANE-MEMBRANE ADHESION AND SEPARATION .2. DISCRETE KINETICALLY TRAPPED MOLECULAR CROSS-BRIDGES. *Biophysical Journal* **48**, 185-192.

Faull, R.J., Kovach, N.L., Harlan, J.M., and Ginsberg, M.H. (1993). AFFINITY MODULATION OF INTEGRIN ALPHA-5-BETA-1 - REGULATION OF THE FUNCTIONAL-RESPONSE BY SOLUBLE FIBRONECTIN. *Journal of Cell Biology* **121**, 155-162.

Friedland, J.C., Lee, M.H., and Boettiger, D. (2009). Mechanically Activated Integrin Switch Controls alpha(5)beta(1) Function. *Science* **323**, 642-644.

Gallant, N.D., Capadona, J.R., Frazier, A.B., Collard, D.M., and Garcia, A.J. (2002). Micropatterned surfaces to engineer focal adhesions for analysis of cell adhesion strengthening. *Langmuir* **18**, 5579-5584.

Gallant, N.D., and Garcia, A.J. (2007). Model of integrin-mediated cell adhesion strengthening. *Journal of Biomechanics* **40**, 1301-1309.

Gallant, N.D., and Michael, K.E. (2005). Cell Adhesion Strengthening: Contributions of Adhesive Area, Integrin Binding, and Focal Adhesion Assembly. *Molecular Biology of the Cell* **16**, 4329-4340.

Garcia, A.J. (2005). Get a grip: integrins in cell-biomaterial interactions. *Biomaterials* **26**, 7525-7529.

Garcia, A.J., Ducheyne, P., and Boettiger, D. (1997). Quantification of cell adhesion using a spinning disc device and application to surface-reactive materials. *Biomaterials* **18**, 1091-1098.

Garcia, A.J., Huber, F., and Boettiger, D. (1998). Force required to break alpha(5)beta(1) integrin-fibronectin bonds in intact adherent cells is sensitive to integrin activation state. *Journal of Biological Chemistry* **273**, 10988-10993.

Garcia, A.J., Vega, M.D., and Boettiger, D. (1999). Modulation of cell proliferation and differentiation through substrate-dependent changes in fibronectin conformation. *Molecular Biology of the Cell* **10**, 785-798.

Gates, B.D., Xu, Q.B., Stewart, M., Ryan, D., Willson, C.G., and Whitesides, G.M. (2005). New approaches to nanofabrication: Molding, printing, and other techniques. *Chemical Reviews* **105**, 1171-1196.

Geiger, B., Spatz, J.P., and Bershadsky, A.D. (2009). Environmental sensing through focal adhesions. *Nat Rev Mol Cell Biol* **10**, 21-33.

Geissler, M., Bernard, A., Bietsch, A., Schmid, H., Michel, B., and Delamarche, E. (2000). Microcontact-printing chemical patterns with flat stamps. *Journal of the American Chemical Society* **122**, 6303-6304.

Giannone, G., Dubin-Thaler, B.J., Rossier, O., Cai, Y.F., Chaga, O., Jiang, G.Y., Beaver, W., Dobereiner, H.G., Freund, Y., Borisy, G.*, et al.* (2007). Lamellipodial actin mechanically links myosin activity with adhesion-site formation. *Cell* **128**, 561-575.

Ginsberg, M.H., Partridge, A., and Shattil, S.J. (2005). Integrin regulation. *Current Opinion in Cell Biology* **17**, 509-516.

Glass, R., Arnold, M., Blummel, J., Kuller, A., Moller, M., and Spatz, J.P. (2003). Micro-nanostructured interfaces fabricated by the use of inorganic block copolymer micellar monolayers as negative resist for electron-beam lithography. *Advanced Functional Materials* **13**, 569-575.

Goffin, J.M., Pittet, P., Csucs, G., Lussi, J.W., Meister, J.J., and Hinz, B. (2006). Focal adhesion size controls tension-dependent recruitment of alpha-smooth muscle actin to stress fibers. *Journal of Cell Biology* **172**, 259-268.

Greenfield, M.A., Hoffman, J.R., Olvera de la Cruz, M., and Stupp, S.I. (2009). Tunable Mechanics of Peptide Nanofiber Gels. *Langmuir*.

Guarnieri, D., Battista, S., Borzacchiello, A., Mayol, L., De Rosa, E., Keene, D.R., Muscariello, L., Barbarisi, A., and Netti, P.A. (2007). Effects of fibronectin and laminin on structural, mechanical and transport properties of 3D collageneous network. *J Mater Sci Mater Med* **18**, 245-253.

Gumbiner, B.M. (1996). Cell adhesion: The molecular basis of tissue architecture and morphogenesis. *Cell* **84**, 345-357.

Gupton, S.L., and Waterman-Storer, C.M. (2006). Spatiotemporal feedback between actomyosin and focal-adhesion systems optimizes rapid cell migration. *Cell* **125**, 1361-1374.

Hammer, D.A., and Lauffenburger, D.A. (1987). A DYNAMIC-MODEL FOR RECEPTOR-MEDIATED CELL-ADHESION TO SURFACES. *Biophysical Journal* **52**, 475-487.

Hato, T., Pampori, N., and Shattil, S.J. (1998). Complementary roles for receptor clustering and conformational change in the adhesive and signaling functions of integrin alpha(IIb)beta(3). *Journal of Cell Biology* **141**, 1685-1695.

Hui, E.E., and Bhatia, S.N. (2007). Microscale control of cell contact and spacing via three-component surface patterning. *Langmuir* **23**, 4103-4107.

Hynes, R.O. (2002). Integrins: Bidirectional, allosteric signaling machines. *Cell* **110**, 673-687.

Isenberg, B.C., Dimilla, P.A., Walker, M., Kim, S., and Wong, J.Y. (2009). Vascular smooth muscle cell durotaxis depends on substrate stiffness gradient strength. *Biophys J* **97**, 1313-1322.

James, C.D., Davis, R.C., Kam, L., Craighead, H.G., Isaacson, M., Turner, J.N., and Shain, W. (1998). Patterned protein layers on solid substrates by thin stamp microcontact printing. *Langmuir* **14**, 741-744.

Jiang, G.Y., Giannone, G., Critchley, D.R., Fukumoto, E., and Sheetz, M.P. (2003). Two-piconewton slip bond between fibronectin and the cytoskeleton depends on talin. *Nature* **424**, 334-337.

Jonkheijm, P., Weinrich, D., Schroder, H., Niemeyer, C.M., and Waldmann, H. (2008). Chemical Strategies for Generating Protein Biochips. *Angewandte Chemie-International Edition* **47**, 9618-9647.

Kandow, C.E., Georges, P.C., Janmey, P.A., and Beningo, K.A. (2007). Polyacrylamide hydrogels for cell mechanics: steps toward optimization and alternative uses. *Methods Cell Biol* **83**, 29-46.

Kato, M., and Mrksich, M. (2004). Using model substrates to study the dependence of focal adhesion formation on the affinity of integrin-ligand complexes. *Biochemistry* **43**, 2699-2707.

Keselowsky, B.G., Collard, D.M., and Garcia, A.J. (2003). Surface chemistry modulates fibronectin conformation and directs integrin binding and specificity to control cell adhesion. *Journal of Biomedical Materials Research Part A* **66A**, 247-259.

Keselowsky, B.G., and Garcia, A.J. (2005). Quantitative methods for analysis of integrin binding and focal adhesion formation on biomaterial surfaces. *Biomaterials* **26**, 413-418.

Khalil, A.S., Ferrer, J.M., Brau, R.R., Kottmann, S.T., Noren, C.J., Lang, M.J., and Belcher, A.M. (2007). Single M13 bacteriophage tethering and stretching. *Proceedings of the National Academy of Sciences of the United States of America* **104**, 4892-4897.

Khatiwala, C.B., Kim, P.D., Peyton, S.R., and Putnam, A.J. (2009). ECM compliance regulates osteogenesis by influencing MAPK signaling downstream of RhoA and ROCK. *J Bone Miner Res* **24**, 886-898.

Klenkler, B.J., Chen, H., Chen, Y., Brook, M.A., and Sheardown, H. (2008). A high-density PEG interfacial layer alters the response to an EGF tethered polydimethylsiloxane surface. *J Biomater Sci Polym Ed* **19**, 1411-1424.

Klenkler, B.J., and Sheardown, H. (2006). Characterization of EGF coupling to aminated silicone rubber surfaces. *Biotechnol Bioeng* **95**, 1158-1166.

Kloboucek, A., Behrisch, A., Faix, J., and Sackmann, E. (1999). Adhesion-induced receptor segregation and adhesion plaque formation: A model membrane study. *Biophysical Journal* **77**, 2311-2328.

Koch, W.H. (2004). Technology platforms for pharmacogenomic diagnostic assays. *Nature Reviews Drug Discovery* **3**, 749-761.

Kong, F., Garcia, A.J., Mould, A.P., Humphries, M.J., and Zhu, C. (2009). Demonstration of catch bonds between an integrin and its ligand. *Journal of Cell Biology* **185**, 1275-1284.

Koo, L.Y., Irvine, D.J., Mayes, A.M., Lauffenburger, D.A., and Griffith, L.G. (2002). Co-regulation of cell adhesion by nanoscale RGD organization and mechanical stimulus. *Journal of Cell Science* **115**, 1423-1433.

Kumagai, S., Yoshii, S., Yamada, K., Matsukawa, N., Fujiwara, I., Iwahori, K., and Yamashita, I. (2006). Electrostatic placement of single ferritin molecules. *Applied Physics Letters* **88**.

Kumar, A., Biebuyck, H.A., and Whitesides, G.M. (1994). Patterning Self-Assembled Monolayers - Applications in Materials Science. *Langmuir* **10**, 1498-1511.

Kumar, A., and Whitesides, G.M. (1993). FEATURES OF GOLD HAVING MICROMETER TO CENTIMETER DIMENSIONS CAN BE FORMED THROUGH A COMBINATION OF STAMPING WITH AN ELASTOMERIC STAMP AND AN ALKANETHIOL INK FOLLOWED BY CHEMICAL ETCHING. *Applied Physics Letters* **63**, 2002-2004.

Kusnezow, W., and Hoheisel, J.D. (2002). Antibody microarrays: Promises and problems. *Biotechniques*, 14-+.

Laflamme, S.E., Akiyama, S.K., and Yamada, K.M. (1992). REGULATION OF FIBRONECTIN RECEPTOR DISTRIBUTION. *Journal of Cell Biology* **117**, 437-447.

Lahiri, J., Isaacs, L., Tien, J., and Whitesides, G.M. (1999a). A strategy for the generation of surfaces presenting ligands for studies of binding based on an active ester as a common reactive intermediate: A surface plasmon resonance study. *Analytical Chemistry* **71**, 777-790.

Lahiri, J., Ostuni, E., and Whitesides, G.M. (1999b). Patterning ligands on reactive SAMs by microcontact printing. *Langmuir* **15**, 2055-2060.

Langer, R., and Tirrell, D.A. (2004). Designing materials for biology and medicine. *Nature* **428**, 487-492.

Lee, K.B., Kim, E.Y., Mirkin, C.A., and Wolinsky, S.M. (2004). The use of nanoarrays for highly sensitive and selective detection of human immunodeficiency virus type 1 in plasma. *Nano Letters* **4**, 1869-1872.

Lee, K.B., Park, S.J., Mirkin, C.A., Smith, J.C., and Mrksich, M. (2002a). Protein nanoarrays generated by dip-pen nanolithography. *Science* **295**, 1702-1705.

Lee, S.W., Mao, C.B., Flynn, C.E., and Belcher, A.M. (2002b). Ordering of quantum dots using genetically engineered viruses. *Science* **296**, 892-895.

Lee, S.W., Oh, B.K., Sanedrin, R.G., Salaita, K., Fujigaya, T., and Mirkin, C.A. (2006). Biologically active protein nanoarrays generated using parallel dip-pen nanolithography. *Advanced Materials* **18**, 1133-+.

Lehnert, D., Wehrle-Haller, B., David, C., Weiland, U., Ballestrem, C., Imhof, B.A., and Bastmeyer, M. (2004). Cell behaviour on micropatterned substrata: limits of extracellular matrix geometry for spreading and adhesion. *Journal of Cell Science* **117**, 41-52.

Lim, J.H., Ginger, D.S., Lee, K.B., Heo, J., Nam, J.M., and Mirkin, C.A. (2003). Direct-write dip-pen nanolithography of proteins on modified silicon oxide surfaces. *Angewandte Chemie-International Edition* **42**, 2309-2312.

Liu, G.Y., and Amro, N.A. (2002). Positioning protein molecules on surfaces: A nanoengineering approach to supramolecular chemistry. *Proceedings of the National Academy of Sciences of the United States of America* **99**, 5165-5170.

Lopez, G.P., Albers, M.W., Schreiber, S.L., Carroll, R., Peralta, E., and Whitesides, G.M. (1993a). CONVENIENT METHODS FOR PATTERNING THE ADHESION OF MAMMALIAN-CELLS TO SURFACES USING SELF-ASSEMBLED MONOLAYERS OF ALKANETHIOLATES ON GOLD. *Journal of the American Chemical Society* **115**, 5877-5878.

Lopez, G.P., Biebuyck, H.A., Harter, R., Kumar, A., and Whitesides, G.M. (1993b). Fabrication and Imaging of 2-Dimensional Patterns of Proteins Adsorbed on Self-Assembled Monolayers by Scanning Electron-Microscopy. *Journal of the American Chemical Society* **115**, 10774-10781.

Lotz, M.M., Burdsal, C.A., Erickson, H.P., and McClay, D.R. (1989). CELL-ADHESION TO FIBRONECTIN AND TENASCIN - QUANTITATIVE MEASUREMENTS OF INITIAL BINDING AND SUBSEQUENT STRENGTHENING RESPONSE. *Journal of Cell Biology* **109**, 1795-1805.

Love, J.C., Estroff, L.A., Kriebel, J.K., Nuzzo, R.G., and Whitesides, G.M. (2005). Self-assembled monolayers of thiolates on metals as a form of nanotechnology. *Chemical Reviews* **105**, 1103-1169.

Lutolf, M.P., and Hubbell, J.A. (2003). Synthesis and physicochemical characterization of end-linked poly(ethylene glycol)-co-peptide hydrogels formed by Michael-type addition. *Biomacromolecules* **4**, 713-722.

Lutolf, M.P., and Hubbell, J.A. (2005). Synthetic biomaterials as instructive extracellular microenvironments for morphogenesis in tissue engineering. *Nature Biotechnology* **23**, 47-55.

Ma, H., Wells, M., Beebe, T.P., and Chilkoti, A. (2006). Surface-initiated atom transfer radical polymerization of oligo(ethylene glycol) methyl methacrylate from a mixed self-assembled monolayer on gold. *Adv Funct Mater* **16**, 640-648.

Malmstrom, J., Christensen, B., Jakobsen, H.P., Lovmand, J., Foldbjerg, R., Sorensen, E.S., and Sutherland, D.S. (2010). Large Area Protein Patterning Reveals Nanoscale Control of Focal Adhesion Development. *Nano Letters* **10**, 686-694.

Mao, C.B., Solis, D.J., Reiss, B.D., Kottmann, S.T., Sweeney, R.Y., Hayhurst, A., Georgiou, G., Iverson, B., and Belcher, A.M. (2004). Virus-based toolkit for the directed synthesis of magnetic and semiconducting nanowires. *Science* **303**, 213-217.

Massia, S.P., and Hubbell, J.A. (1991). AN RGD SPACING OF 440NM IS SUFFICIENT FOR INTEGRIN ALPHA-V-BETA-3-MEDIATED FIBROBLAST SPREADING AND 140NM FOR FOCAL CONTACT AND STRESS FIBER FORMATION. *Journal of Cell Biology* **114**, 1089-1100.

Mayer, M., Yang, J., Gitlin, I., Gracias, D.H., and Whitesides, G.M. (2004). Micropatterned agarose gels for stamping arrays of proteins and gradients of proteins. *Proteomics* **4**, 2366-2376.

Mei, Y., Cannizzaro, C., Park, H.S., Xu, Q.B., Bogatyrev, S.R., Yi, K., Goldman, N., Langer, R., and Anderson, D.G. (2008). Cell-Compatible, Multicomponent Protein Arrays with Subcellular Feature Resolution. *Small* **4**, 1600-1604.

Michael, K.E., Dumbauld, D.W., Burns, K.L., Hanks, S.K., and Garcia, A.J. (2009). Focal Adhesion Kinase Modulates Cell Adhesion Strengthening via Integrin Activation. *Molecular Biology of the Cell* **20**, 2508-2519.

Miyamoto, S., Akiyama, S.K., and Yamada, K.M. (1995a). SYNERGISTIC ROLES FOR RECEPTOR OCCUPANCY AND AGGREGATION IN INTEGRIN TRANSMEMBRANE FUNCTION. *Science* **267**, 883-885.

Miyamoto, S., Teramoto, H., Coso, O.A., Gutkind, J.S., Burbelo, P.D., Akiyama, S.K., and Yamada, K.M. (1995b). INTEGRIN FUNCTION - MOLECULAR HIERARCHIES OF CYTOSKELETAL AND SIGNALING MOLECULES. *Journal of Cell Biology* **131**, 791-805.

Mossman, K.D., Campi, G., Groves, J.T., and Dustin, M.L. (2005). Altered TCR signaling from geometrically repatterned immunological synapses. *Science* **310**, 1191-1193.

Munevar, S., Wang, Y.L., and Dembo, M. (2001). Distinct roles of frontal and rear cell-substrate adhesions in fibroblast migration. *Molecular Biology of the Cell* **12**, 3947-3954.

Nam, K.T., Kim, D.W., Yoo, P.J., Chiang, C.Y., Meethong, N., Hammond, P.T., Chiang, Y.M., and Belcher, A.M. (2006). Virus-enabled synthesis and assembly of nanowires for lithium ion battery electrodes. *Science* **312**, 885-888.

Nam, K.T., Wartena, R., Yoo, P.J., Liau, F.W., Lee, Y.J., Chiang, Y.M., Hammond, P.T., and Belcher, A.M. (2008). Stamped microbattery electrodes based on self-assembled M13

viruses. *Proceedings of the National Academy of Sciences of the United States of America* **105**, 17227-17231.

Narumiya, S., Ishizaki, T., and Uehata, M. (2000). Use and properties of ROCK-specific inhibitor Y-27632. *Methods in Enzymology* **325**, 273-284.

Nobes, C.D., and Hall, A. (1995). RHO, RAC, AND CDC42 GTPASES REGULATE THE ASSEMBLY OF MULTIMOLECULAR FOCAL COMPLEXES ASSOCIATED WITH ACTIN STRESS FIBERS, LAMELLIPODIA, AND FILOPODIA. *Cell* **81**, 53-62.

Olivier, L.A., and Truskey, G.A. (1993). A NUMERICAL-ANALYSIS OF FORCES EXERTED BY LAMINAR-FLOW ON SPREADING CELLS IN A PARALLEL-PLATE FLOW CHAMBER ASSAY. *Biotechnology and Bioengineering* **42**, 963-973.

Paszek, M.J., Zahir, N., Johnson, K.R., Lakins, J.N., Rozenberg, G.I., Gefen, A., Reinhart-King, C.A., Margulies, S.S., Dembo, M., Boettiger, D.*, et al.* (2005). Tensional homeostasis and the malignant phenotype. *Cancer Cell* **8**, 241-254.

Petrenko, V.A., Smith, G.P., Gong, X., and Quinn, T. (1996). A library of organic landscapes on filamentous phage. *Protein Engineering* **9**, 797-801.

Petrie, T.A., Capadona, J.R., Reyes, C.D., and Garcia, A.J. (2006). Integrin specificity and enhanced cellular activities associated with surfaces presenting a recombinant fibronectin fragment compared to RGD supports. *Biomaterials* **27**, 5459-5470.

Petrie, T.A., Stanley, B.T., and Garcia, A.J. (2009). Micropatterned surfaces with controlled ligand tethering. *J Biomed Mater Res A* **90**, 755-765.

Peyton, S.R., Raub, C.B., Keschrumrus, V.P., and Putnam, A.J. (2006). The use of poly(ethylene glycol) hydrogels to investigate the impact of ECM chemistry and mechanics on smooth muscle cells. *Biomaterials* **27**, 4881-4893.

Piner, R.D., Zhu, J., Xu, F., Hong, S.H., and Mirkin, C.A. (1999). "Dip-pen" nanolithography. *Science* **283**, 661-663.

Ponti, A., Machacek, M., Gupton, S.L., Waterman-Storer, C.M., and Danuser, G. (2004). Two distinct actin networks drive the protrusion of migrating cells. *Science* **305**, 1782-1786.

Psaltis, D., Quake, S.R., and Yang, C. (2006). Developing optofluidic technology through the fusion of microfluidics and optics. *Nature* **442**, 381-386.

Ranzinger, J., Krippner-Heidenreich, A., Haraszti, T., Bock, E., Tepperink, J., Spatz, J.P., and Scheurich, P. (2009). Nanoscale Arrangement of Apoptotic Ligands Reveals a Demand for a Minimal Lateral Distance for Efficient Death Receptor Activation. *Nano Letters* **9**, 4240-4245.

Renault, J.P., Bernard, A., Bietsch, A., Michel, B., Bosshard, H.R., Delamarche, E., Kreiter, M., Hecht, B., and Wild, U.P. (2003). Fabricating arrays of single protein molecules on glass using microcontact printing. *Journal of Physical Chemistry B* **107**, 703-711.

Renault, J.P., Bernard, A., Juncker, D., Michel, B., Bosshard, H.R., and Delamarche, E. (2002). Fabricating microarrays of functional proteins using affinity contact printing. *Angewandte Chemie-International Edition* **41**, 2320-2323.

Riveline, D., Zamir, E., Balaban, N.Q., Schwarz, U.S., Ishizaki, T., Narumiya, S., Kam, Z., Geiger, B., and Bershadsky, A.D. (2001). Focal contacts as mechanosensors: Externally applied local mechanical force induces growth of focal contacts by an mDia1-dependent and ROCK-independent mechanism. *Journal of Cell Biology* **153**, 1175-1185.

Roca-Cusachs, P., Gauthier, N.C., del Rio, A., and Sheetz, M.P. (2009). Clustering of α5β1 integrins determines adhesion strength whereas αvβ3 and talin enable mechanotransduction. *Proceedings of the National Academy of Sciences* **106**, 16245-16250.

Rundqvist, J., Mendoza, B., Werbin, J.L., Heinz, W.F., Lemmon, C., Romer, L.H., Haviland, D.B., and Hoh, J.H. (2007). High fidelity functional patterns of an extracellular matrix protein by electron beam-based inactivation. *Journal of the American Chemical Society* **129**, 59-67.

Salaita, K., Wang, Y.H., Fragala, J., Vega, R.A., Liu, C., and Mirkin, C.A. (2006). Massively parallel dip-pen nanolithography with 55000-pen two-dimensional arrays. *Angewandte Chemie-International Edition* **45**, 7220-7223.

Schmidt, R.C., and Healy, K.E. (2009). Controlling biological interfaces on the nanometer length scale. *Journal of Biomedical Materials Research Part A* **90A**, 1252-1261.

Selhuber-Unkel, C., Erdmann, T., Lopez-Garcia, M., Kessler, H., Schwarz, U.S., and Spatz, J.P. (2010). Cell Adhesion Strength Is Controlled by Intermolecular Spacing of Adhesion Receptors. *Biophysical Journal* **98**, 543-551.

Seo, J.H., Matsuno, R., Konno, T., Takai, M., and Ishihara, K. (2008). Surface tethering of phosphorylcholine groups onto poly(dimethylsiloxane) through swelling--deswelling methods with phospholipids moiety containing ABA-type block copolymers. *Biomaterials* **29**, 1367-1376.

Slater, J.H., and Frey, W. (2008). Nanopatterning of fibronectin and the influence of integrin clustering on endothelial cell spreading and proliferation. *Journal of Biomedical Materials Research Part A* **87A**, 176-195.

Sniadecki, N., Desai, R.A., Ruiz, S.A., and Chen, C.S. (2006). Nanotechnology for cell-substrate interactions. *Annals of Biomedical Engineering* **34**, 59-74.

Souza, G.R., Christianson, D.R., Staquicini, F.I., Ozawa, M.G., Snyder, E.Y., Sidman, R.L., Miller, J.H., Arap, W., and Pasqualini, R. (2006). Networks of gold nanoparticles and

bacteriophage as biological sensors and cell-targeting agents. *Proceedings of the National Academy of Sciences of the United States of America* **103**, 1215-1220.

Spatz, J.P., Herzog, T., Mossmer, S., Ziemann, P., and Moller, M. (1999). Micellar inorganic-polymer hybrid systems - A tool for nanolithography. *Advanced Materials* **11**, 149-153.

Stamou, D., Duschl, C., Delamarche, E., and Vogel, H. (2003). Self-assembled microarrays of attoliter molecular vessels. *Angewandte Chemie International Edition* **42**, 5580-5583.

Stevens, M.M., and George, J.H. (2005). Exploring and engineering the cell surface interface. *Science* **310**, 1135-1138.

Stupack, D.G., Li, E.G., Silletti, S.A., Kehler, J.A., Geahien, R.L., Hahn, K., Nemerow, G.R., and Cheresh, D.A. (1999). Matrix valency regulates integrin-mediated lymphoid adhesion via Syk kinase. *Journal of Cell Biology* **144**, 777-787.

Suh, K.Y., Khademhosseini, A., Jon, S., and Langer, R. (2006). Direct confinement of individual viruses within polyethylene glycol (PEG) nanowells. *Nano Letters* **6**, 1196-1201.

Tadokoro, S., Shattil, S.J., Eto, K., Tai, V., Liddington, R.C., de Pereda, J.M., Ginsberg, M.H., and Calderwood, D.A. (2003). Talin binding to integrin beta tails: A final common step in integrin activation. *Science* **302**, 103-106.

Takeuchi, H., Matsuno, M., Overman, S.A., and Thomas, G.J. (1996). Raman linear intensity difference of flow-oriented macromolecules: Orientation of the indole ring of tryptophan-26 in filamentous virus fd. *Journal of the American Chemical Society* **118**, 3498-3507.

Tan, J.L., Tien, J., and Chen, C.S. (2002). Microcontact printing of proteins on mixed self-assembled monolayers. *Langmuir* **18**, 519-523.

Tan, J.L., Tien, J., Pirone, D.M., Gray, D.S., Bhadriraju, K., and Chen, C.S. (2003). Cells lying on a bed of microneedles: An approach to isolate mechanical force. *Proceedings of the National Academy of Sciences of the United States of America* **100**, 1484-1489.

Vega, R.A., Maspoch, D., Salaita, K., and Mirkin, C.A. (2005). Nanoarrays of single virus particles. *Angewandte Chemie-International Edition* **44**, 6013-6015.

Vega, R.A., Shen, C.K.F., Maspoch, D., Robach, J.G., Lamb, R.A., and Mirkin, C.A. (2007). Monitoring single-cell infectivity from virus-particle nanoarrays fabricated by parallel dip-pen nanotithography. *Small* **3**, 1482-1485.

Vogel, V., and Sheetz, M. (2006). Local force and geometry sensing regulate cell functions. *Nat Rev Mol Cell Biol* **7**, 265-275.

Vogel, V., and Sheetz, M.P. (2009). Cell fate regulation by coupling mechanical cycles to biochemical signaling pathways. *Curr Opin Cell Biol* **21**, 38-46.

Von Philipsborn, A.C., Lang, S., Bernard, A., Loeschinger, J., David, C., Lehnert, D., Bastmeyer, M., and Bonhoeffer, F. (2006). Microcontact printing of axon guidance molecules for generation of graded patterns. *Nature Protocols* **1**, 1322-1328.

Wang, H.B., Dembo, M., Hanks, S.K., and Wang, Y.Y. (2001). Focal adhesion kinase is involved in mechanosensing during fibroblast migration. *Proc Natl Acad Sci U S A* **98**, 11295-11300.

Ward, M.D., and Hammer, D.A. (1993). A THEORETICAL-ANALYSIS FOR THE EFFECT OF FOCAL CONTACT FORMATION ON CELL-SUBSTRATE ATTACHMENT STRENGTH. *Biophysical Journal* **64**, 936-959.

Whitesides, G.M. (2006). The origins and the future of microfluidics. *Nature* **442**, 368-373.

Whitesides, G.M., Ostuni, E., Takayama, S., Jiang, X.Y., and Ingber, D.E. (2001). Soft lithography in biology and biochemistry. *Annual Review of Biomedical Engineering* **3**, 335-373.

Wu, Y., Huang, Y., and Ma, H. (2007). A facile method for permanent and functional surface modification of poly(dimethylsiloxane). *J Am Chem Soc* **129**, 7226-7227.

Yan, H., Park, S.H., Finkelstein, G., Reif, J.H., and Labean, T.H. (2003). DNA-templated self-assembly of protein arrays and highly conductive nanowires. *Science* **301**, 1882-1884.

Yan, L., Huck, W.T.S., Zhao, X.M., and Whitesides, G.M. (1999). Patterning thin films of poly(ethylene imine) on a reactive SAM using microcontact printing. *Langmuir* **15**, 1208-1214.

Yan, L., Zhao, X.M., and Whitesides, G.M. (1998). Patterning a preformed, reactive SAM using microcontact printing. *Journal of the American Chemical Society* **120**, 6179-6180.

Yang, L.H., Liang, H.J., Angelini, T.E., Butler, J., Coridan, R., Tang, J.X., and Wong, G.C.L. (2004). Self-assembled virus-membrane complexes. *Nature Materials* **3**, 615-619.

Yi, H.M., Nisar, S., Lee, S.Y., Powers, M.A., Bentley, W.E., Payne, G.F., Ghodssi, R., Rubloff, G.W., Harris, M.T., and Culver, J.N. (2005). Patterned assembly of genetically modified viral nanotemplates via nucleic acid hybridization. *Nano Letters* **5**, 1931-1936.

Zaidel-Bar, R., Ballestrem, C., Kam, Z., and Geiger, B. (2003). Early molecular events in the assembly of matrix adhesions at the leading edge of migrating cells. *Journal of Cell Science* **116**, 4605-4613.

Zaidel-Bar, R., Itzkovitz, S., Ma'ayan, A., Iyengar, R., and Geiger, B. (2007). Functional atlas of the integrin adhesome. *Nat Cell Biol* **9**, 858-867.

Zhong, C.L., Kinch, M.S., and Burridge, K. (1997). Rho-stimulated contractility contributes to the fibroblastic phenotype of ras-transformed epithelial cells. *Molecular Biology of the Cell* **8**, 2329-2344.

Zimerman, B., Volberg, T., and Geiger, B. (2004). Early molecular events in the assembly of the focal adhesion-stress fiber complex during fibroblast spreading. *Cell Motility and the Cytoskeleton* **58**, 143-159.

Zimmermann, K., Hagedorn, H., Heuck, C.C., Hinrichsen, M., and Ludwig, H. (1986). THE IONIC PROPERTIES OF THE FILAMENTOUS BACTERIOPHAGES PF1 AND FD. *Journal of Biological Chemistry* **261**, 1653-1655.